

THE SURFACE IMPOUNDMENT ELEMENT FOR  
THE WATER EROSION PREDICTION PROJECT

By

MARK R. LINDLEY

Bachelor of Science

University of Kentucky

Lexington, Kentucky

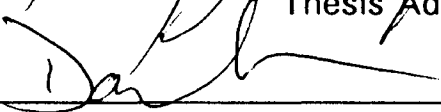
1989

Submitted to the Faculty of the  
Graduate College of the  
Oklahoma State University  
in partial fulfillment of  
the requirements for  
the Degree of  
MASTER OF SCIENCE  
July, 1994


THE SURFACE IMPOUNDMENT ELEMENT FOR  
THE WATER EROSION PREDICTION PROJECT

Thesis Approved:

  
\_\_\_\_\_  
Thesis Adviser

  
\_\_\_\_\_

  
\_\_\_\_\_

  
\_\_\_\_\_  
Dean of the Graduate College

## ACKNOWLEDGEMENTS

I wish to thank my major advisor, Dr. Bill Barfield. Bill provided not only the technical guidance that made this study possible, but also the moral and personal support required to see this project to completion and to help me grow and mature as a human being. I would also like to thank Dr. Bruce Wilson for his excellent suggestions in this modelling effort.

I would like to thank Dr. John Laflen, the Agricultural Research Service, and the National Soil Erosion Laboratory for the patience and financial support required for this project. Further, I need to express my appreciation to the Biosystems and Agricultural Engineering Department at the Oklahoma State University and the Biological and Agricultural Engineering Department at the University of Kentucky for the support they provided this project.

Alex Fogle and Dr. James Ascough II provided excellent knowledge of FORTRAN code, and Dr. George Sabbah checked the final code line by line.

I must also thank my parents Christine and Carl Lindley for the genetic material and upbringing that form the basis of my being. Dr. Blaine Parker, Dr. Richard Warner, John Moredock, Bob Poole, Bruce Odze, Doris Plant, Bill Blasewitz, Metta Montin, and the Grateful Dead have all played instrumental roles in forming the intellectual and spiritual being that performed this study.

## TABLE OF CONTENTS

Chapter	Page
I. INTRODUCTION . . . . .	1
Background . . . . .	1
Water Erosion Prediction Project . . . . .	3
Impoundment Routines . . . . .	4
Objective . . . . .	7
Thesis Structure . . . . .	8
II. LITERATURE REVIEW . . . . .	10
Hydraulic Routing . . . . .	11
Stage-Discharge Relationships . . . . .	20
Drop Spillway . . . . .	20
Perforated Riser . . . . .	30
Culvert . . . . .	35
Open Channel and Emergency Spillway . . . . .	45
Rock Fill Check Dam . . . . .	51
Filter Fence and Straw Bale . . . . .	57
Stage-Area Relationship . . . . .	64
Sedimentation . . . . .	64
Effect of Particle Size Distribution . . . . .	66
Steady-State Flow Models . . . . .	69
Overflow Rate Model - Quiescent Flow . . . . .	69
Overflow Rate Model - Turbulent Flow . . . . .	73
EPA Urban Methodology . . . . .	74
Variable Flow Rate Models . . . . .	83
Modified Overflow Rate Models . . . . .	83
Plug Flow Model . . . . .	88
CSTRS Model . . . . .	92
BASIN Model . . . . .	98
Evaluation of Accuracy . . . . .	100

Chapter	Page
III. MODEL DEVELOPMENT . . . . .	102
Hydraulic Routing . . . . .	106
Continuity Expression . . . . .	107
Runge-Kutta Numerical Integration . . . . .	109
Adaptive Time Step . . . . .	110
Stage-Discharge Relationships . . . . .	113
Drop Spillway . . . . .	115
Perforated Riser . . . . .	118
Culvert . . . . .	121
Open Channel and Emergency Spillway . . . . .	122
Rock Fill Check Dam . . . . .	123
Filter Fence and Straw Bale . . . . .	125
User Defined . . . . .	127
Overall Outflow Expression . . . . .	128
Stage-Area Relationship . . . . .	129
Evaporation and Infiltration . . . . .	130
Sedimentation . . . . .	131
Conservation of Mass . . . . .	132
Deposition . . . . .	134
Quiescent Settling . . . . .	142
IV. CALIBRATION COEFFICIENTS . . . . .	144
Optimal Values of $c_t$ and $c_d$ . . . . .	145
Statistical Analysis . . . . .	149
Estimation Models . . . . .	156
Comparison to CSTRS Database . . . . .	160

Chapter	Page
V. VALIDATION . . . . .	178
Hydraulic Routing . . . . .	178
Stage-Discharge Relationships . . . . .	184
Perforated Risers . . . . .	187
Open Channels and Emergency Spillways . . . . .	188
Rock Fill Check Dams . . . . .	194
Sedimentation Algorithms . . . . .	195
VI. SUMMARY AND CONCLUSIONS . . . . .	217
Summary . . . . .	217
Conclusions . . . . .	219
Recommendations for Further Study . . . . .	221
REFERENCES . . . . .	222

## LIST OF TABLES

Table	Page
2.1. Friction loss coefficients for circular conduits flowing full (SCS, 1951). . . . .	28
2.2. Friction loss coefficients for square conduits flowing full (SCS, 1951). . . . .	29
2.3. Constants for inlet control culvert discharge equations (FHA, 1985). . . . .	44
2.4. Slurry flow rates recommended by state regulatory agencies (Haan et al., 1994). . . . .	62
2.5. Slurry flow rates for various fabrics with different size distributions (Fisher and Jarrett, 1984). . . . .	63
2.6. Rainfall statistical parameters (Driscoll et al., 1986). . . . .	82
4.1. Description of small impoundments used in the optimization runs. . . . .	150
4.2. Description of inflow hydrographs utilized in the small impoundment optimization runs. . . . .	151
4.3. Description of large impoundments used in the optimization runs. . . . .	152
4.4. Description of inflow hydrographs utilized in the large impoundment optimization runs. . . . .	153
4.5. Variables considered for inclusion in $c_t$ and $c_d$ estimation models. . . . .	154
4.6. Small impoundment models. . . . .	158

Table	Page
4.7. Large impoundment models. . . . .	159
4.8. Description of small impoundments used in the comparison runs. . . . .	162
4.9. Description of large impoundments used in the comparison runs. . . . .	163
4.10. Results on small impoundments using the prediction models presented above. . . . .	166
4.11. Results on small impoundments using the mean values of $c_t$ and $c_d$ computed with the optimization data for small impoundments. . . . .	167
4.12. Results on small impoundments using the mean values of $c_t$ and $c_d$ computed with the optimization data for both small and large impoundments. . . . .	168
4.13. Results on large impoundments using the prediction models presented above. . . . .	172
4.14. Results on large impoundments using the mean values of $c_t$ and $c_d$ computed with the optimization data for large impoundments. . . . .	173
4.15. Results on large impoundments using the mean values of $c_t$ and $c_d$ computed with the optimization data for both small and large impoundments. . . . .	174
5.1. Summary of input data used for validation of the hydraulic routing. . . . .	180
5.2. Summary of inflow rates and influent sediment concentrations for empirical validation runs. . . . .	199



Table	Page
5.3. Predicted and observed trapping efficiencies for the Tapp et al. (1981) and Wilson et al. (1984) data sets. . . . .	203

## LIST OF FIGURES

Figure	Page
2.1. Change of storage in an impoundment (Kao, 1975). . . . .	12
2.2. Inflow and outflow hydrographs (Kao, 1975). . . . .	13
2.3. Storage characteristic curves illustrating the PULS method (Barfield et al., 1981). . . . .	16
2.4. Outflow hydrograph comparison. . . . .	18
2.5. Outflow Hydrograph comparison. . . . .	19
2.6. Drop inlet with weir control (Barfield et al., 1981). . . . .	22
2.7. Drop inlet with orifice flow control (Barfield et al., 1981). . . . .	24
2.8. Drop inlet with pipe flow and a free outfall (Barfield et al., 1981). . . . .	25
2.9. Drop inlet with pipe flow and a submerged outfall (Barfield et al., 1981). . . . .	26
2.10. Energy losses for a drop inlet flowing full (Barfield et al., 1981). . . . .	27
2.11. Stage-discharge relationship for a drop inlet (Barfield et al. 1994). . . . .	31
2.12. Perforated riser definition sketch (McEnroe et al., 1988). . . . .	32
2.13. Culvert used as an outlet to a farm pond (Barfield et al., 1981). . . . .	37
2.14. Types of culvert flow (Chow, 1959). . . . .	38

Figure	Page
2.15. Criteria for hydraulically short and long concrete culverts Type 3 is short and Type 2 is long (Carter, 1957). . . . .	39
2.16. Criteria for hydraulically short and long culverts with rough corrugated pipes. Type 3 is short and Type 2 is long (Carter, 1957). . . . .	40
2.17. Stage-discharge relationship for a circular pipe with control at the inlet (Mavis, 1942). . . . .	42
2.18. Broad Crested Spillway with a control section (Barfield et al., 1981). . . . .	47
2.19. Schematic for flow in porous rock fill (Haan et al., 1994). . . . .	52
2.20. Coefficients for the rock fill stage-discharge power function (after Haan et al., 1994). . . . .	58
2.21. Straw bale check dam schematic (Barfield et al., 1981). . . . .	59
2.22. Filter fence check dam schematic (Barfield et al., 1981). . . . .	60
2.23. Sediment diameter vs. settling velocity in water assuming a specific gravity for sediment of 2.65 (Barfield et al., 1981). . . . .	68
2.24. Illustration of the overflow rate concept in an ideal rectangular basin (Barfield et al., 1981). . . . .	72
2.25. Trapping efficiency in a rectangular basin with turbulent steady-state flow (Camp, 1946). . . . .	75
2.26. Trapping efficiency verses the ratio of settling velocity to overflow rate for a high turbulence model (Barfield et al., 1981; after Chen, 1975). . . . .	76

Figure	Page
2.27. Comparison of the EPA and overflow rate models (after Haan et al., 1994). . . . .	79
2.28. Long term sediment trapping in ponds under storm flow conditions (Driscoll et al., 1986). . . . .	80
2.29. Regions for rainfall statistical parameters (Driscoll et al., 1986). . . . .	81
2.30. Ratio of the mean storage volume to the mean runoff volume (after Driscoll, 1986). . . . .	84
2.31. Long term removal ratio for impoundments under quiescent conditions between storms (after Driscoll, 1986). . . . .	85
2.32. The plug flow concept (Wilson et al., 1982). . . . .	90
2.33. An impoundment with short-circuiting and dead storage (Wilson et al., 1982). . . . .	91
2.34. The inflow and outflow hydrographs split into plugs (Wilson et al., 1982). . . . .	93
2.35. Layers for mass balance computations (Wilson et al., 1982). . . . .	94
2.36. Pond divided into a series of CSTRS (Wilson and Barfield, 1985). . . . .	96
2.37. An impoundment split into reactors and vertical layers (Wilson and Barfield, 1985). . . . .	99
3.1. WEPPSIE flow chart. . . . .	104
3.2. Illustration of Runge-Kutta integration (Press et al., 1986). . . .	112

Figure	Page
3.3. Schematic of an impoundment with multiple outlet structures. . . . .	116
3.4. Stage-discharge relationship for individual structures and all structures combined including transitions between flow regimes. . . . .	117
3.5. Division of a particle size distribution into four subclasses. . . . .	136
3.6. Locations in time for which each deposition statement is used (Lindley et al., 1993). . . . .	141
4.1. Locations in time for which optimizations took place (Lindley et al., 1993). . . . .	146
4.2. Trapping efficiency difference between the WEPPSIE and CSTRS predictions for small impoundments. . . . .	169
4.3. Trapping efficiency difference between the WEPPSIE and CSTRS predictions for small impoundments. . . . .	170
4.4. Trapping efficiency difference between the WEPPSIE and CSTRS predictions for large impoundments. . . . .	175
4.5. Trapping efficiency difference between the WEPPSIE and CSTRS predictions for large impoundments. . . . .	176
5.1. Outflow hydrograph comparison for the 7770 m <sup>3</sup> pond. . . . .	181
5.2. Outflow hydrograph comparison for a 15,663 m <sup>3</sup> pond. . . . .	182
5.3. Comparison of peak outflows for the 10 impoundments presented in Table 5.1. . . . .	183

Figure	Page
5.4. Comparison of the outflow hydrographs computed with WEPPSIE and with the CSTRS model when only 5 stage-area-discharge points are entered into the CSTRS model. . . . .	185
5.5. Comparison of the outflow hydrographs computed with WEPPSIE and with the CSTRS model when only 5 stage-area-discharge points are entered into the CSTRS model. . . . .	186
5.6. Comparison between the stage-discharge relationship computed according to the McEnroe et al. (1988) procedure and the regression relationship in WEPPSIE ( $h_b = 0.0$ m). . . . .	189
5.7. Comparison between the stage-discharge relationship computed according to the McEnroe et al. (1988) procedure and the regression relationship in WEPPSIE ( $h_b = 0.9$ m). . . . .	190
5.8. Comparison of the stage-discharge relationship for an open channel outlet without control produced by the steady-state standard step method and the polynomial regression equation included in WEPPSIE. . . . .	192
5.9. Comparison of the stage-discharge relationship for an emergency spillway with control outlet produced by the steady-state standard step method and the polynomial regression equation included in WEPPSIE. . . . .	193
5.10. Comparison of the stage-discharge relationship for a rock fill check dam produced by the Herrera (1989) procedure included in WEPPSIE. . . . .	196

Figure	Page
5.11. Predicted and observed effluent sediment concentrations for Tapp et al. (1981) Run 18. . . . .	204
5.12. Predicted and observed effluent sediment concentrations for Tapp et al. (1981) Run 19. . . . .	205
5.13. Predicted and observed effluent sediment concentrations for Tapp et al. (1981) Run 22. . . . .	206
5.14. Predicted and observed effluent sediment concentrations for Tapp et al. (1981) Run 24. . . . .	207
5.15. Predicted and observed effluent sediment concentrations for Tapp et al. (1981) Run 28. . . . .	208
5.16. Predicted and observed effluent sediment concentrations for Wilson et al. (1984) Run 1. . . . .	209
5.17. Predicted and observed effluent sediment concentrations for Wilson et al. (1984) Run 2. . . . .	210
5.18. Predicted and observed effluent sediment concentrations for Wilson et al. (1984) Run 3. . . . .	211
5.19. Predicted and observed effluent sediment concentrations for Wilson et al. (1984) Run 4. . . . .	212
5.20. Predicted and observed effluent sediment concentrations for Wilson et al. (1984) Run 5. . . . .	213
5.21. Predicted and observed effluent sediment concentrations for Wilson et al. (1984) Run 6. . . . .	214

## Chapter 1: Introduction

As society moves into the twenty-first century, humankind is faced by a multitude of problems that threaten its very existence on the planet. Deforestation, declining biodiversity, the greenhouse effect, ozone depletion, soil erosion, ground water contamination, pollution, and violence are all evidence of the real and complex problems that challenge society.

Soil erosion is one of the major threats to environmental stability world wide. Estimates of soil erosion in the United States range from 1.7 billion tons to 3 billion tons of soil lost each year to erosion (Lake and Shady, 1993). Global estimates are as high as 24 billion tons of soil lost each year (Lake and Shady, 1993). Water erosion is estimated to account for 55% of the losses (Lake and Shady, 1993).

The cost of this enormous loss of top soil every year is staggering. Degradation of agricultural lands is the most apparent. Between 1945 and 1990, 1.2 billion hectares (ha), an area approximately the size of China and India combined, has experienced moderate to extreme degradation (Lake and Shady, 1993). This represents 10.5% of all vegetated land world wide (Lake and Shady, 1993).

There are also secondary costs of erosion. Eroded material may be deposited down slope, causing crop damage. Sediment can block culverts and spillways increasing the risk of flooding. Sediment laden runoff damages



aquaculture, fisheries, and wildlife. Sediment deposited in reservoirs causes an estimated \$10 billion in damage annually; approximately 36% of this comes from agricultural lands (Lake and Shady, 1993).

Soil erosion can be limited by farm practices such as contouring and strip cropping. Once sediment is detached from the land, the damage it causes down slope can be minimized by the use of impoundments. Typical impoundments include terraces, farm ponds, and check dams. Impoundments form small ponds which reduce the flow velocity, and thus decreasing the sediment carrying capacity allowing sediment to settle out of suspension. Impoundments can significantly reduce sediment yield by trapping as much as 90% to 100% of incoming sediment, dependent upon particle size, impoundment size, and inflow and outflow rates (Haan et al., 1994).

Clearly water erosion is a very serious problem. Unfortunately, given the limited resources of federal, state, and local agencies, it is impossible to address the issue fully. The answer to this problem lies in carefully allocating the available funds to projects that best improve on the current situation. How do we determine where the most serious problems exist and what measures are necessary to limit the damage caused by erosion? At this point modeling becomes a very useful tool. Using a model one can estimate the sediment loss from a field or an entire watershed under a variety of land use scenarios including a variety of sediment control structures, thus enabling decision makers to determine where and what kind of erosion control measures are needed.

## **Water Erosion Prediction Project**

An example of the models available to estimate sediment loss is the Water Erosion Prediction Project, WEPP, a process-oriented, continuous simulation model based upon state-of-art hydrologic and erosion theory. WEPP is being developed by the United States Department of Agriculture - Agricultural Research Service (USDA-ARS). The goals of WEPP are to predict runoff and sediment yield for areas ranging from small field size plots to small watersheds. Projected users for WEPP include the Soil Conservation Service, Forest Service, Bureau of Land Management, and others involved in soil and water conservation and environmental planning and assessment (Foster et al., 1987). In the future, WEPP will be an indispensable tool to identify areas with high risks of erosion and identify control practices necessary to limit erosion.

The WEPP technology includes a climate generator, hillslope profile routines, channel routines, and impoundment routines. The hillslope profile routines form the core of the WEPP technology. In the hillslope profile routines, predictions of runoff, erosion, deposition, sediment yield, and sediment characteristics are made based on of the influence of climate, topography, cover, management, and supporting practices. For similar landscape profiles, the hillslope profile routines are intended to be a technological update of the Universal Soil Loss Equation, (USLE). The channel routines in WEPP incorporate hydraulic routing as well as detachment and deposition in small channels. The impoundment routines route runoff and sediment through an impoundment

determining the total amount of runoff leaving the structure, the amount of sediment deposited in the structure, and the amount and size of sediment leaving the structure. Since impoundments are our best off-site method to limit the damage water erosion causes, the impoundment routines are crucial to the usefulness of WEPP.

The WEPP technology is intended to estimate runoff and sediment yield for small agricultural and silvicultural watersheds located through out the United States. In such watersheds, many impoundments possessing a variety of shapes and outflow structures may be present. The WEPP technology is intended to run a twenty year continuous daily simulation in fifteen to twenty minutes. Due to this time constraint, WEPP routines must function quickly. In order to balance simulation complexity with the run time limitations, WEPP includes many simplifying assumptions.

#### **WEPP Surface Impoundment Element**

This thesis addresses the development of the WEPP Surface Impoundment Element, (WEPPSIE). Thus, the subsequent discussion addresses WEPPSIE.

User requirements dictate that the impoundment routines utilized in the WEPP technology must simulate several types of impoundments: farm ponds, terraces, culverts, filter fences, and check dams. WEPP will be utilized to determine the impact of sediment laden runoff. In order to make this analysis, the user will need WEPPSIE to determine peak outflow, outflow volume, peak

effluent sediment concentration, total sediment yield, and the time required to fill a given impoundment.

One possible solution would be to use a model such as the Continuously STirred Reactors in Series, (CSTRS) (Wilson and Barfield, 1984), or the Basin Analysis of Sediment laden INflow, (BASIN) (Wilson and Barfield, 1985), models. Both CSTRS and BASIN have been validated against pilot scale impoundment data. The CSTRS model has enjoyed wide spread use as the pond component included in the SEDIMOT (Wilson et al., 1982) and SEDCAD (Warner and Schwab, 1992) single storm models. Both BASIN and CSTRS divide an impoundment into several horizontal reactors and further split the reactors into eight vertical chambers determining sedimentation by performing a mass balance on each chamber. This is very time consuming. Considering the length of the WEPP continuous daily simulation and that a modeled watershed could include several impoundments, the computation time required to run CSTRS or BASIN would be unacceptable.

With the user's needs in mind, the algorithms and code for WEPPSIE were developed to perform quickly and accurately. The basic framework of WEPPSIE daily simulation includes four sections: daily input, hydraulic simulation, sedimentation simulation, and daily output. WEPPSIE also includes a front end user interface that develops stage-discharge and stage-area relationships for a given impoundment run one time at the beginning of the WEPP simulation.

The input section of the impoundment element receives daily hydraulic inputs and sedimentologic inputs from the hillslope and channel components. The WEPP convention dictates that hydraulic inputs consist of incoming storm volume and incoming flow rate utilizing a rectangular hydrograph shape. The WEPP convention also defines the sedimentologic inputs based upon the CREAMS criteria (Foster et al., 1985) including the five particle size classes clay, silt, sand, small aggregates, and large aggregates. The sedimentologic inputs include total suspended sediment concentration, percent in each size class, and the median particle size diameter ( $d_{50}$ ) for each size class. The rectangular hydrograph and sediment graph shape along with the use of only five particle size class divisions are simplifying assumptions made by the WEPP code that balance complexity with run time.

The hydraulic simulation section performs a direct numerical integration of an expression of continuity using an adaptive time step which increases when the inflow and outflow rates are relatively constant. A temporary file of the predicted outflow hydrograph including the time, stage and outflow at each time step included in the integration is created. The sedimentation simulation section then determines the amount of sediment deposited and the outflow concentration for each time step. Deposition and effluent sediment concentration are predicted using conservation of mass and overflow rate concepts. The output section returns daily hydrologic and sedimentologic information similar to the input information for further use in the WEPP code.

The output section also creates daily, monthly, and yearly summaries of impoundment performance.

### **Objective**

The objective of this project includes the development and evaluation of the algorithms for the WEPPSIE. Specifically, this includes:

1. Develop an fast, accurate impoundment routine which determines:
  - a. Peak outflow rate and volume leaving the impoundment each day.
  - b. Peak effluent sediment concentration and the total sediment yield in the five sediment size classes.
  - c. The median particle size diameter of the sediment leaving the impoundment for each of the five sediment size classes.
2. Evaluate the accuracy of WEPPSIE as compared to both field data and data from a widely used and more complex model.

The impoundment routines must function for a wide range of impoundment sizes and shapes. The impoundment routines must also function for number of possible hydraulic outflow structures:

1. Drop spillways.
2. Perforated risers.
3. Culverts.
4. Open channels and emergency spillways.
5. Rock fill check dams.

6. Filter fences (silt fence) and straw bales.

### **Thesis Structure**

The main body of this thesis contains the following chapters:

1. **Literature Review.** The literature review chapter examines the work that has been done in the past to determine the hydraulic routing of flow through an impoundment and the sedimentation occurring within the impoundment. The literature review follows the basic structure of the WEPP impoundment element. First, pertinent information on routing of flow through impoundments is presented. Then a detailed description of methods to determine the flow through each possible outflow structure is presented. Finally, the most accepted methods of determining sedimentation within an impoundment are described.
2. **Model Development.** The model development chapter details the algorithms included in the WEPP impoundment element. First, the method used to determine the hydraulic routing of flow through an impoundment is presented. Then the overall stage-discharge and stage-area functions is described; detailing the stage-discharge function for each possible outflow structure. Finally, the sedimentation algorithms are presented including two calibration coefficients used to modify the overflow rate concept to account for impoundment geometry, hydraulic response, and stratification.

3. **Calibration Coefficients.** The calibration coefficients chapter describes how the more complex Continuous STirred Reactors in Series, CSTRS, model was used to determine optimal values of the calibration coefficients for numerous storm events simulated on numerous impoundments. This chapter also details how regression equations based upon easily determined hydraulic parameters were developed to estimate the calibration coefficients.
4. **Validation.** The validation chapter presents a comparison of results obtained with WEPPSIE to data gathered in the field, and a larger data set created with the CSTRS model.



## **Chapter 2: Literature Review**

The objective of the literature review is to provide a foundation for the development of WEPPSIE algorithms by examining work that has been done in the past to determine the hydraulic routing of flow through an impoundment and the sedimentation occurring within the impoundment. The literature review will follow the basic structure of WEPPSIE. First, pertinent information on routing of flow through impoundments will be presented. Then a detailed description of methods to determine the flow through each possible outflow structure will be presented. Finally, the most accepted methods of determining sedimentation within an impoundment will be described.

### **Hydraulic Routing**

Routing of flow through an impoundment is the first task the impoundment element completes on a daily basis. Daily hydraulic inputs dictated by the WEPP convention include the peak flow rate and the incoming volume, forming a rectangular hydrograph of known duration. The impoundment element routes the inflow through the impoundment determining the volume of flow leaving the impoundment and the peak outflow rate for each day.

Routing flow through an impoundment starts with an inflow hydrograph. As the inflow enters the impoundment, the impoundment begins to fill with water. When the stage of the outflow structure is exceeded, water begins to

exit the impoundment at a rate that is proportional to the driving head above the outflow structure. At some point after the peak of the inflow hydrograph, the outflow begins to exceed the inflow causing the stage to decrease. After all the inflow enters the impoundment, the stage and outflow continue to decrease until the stage falls below the inlet stage of the outflow structure. An illustration of hydraulic routing is presented in Figures 2.1 and 2.2 (Kao, 1975).

The continuity equation forms the basis for routing flow through an impoundment (Haan et al., 1994; Gupta, 1989):

$$\frac{\Delta S}{\Delta t} = I - O \quad (2.1)$$

where  $\Delta$  designates change,  $S$  is the storage volume,  $t$  is time,  $I$  is the inflow rate, and  $O$  is the outflow rate. Using the subscripts 1 and 2 to denote the storage, inflow, and outflow at the beginning and end of a time step of duration  $\Delta t$ , Equation 2.1 can be rewritten as (Haan et al., 1994; Gupta, 1989):

$$S_2 - S_1 = \frac{I_2 + I_1}{2} \Delta t - \frac{O_2 + O_1}{2} \Delta t \quad (2.2)$$

or

$$\left( S_2 + \frac{O_2}{2} \Delta t \right) - \left( S_1 + \frac{O_1}{2} \Delta t \right) = \frac{I_2 + I_1}{2} \Delta t \quad (2.3)$$

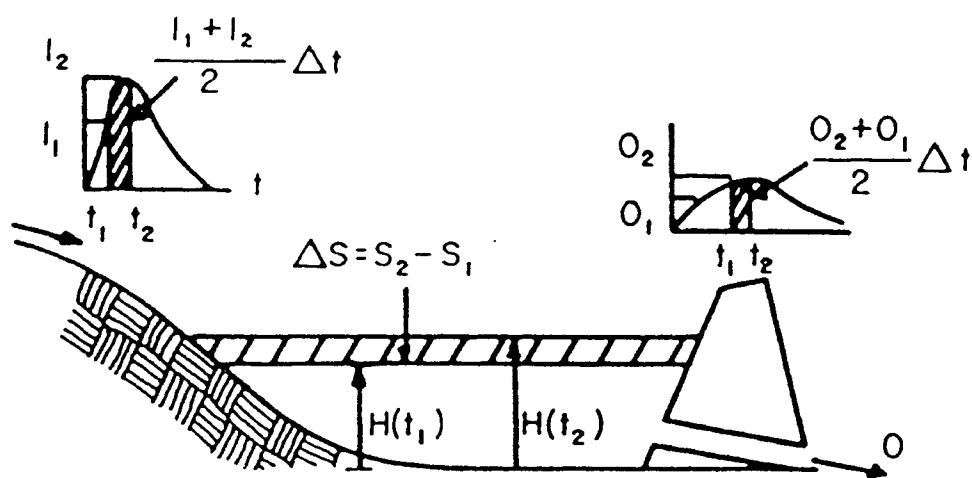


Figure 2.1: Change of storage in an impoundment (Kao, 1975).

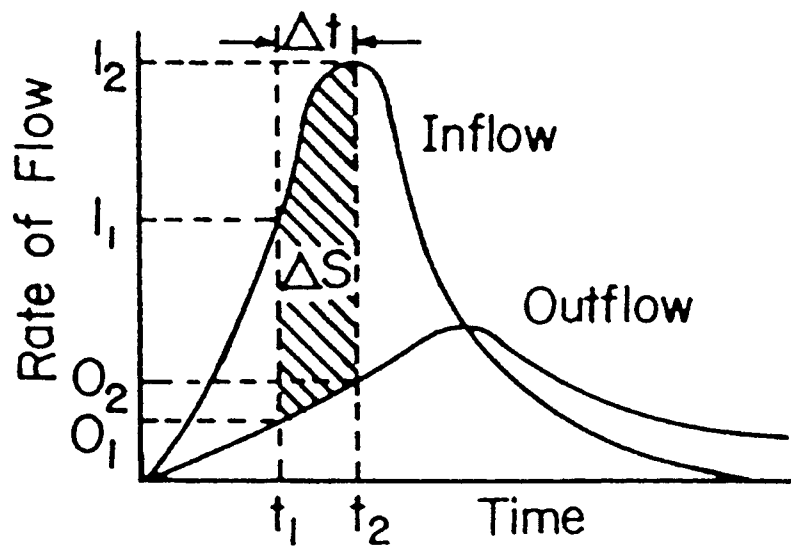


Figure 2.2: Inflow and outflow hydrographs (Kao, 1975).

Traditional flood routing involves solving Equation 2.3 either graphically or numerically to develop an outflow hydrograph.

The graphical solution to Equation 2.3 is called the PULS method which is the most widely used hydraulic routing procedure. A numerical adaptation of the PULS method is included in the Continuous STirred Reactors in Series model, CSTRS, which is utilized in two widely used hydrology and sedimentology models, SEDIMOT II (Wilson et al., 1982) and SEDCAD (Warner and Schawb, 1992). The PULS method utilizes storage characteristic curves developed from stage-storage and stage-discharge curves. The two storage characteristic curves take the following form:

$$H \text{ vs. } S + \frac{O}{2} \Delta t \quad (2.4)$$

and

$$H \text{ vs. } S - \frac{O}{2} \Delta t \quad (2.5)$$

where H is the stage. Using the storage characteristic curves in Equation 2.3 enables one to solve for the stage and therefore the discharge at the end of a time step of duration  $\Delta t$ . A step-by-step procedure to utilize the PULS routing method follows (Haan et al., 1994):

1. Develop stage-storage curves and stage-discharge curves.

2. Select a  $\Delta t$  (up to 25% of the time to the peak of the inflow hydrograph).
3. Using the information from step 1 and 2, compute the storage characteristic curves given in Equations 2.4 and 2.5.
4. For a given time step of  $\Delta t$ ,  $I_1$  and  $I_2$  are known from the inflow hydrograph and  $H_1$  is known from the previous time step. Knowing  $H_1$ ,  $\{S_1 - (O_1 / 2) \Delta t\}$  can be found from the storage characteristic curve.
5. Utilizing  $\Delta t$ ,  $I_1$ ,  $I_2$ , and  $\{S_1 - (O_1 / 2) \Delta t\}$  in Equation 2.3, solve for  $\{S_2 + (O_2 / 2) \Delta t\}$ .
6. Using the storage characteristic curve, determine the stage,  $H_2$ , that corresponds to  $\{S_2 + (O_2 / 2) \Delta t\}$ .
7. The outflow,  $O_2$ , corresponding to  $H_2$  is determined with the stage-discharge curve.
8. Set  $I_1$ ,  $H_1$ ,  $O_1$ , and  $S_1$  equal to  $I_2$ ,  $H_2$ ,  $O_2$ , and  $S_2$  and repeat steps 4 through 7. This procedure is repeated until all the inflow is routed through the impoundment.

An example of this procedure is presented in Figure 2.3.

The numerical adaptation of the PULS method included in the CSTRS model utilizes up to twenty-four user entered stage points, with the

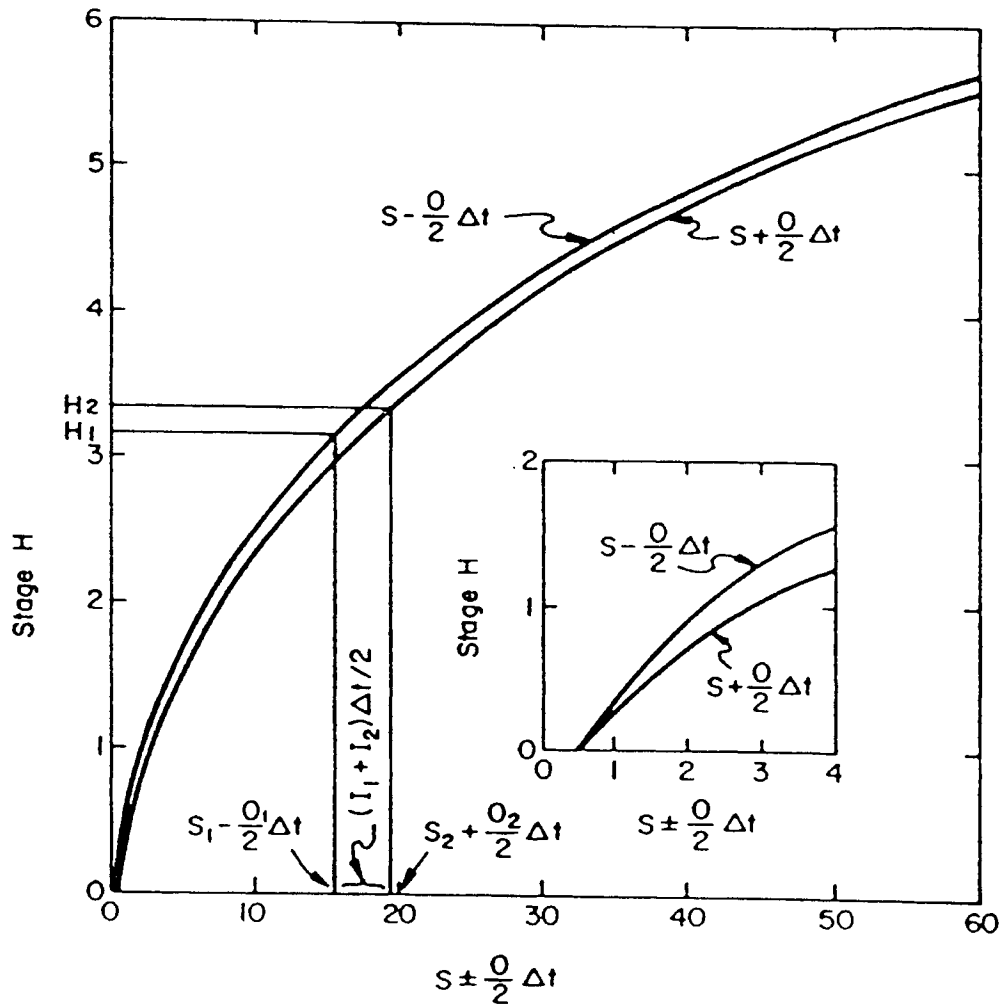


Figure 2.3: Storage characteristic curves illustrating the PULS method (Barfield et al., 1981).

corresponding areas and discharges either computed by the model or entered by the user. Linear interpolation is utilized between the stage points when computing the stage-discharge and storage characteristic curves. Provided the user enters sufficient stage-area-discharge points, the error introduced by the use of linear interpolation is minimal. However, if the user enters only a few stage-area-discharge points, the use of linear interpolation can introduce large errors in the computed outflow hydrograph. Figures 2.4 and 2.5 illustrate the error in outflow hydrographs computed with the CSTRS model when the user entered five as compared to fifteen stage-area-discharge points (Lindley et al., 1992).

It is also possible to solve Equation 2.3 numerically. For a given time step,  $\Delta t$ ,  $H_1$ ,  $S_1$ ,  $O_1$ ,  $I_1$ , and  $I_2$  are known, and  $H_2$ ,  $S_2$ , and  $O_2$  must be determined. Since there is one equation with two unknowns,  $S_2$  and  $O_2$ , no explicit solution exists, and Equation 2.3 must be solved iteratively. Haan et al. (1994) indicates that convergence should occur within a couple of iterations.

The hydraulic routing procedure utilized in WEPPSIE is also based upon the continuity principle. However, it departs from the traditional routing procedures presented here by utilizing a direct numerical integration of the continuity expression presented in Equation 2.1. In the WEPPSIE routing procedure, storage,  $S$ , is split into stage and area with area being expressed as a function of stage. Thus, both the discharge and the area are functionally related to stage. A detailed description of the hydraulic routing procedure



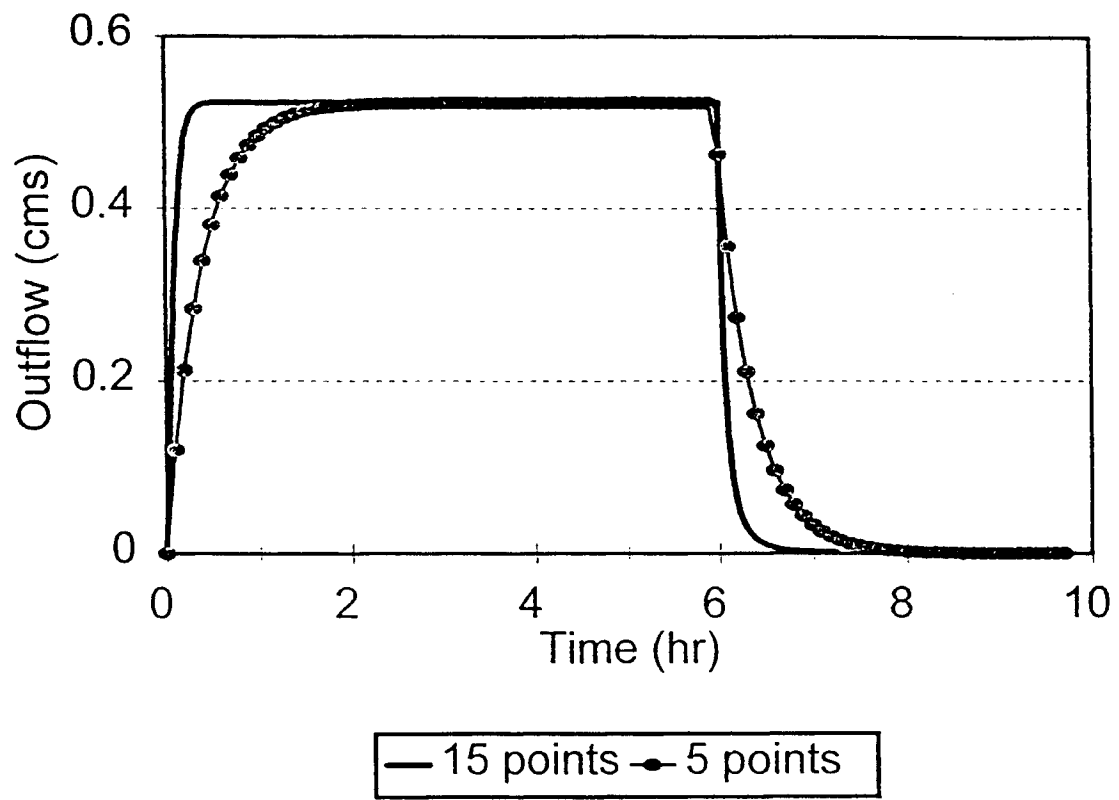


Figure 2.4: Outflow hydrograph comparison.

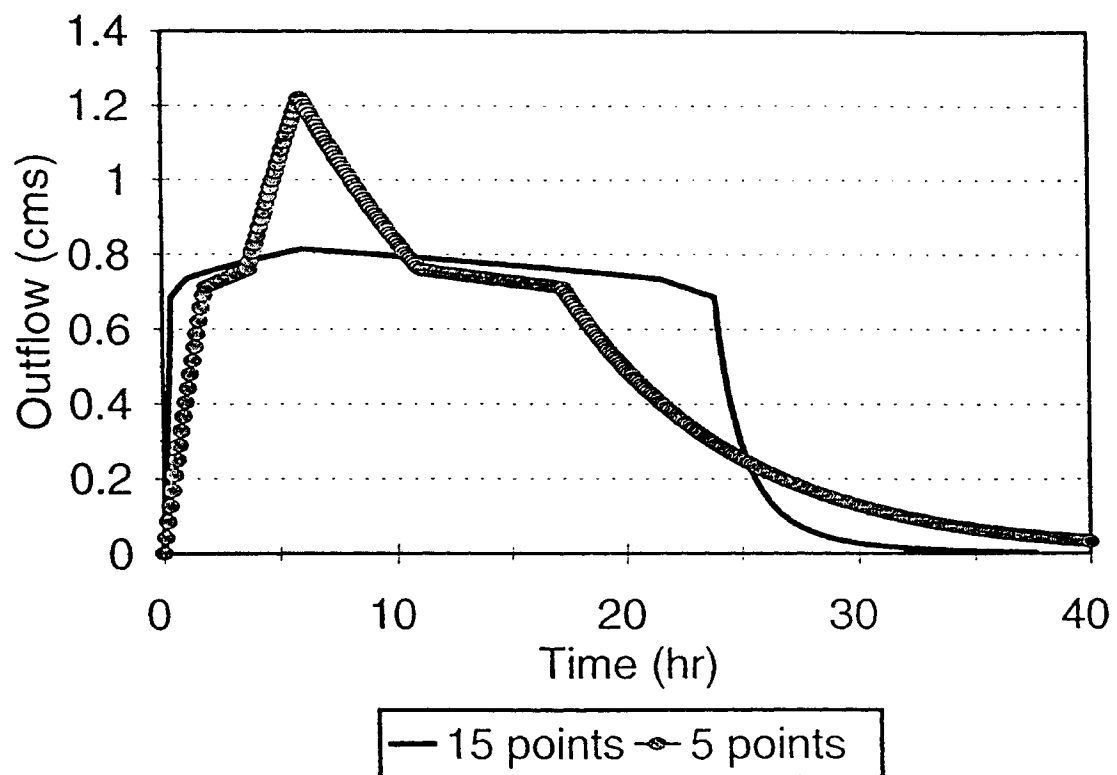


Figure 2.5: Outflow Hydrograph comparison.

utilized in WEPPSIE Impoundment element is presented in the Model Development section.

## **Stage-Discharge Relationships**

The discharge through an outflow structure is driven by the head above the outflow structure inlet. As the stage increases above the outflow structure, the driving head increases and therefore outflow increases. In order to hydraulically route flow through an impoundment, the relationship between stage and discharge must be known. This section examines currently accepted methods for determining the discharge through the outflow structures that will be covered in WEPPSIE:

1. Drop spillways.
2. Perforated risers.
3. Culverts.
4. Open channels and emergency spillways.
5. Rock fill check dams.
6. Filter fences and straw bales.

### **Drop Spillway**

A drop spillway is a common outflow structure used in farm ponds and sediment detention basins. It consists of a vertical riser connected to a horizontal or near horizontal barrel, as shown in Figures 2.6 through 2.10. Depending upon the driving head, either weir flow, orifice flow, or pipe flow controls the discharge.

As the stage rises above the riser inlet, water starts to flow over edge of the riser, and the riser acts as a sharp crested weir with a length equivalent to the circumference of the riser. The discharge over a sharp crested weir is related to the driving head by the following commonly used sharp crested weir equation (Haan et al., 1994; SCS, 1984; and Schwab et al., 1981):

$$Q = CLH^{\frac{3}{2}} \quad (2.6)$$

where Q is the discharge in ft<sup>3</sup>/sec, C is the weir coefficient, L is the length of the weir in ft (circumference of the riser), and H is the driving head in ft. For risers, C is generally between 3.0 and 3.2. Figure 2.6 illustrates a drop inlet with weir flow control. For a detailed discussion of the dynamics of weir flow, Grant (1978) can be consulted.

As the stage above the riser inlet continues to increase, the riser inlet becomes submerged and starts to behave as an orifice. The discharge through an orifice can be determined with the following equation (Haan et al., 1994;SCS, 1984; and Schwab et al., 1981):

$$Q = C'A\sqrt{2gH} \quad (2.7)$$

where C' is the orifice coefficient, A is the cross sectional area of the orifice in ft<sup>2</sup> (flow area of the riser), g is the gravitational constant, and H is the head on the orifice in ft. For a riser inlet, C' is 0.6. Figure 2.7 illustrates a drop inlet

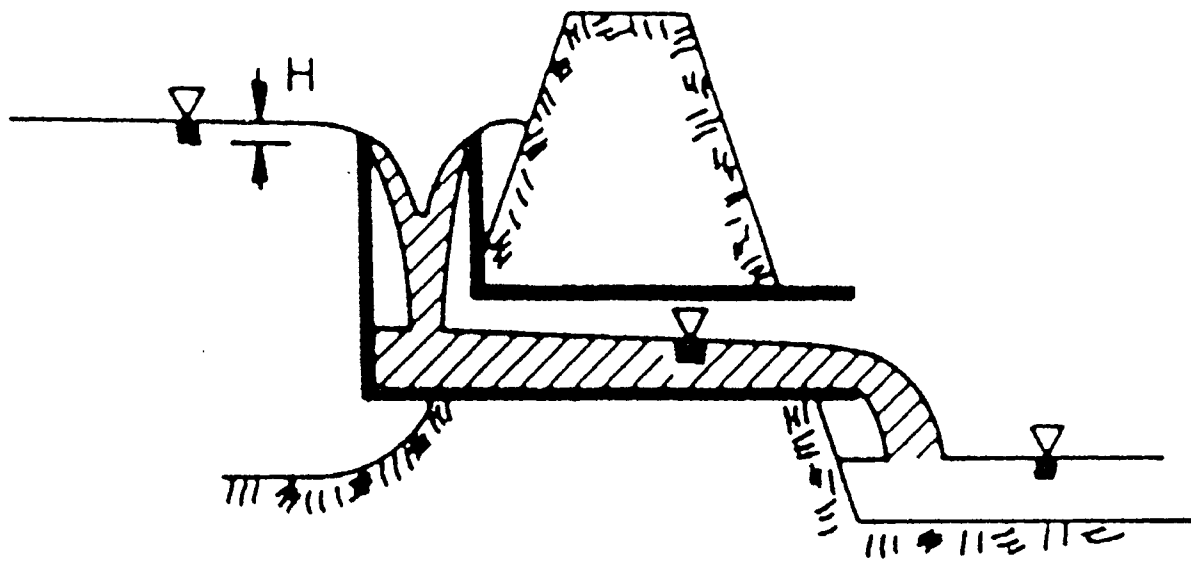


Figure 2.6: Drop inlet with weir control (Barfield et al., 1981).

with orifice flow control. Detailed discussions of the theory behind Equation 2.7 can be found in Streeter (1971) and SCS (1984).

As the stage above the riser inlet continues to increase, eventually the riser and barrel flow full, and pipe flow controls the discharge. The discharge through a pipe flowing full can be determined by the following equation (Haan et al., 1994; SCS, 1984; and Schwab et al., 1981):

$$Q = \frac{a\sqrt{2gH'}}{\sqrt{1 + K_e + K_b + K_cL}} \quad (2.8)$$

where  $H'$  is the driving head in ft as shown in Figures 2.8 through 2.10,  $K_e$  is the entrance head loss coefficient,  $K_b$  is the bend loss coefficient,  $K_c$  is the friction loss coefficient, and  $L$  is the length of the pipe (including the riser) in ft. Figures 2.8 and 2.9 illustrate a drop inlet with pipe flow control. The driving head,  $H'$ , is dissipated by entrance head loss, transition head loss, bend head loss, friction head loss, and velocity head as shown in Figure 2.10. The dissipation of energy due to entrance losses is accounted for by  $K_e$ ; a typical value for  $K_e$  for a drop inlet is 1.0. The energy dissipation caused by the bend where the barrel meets the riser is accounted for by  $K_b$ . For a drop inlet with a single bend,  $K_b$  is 0.5. The energy dissipation due to friction is accounted for by  $K_cL$ ; where  $K_c$  is a parameter dependant upon the size and roughness of the conduit. Values of  $K_c$  are presented in Tables 2.1 and 2.2.

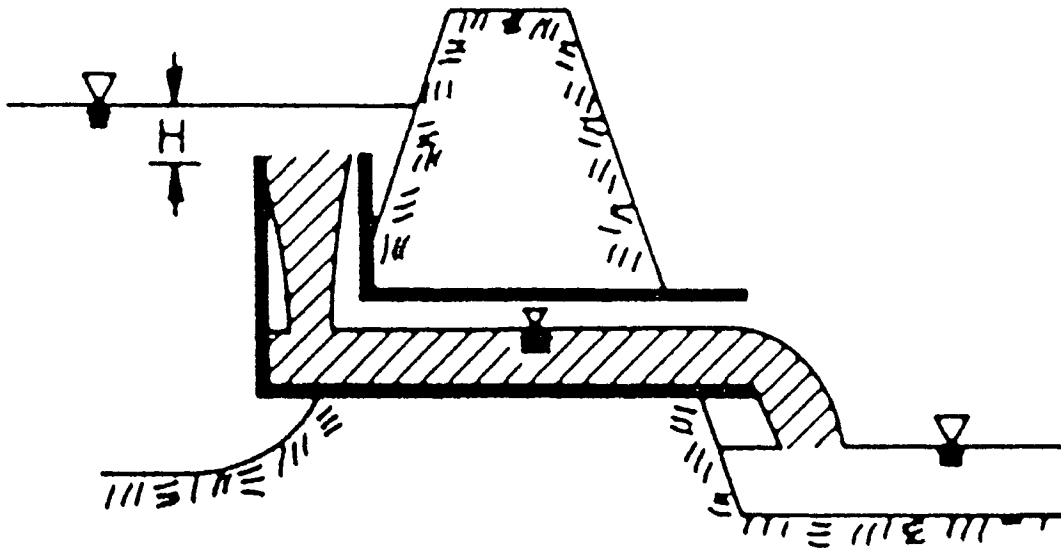


Figure 2.7: Drop inlet with orifice flow control (Barfield et al., 1981).

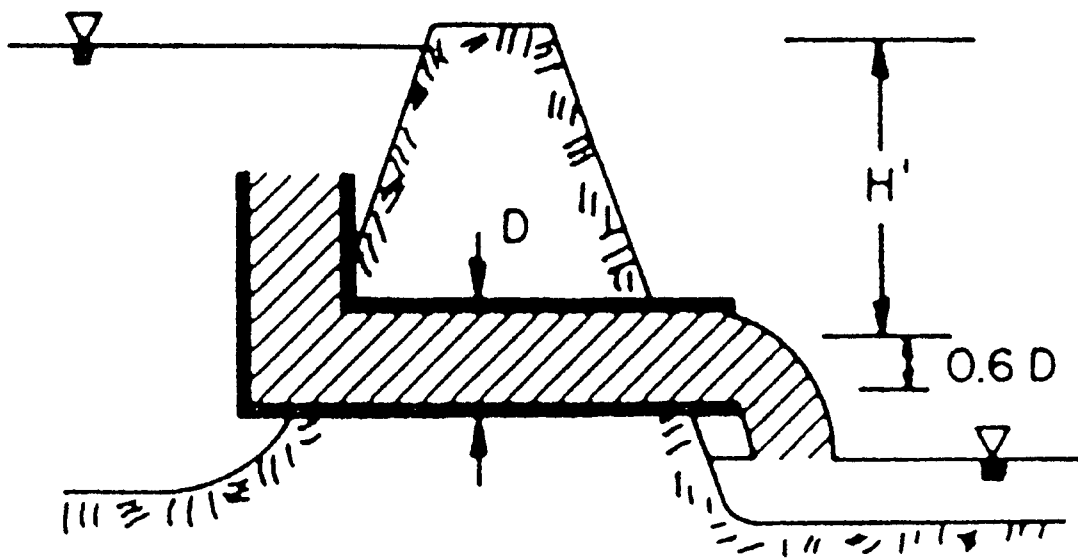


Figure 2.8: Drop inlet with pipe flow and a free outfall (Barfield et al., 1981).



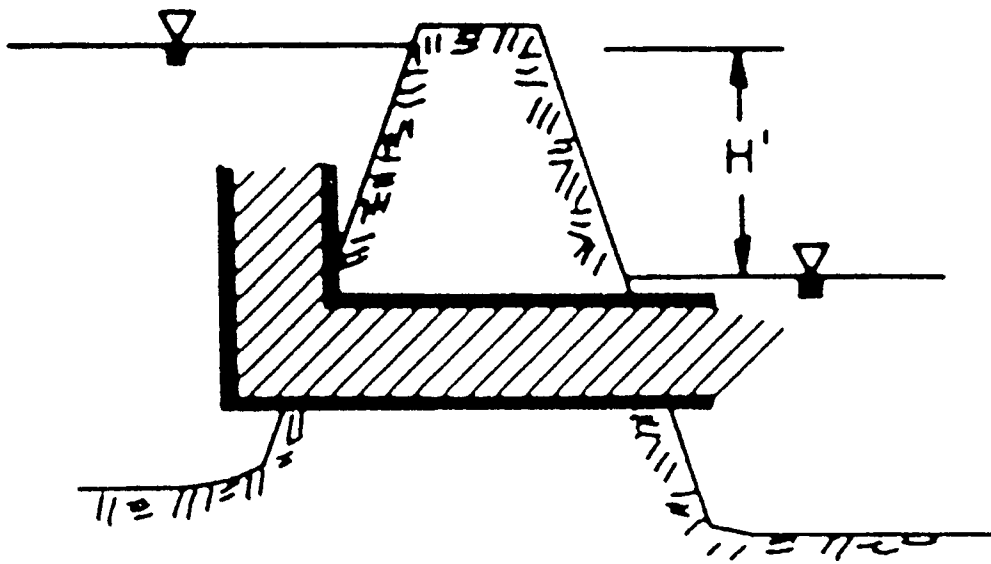


Figure 2.9: Drop inlet with pipe flow and a submerged outfall (Barfield et al., 1981).

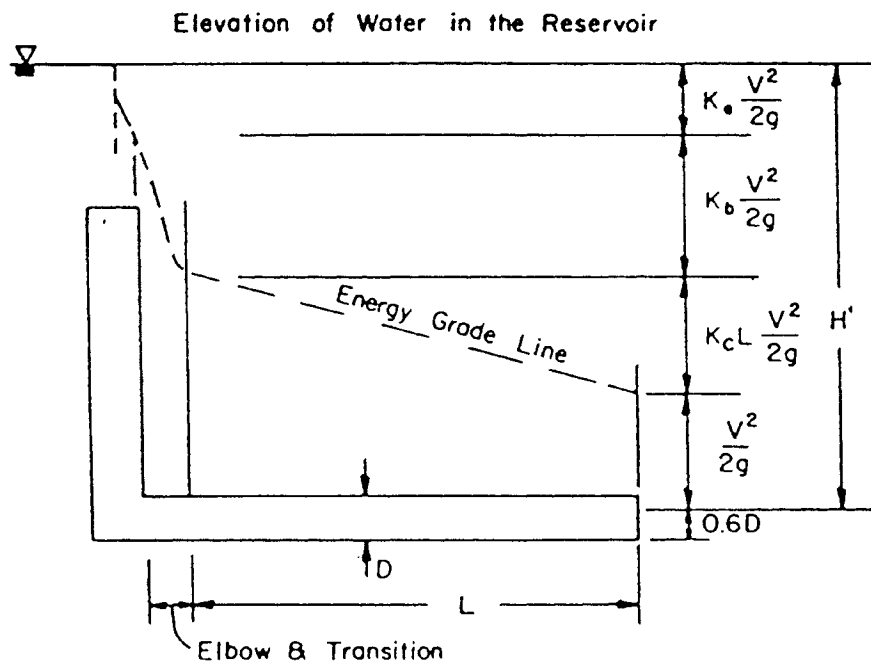


Figure 2.10: Energy losses for a drop inlet flowing full (Barfield et al., 1981).

Table 2.1: Friction loss coefficients for circular conduits flowing full (SCS, 1951).

Head Loss Coefficient,  $K_c$ , for Circular Pipe Flowing Full  $K_c = \frac{5087 n^2}{d_f^{4/3}}$

Pipe diam. inches	Flow area sq. ft.	Manning's Coefficient of Roughness "n"															
		0.010	0.011	0.012	0.013	0.014	0.015	0.016	0.017	0.018	0.019	0.020	0.021	0.022	0.023	0.024	0.025
6	0.196	0.0467	0.0565	0.0672	0.0789	0.0914	0.1050	0.1194	0.1348	0.1510	0.1680	0.1870	0.2060	0.2260	0.2470	0.2690	0.2920
8	0.349	.0318	.0385	.0458	.0537	.0623	.0715	.0814	.0919	.1030	.1148	.1272	.1400	.1540	.1680	.1830	.1990
10	0.545	.0236	.0286	.0340	.0399	.0463	.0531	.0604	.0682	.0765	.0852	.0944	.1041	.1143	.1249	.1360	.1480
12	0.785	.0185	.0224	.0267	.0313	.0363	.0417	.0474	.0535	.0600	.0668	.0741	.0817	.0896	.0980	.1067	.1157
14	1.069	.0151	.0182	.0217	.0255	.0295	.0339	.0386	.0436	.0488	.0544	.0603	.0665	.0730	.0798	.0868	.0942
15	1.230	.0138	.0166	.0198	.0232	.0270	.0309	.0352	.0397	.0446	.0496	.0550	.0606	.0666	.0727	.0792	.0859
16	1.400	.0126	.0153	.0182	.0213	.0247	.0284	.0323	.0365	.0409	.0455	.0505	.0556	.0611	.0667	.0727	.0789
18	1.770	.10178	.0130	.0155	.0182	.0211	.0243	.0276	.0312	.0349	.0389	.0431	.0476	.0522	.0570	.0621	.0674
21	2.410	.00878	.01062	.0126	.0148	.0172	.0198	.0225	.0254	.0284	.0317	.0351	.0387	.0425	.0464	.0506	.0549
24	3.140	.00735	.00889	.01058	.0124	.0144	.0165	.0188	.0212	.0238	.0265	.0294	.0324	.0356	.0389	.0423	.0459
27	3.980	.00628	.00760	.00904	.01061	.0123	.0141	.0161	.0181	.0203	.0227	.0251	.0277	.0304	.0332	.0362	.0393
30	4.910	.00546	.00660	.00786	.00922	.01070	.01228	.0140	.0158	.0177	.0197	.0218	.0241	.0264	.0289	.0314	.0341
36	7.070	.00428	.00518	.00616	.00723	.00839	.00963	.01096	.0124	.0139	.0154	.0171	.0189	.0207	.0226	.0246	.0267
42	9.620	.00348	.00422	.00502	.00589	.00683	.00784	.00892	.01007	.01129	.0126	.0139	.0154	.0169	.0184	.0201	.0218
48	12.570	.00292	.00353	.00420	.00493	.00572	.00656	.00747	.00843	.00945	.01053	.01166	.0129	.0141	.0154	.0168	.0182
54	15.900	.00249	.00302	.00359	.00421	.00488	.00561	.00638	.00720	.00808	.00900	.00997	.01099	.0121	.0132	.0144	.0156
60	19.630	.00217	.00262	.00312	.00366	.00424	.00487	.00554	.00622	.00702	.00782	.00866	.00955	.01048	.0115	.0125	.0135

Table 2.2: Friction loss coefficients for square conduits flowing full (SCS, 1951).

$$K_c = \frac{29.16 n^2}{R^{4/3}}$$

Conduit Size ft	Flow Area ft <sup>2</sup>	Manning Coefficient of Roughness n				
		0.012	0.013	0.014	0.015	0.016
2 x 2	4.00	0.01058	0.01212	0.01440	0.01653	0.01880
2½ x 2½	6.25	.00786	.00922	.01070	.01228	.01397
3 x 3	9.00	.00616	.00723	.00839	.00963	.01096
3½ x 3½	12.25	.00502	.00589	.00683	.00784	.00892
4 x 4	16.00	.00420	.00493	.00572	.00656	.00746
4½ x 4½	20.25	.00359	.00421	.00488	.00561	.00638
5 x 5	25.00	.00312	.00366	.00425	.00487	.00554
5½ x 5½	30.25	.00275	.00322	.00374	.00429	.00488
6 x 6	36.00	.00245	.00287	.00333	.00382	.00435
6½ x 6½	42.25	.00220	.00258	.00299	.00343	.00391
7 x 7	49.00	.00199	.00234	.00271	.00311	.00354
7½ x 7½	56.25	.00182	.00213	.00247	.00284	.00323
8 x 8	64.00	.00167	.00196	.00227	.00260	.00296
8½ x 8½	72.25	.00154	.00180	.00209	.00240	.00273
9 x 9	81.00	.00142	.00167	.00194	.00223	.00253
9½ x 9½	90.25	.00133	.00156	.00180	.00207	.00236
10 x 10	100.00	.00124	.00145	.00168	.00193	.00220

\* From Soil Conservation Service, 1951.

The overall stage-discharge relationship can be determined graphically. First the stage-discharge relationship for weir flow, orifice flow, and pipe flow are plotted on the same graph. Then the controlling flow is the smallest discharge for any given head, as illustrated in Figure 2.11.

### Perforated Riser

Terraces are commonly used to limit sediment loss from agricultural lands. Perforated risers are often used as outlet structures for these terrace systems. A perforated riser is similar to a drop inlet in that both employ a riser that empties into a subsurface conduit. The perforated riser includes a bottom orifice plate to limit flow to the subsurface conduit and slots along the riser to allow complete drainage of the terrace.

A typical perforated riser contains  $N$  horizontal rows of side orifices spaced a uniform distance  $S$ . The side orifices have a total area,  $A_s$ , distributed over a length,  $h_s$ . This typical perforated riser also incorporates a bottom orifice plate with a flow area,  $A_b$ , located a distance,  $h_b$ , below the slots. An illustration of this typical perforated riser appears in Figure 2.12.

In a properly designed perforated riser, the bottom orifice plate limits the flow to the subsurface conduit (Laflen, 1972). A simple equation to determine the flow through the bottom orifice plate is (Laflen, 1972):

$$Q = C_b A_b \sqrt{2g(h + h_b)} \quad (2.9)$$

where  $Q$  is the flow through the bottom orifice plate in  $\text{ft}^3/\text{sec}$ ,  $C_b$  is the orifice

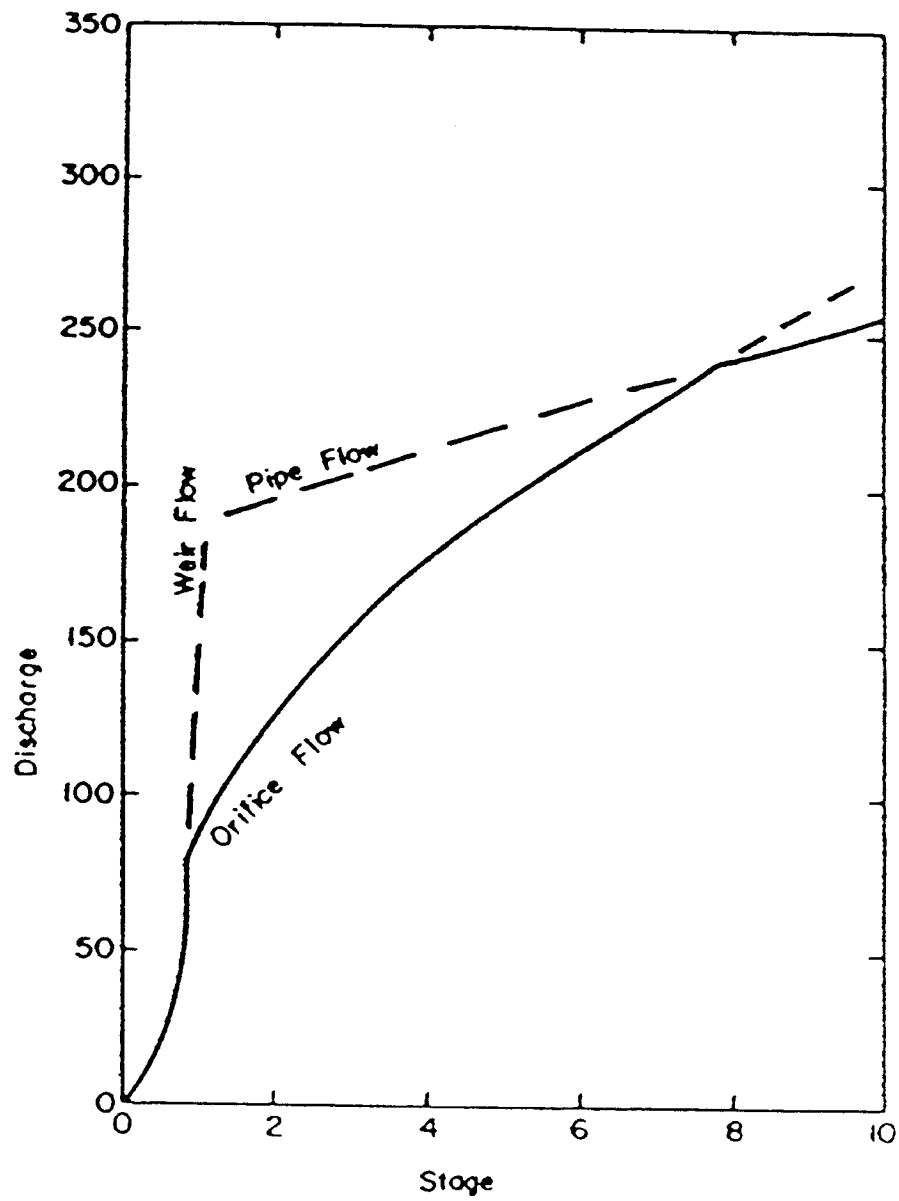


Figure 2.11: Stage-discharge relationship for a drop inlet (Barfield et al. 1994).

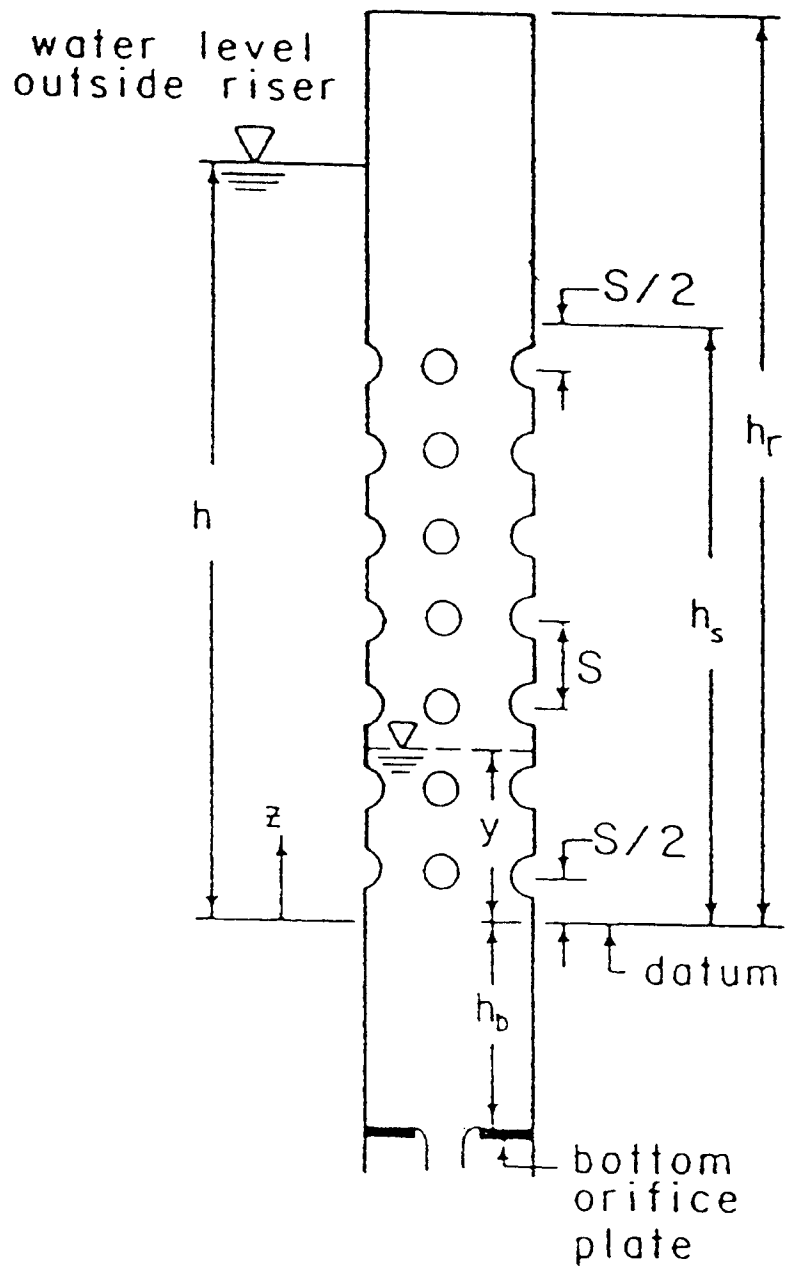


Figure 2.12: Perforated riser definition sketch (McEnroe et al., 1988).

coefficient,  $A_b$  is the flow area of the orifice in  $\text{ft}^2$ ,  $g$  is gravitational constant, and  $(h + h_b)$  is the driving head in ft. It is also possible for flow through the riser slots to be the limiting flow. Laflen (1972) derived the following expression for flow through a series of equal area slots spaced a distance,  $S$ , along a riser pipe:

$$Q = (2/3)(C_s A_s / h_s) (2g)^{1/2} (h + h_b)^{3/2} \quad (2.10)$$

where  $C_s$  is the orifice coefficient for the slots,  $A_s$  is the total area of the slots in  $\text{ft}^2$ ,  $h_s$  is the height of the slots in ft. The accepted value of  $C_s$  is 0.611 (McEnroe et al., 1988). The driving head term,  $(h + h_b)$ , is raised to the three halves power indicating that the slots are behaving as small weirs. The actual flow to the subsurface conduit is the value of  $Q$  computed by either Equation 2.9 or Equation 2.10 that is smallest, i.e. the limiting  $Q$ . Provided that  $A_s$  and  $A_b$  are properly sized;  $y$  is very close to  $h$  (see Figure 2.12), flow through the bottom orifice is the limiting flow, and Equation 2.9 does an adequate job of predicting  $Q$ . However, if  $A_s$  is too small or  $A_b$  is too large,  $y$  will be much smaller than  $h$ , and Equations 2.9 and 2.10 will be inadequate for predicting  $Q$ .

A more accurate approach presented by McEnroe et al. (1988) incorporates the level of zero gage pressure or free water surface inside the riser. The distance between the datum and this free water surface is  $y$  (see Figure 2.12). McEnroe et al. (1988) derived six equations to determine to flow to the subsurface conduit for  $h < h_r$ .



Flow through the bottom plate orifice to the subsurface conduit can be determined from (McEnroe et al., 1988):

$$Q = C_b A_b [2g(h_b + y)]^{1/2} \quad (2.11)$$

When  $h < h_s$  and  $y < 0$ , the slots behave as weirs. The flow to the bottom orifice plate through the slots can be determined with (McEnroe et al., 1988):

$$Q = (2/3)(C_s A_s / h_s)(2g)^{1/2} h^{3/2} \quad (2.12)$$

When  $h < h_s$  and  $y > 0$ , the slots behave as orifices over a length  $y$  and as weirs between  $y$  and  $h$ . The following equation yields the flow to the bottom orifice plate (McEnroe et al., 1988):

$$Q = (C_s A_s / h_s)(2g)^{1/2} [y(h-y)^{1/2} + (2/3)(h-y)^{3/2}] \quad (2.13)$$

When  $h_s < h < h_r$  and  $y < 0$ , the slots behave as weirs, and the flow to the bottom orifice plate through the slots can be determined with (McEnroe et al., 1988):

$$Q = (2/3)(C_s A_s / h_s)(2g)^{1/2} [h^{3/2} - (h - h_s)^{3/2}] \quad (2.14)$$

When  $h_s < h < h_r$  and  $0 < y < h_s$ , the slots behave as orifices over a length  $y$  and as weirs between  $y$  and  $h_s$ . The following equation yields the flow to the

bottom orifice plate (McEnroe et al., 1988):

$$Q = (C_s A_s / h_s) (2g)^{1/2} \left( y(h-y)^{1/2} + (2/3) [(h-y)^{3/2} - (h-h_s)^{3/2}] \right) \quad (2.15)$$

When  $h < h_r$  and  $y > h_s$ , the slots behave entirely as orifices, and the flow to the bottom orifice plate through the slots can be determined with (McEnroe et al., 1988):

$$Q = (C_s A_s) [2g(h-y)^{1/2}] \quad (2.16)$$

Equations 2.11 through 2.16 each have two unknowns,  $Q$  and  $y$ , and therefore can not be solved explicitly. However, the flow through the slots must be equal to the flow through the bottom orifice plate. To determine  $Q$ , Equation 2.11 which yields the flow through bottom orifice plate must be solved simultaneously with one of Equations 2.12 through 2.16 which yield the flow through the slots. Thus, using Equations 2.11 through 2.16, a stage-discharge relationship can be developed for stages up to the stage of the riser.

### Culverts

Culverts (sometimes called trickle tube spillways) can be used as outlet structures for farm ponds and sediment basins as shown in Figure 2.13. Culverts are also be used to control flows under roadways, often resulting in ponding upstream of the culvert forming an impoundment. Discharge through a culvert is dependant upon many factors: upstream depth, downstream depth,

culvert length, size, roughness, slope, entrance characteristics, and exit characteristics.

Based upon the headwater depth, outlet depth, and flow depth within the culvert, flow can be divided into six categories as illustrated in Figure 2.14 (Chow, 1959). If the headwater is below a critical value,  $H^*$ , and the outlet is unsubmerged, then the inlet will be unsubmerged (Chow, 1959). Depending upon entrance geometry, barrel characteristics, and approach conditions, the critical headwater depth,  $H^*$ , is usually in the range of 1.2 to 1.5 times the culvert height (Haan et al., 1994 and Chow, 1959). The six classes of flow are:

*Type 1 - Outlet Submerged.* When the outlet is submerged, the pipe will flow full. The discharge can be computed from the pipe flow equation given in the drop spillway section, Equation 2.8 (Haan et al., 1994 and Chow, 1959).

*Type 2 - Inlet Submerged, Outlet Unsubmerged, Full Pipe Flow.* When the culvert is hydraulically long as determined by Figure 2.15 for concrete pipes or Figure 2.16 for corrugated pipes and  $H > H^*$  with an unsubmerged outlet, the pipe will flow full. The discharge can be computed from the pipe flow equation given in the drop spillway section, Equation 2.8 (Haan et al., 1994 and Chow, 1959).

*Type 3 - Inlet Submerged, Outlet Unsubmerged, Pipe not Flowing Flow.* When the culvert is hydraulically short as determined by Figure 2.15 for

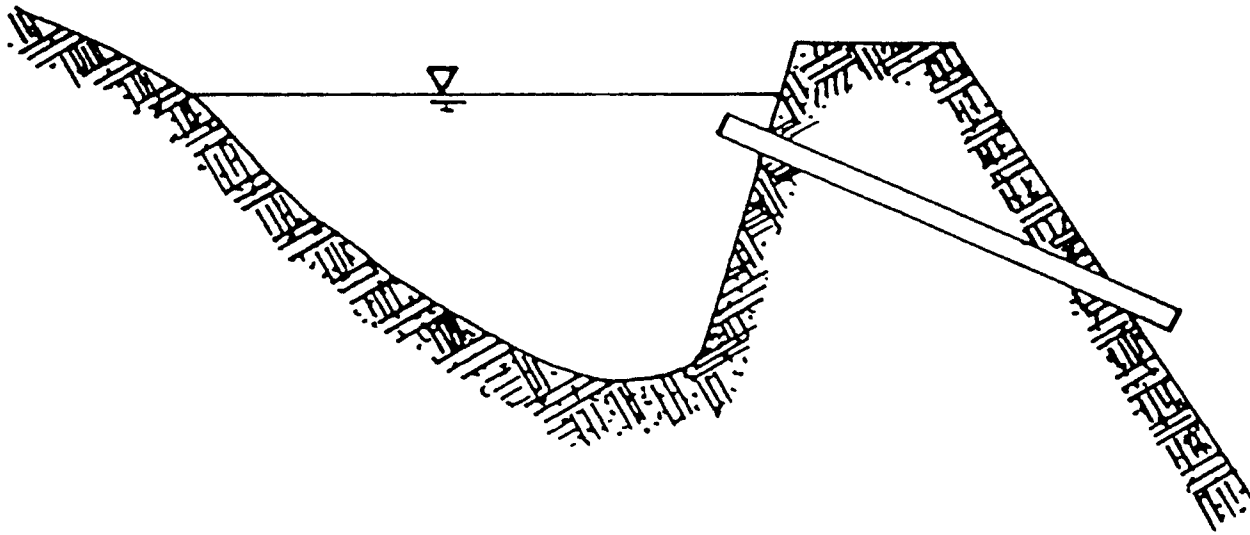


Figure 2.13: Culvert used as an outlet to a farm pond (Barfield et al., 1981).

## FLOW THROUGH NONPRISMATIC CHANNEL SECTIONS

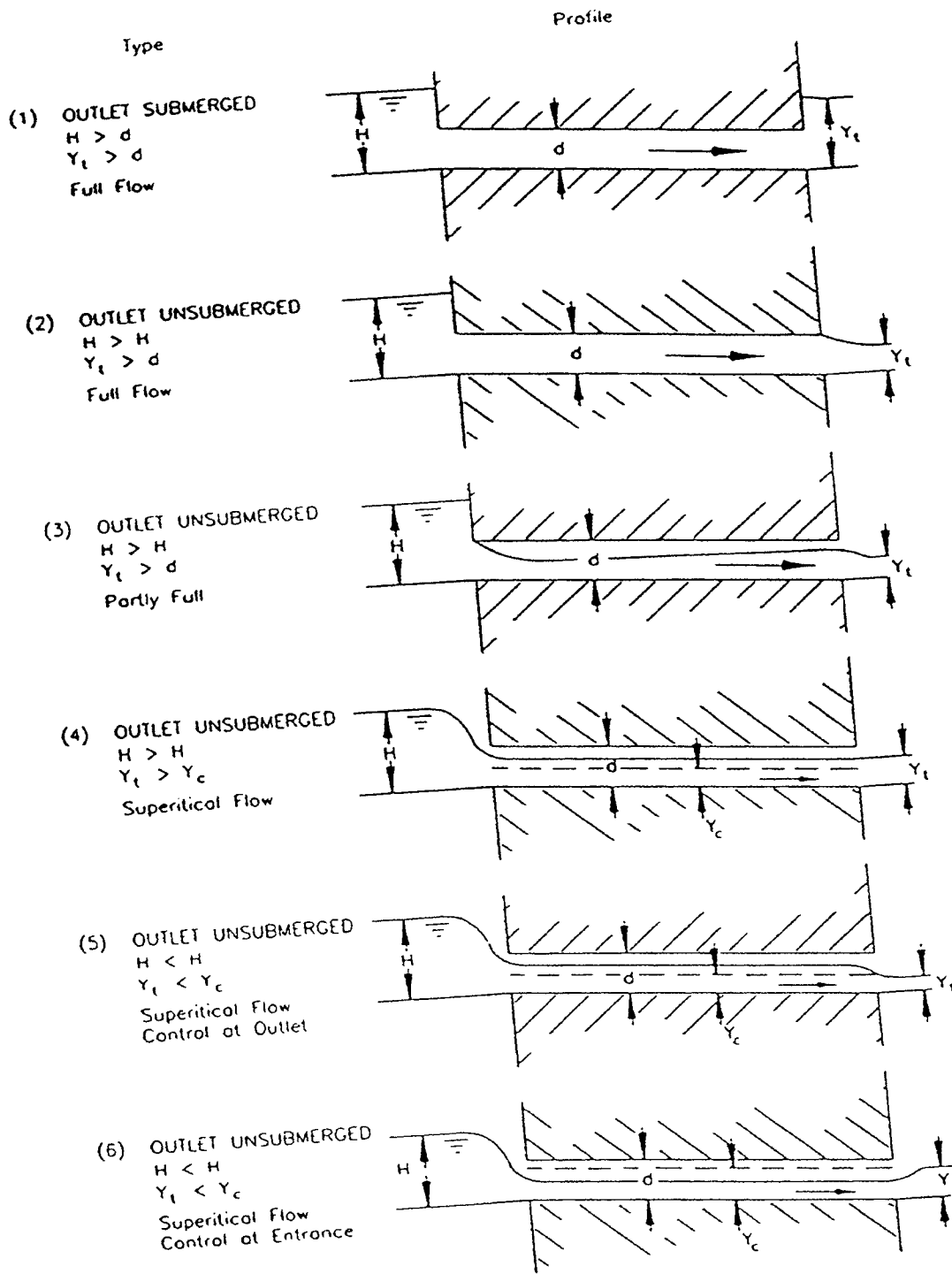


Figure 2.14: Types of culvert flow (Chow, 1959).

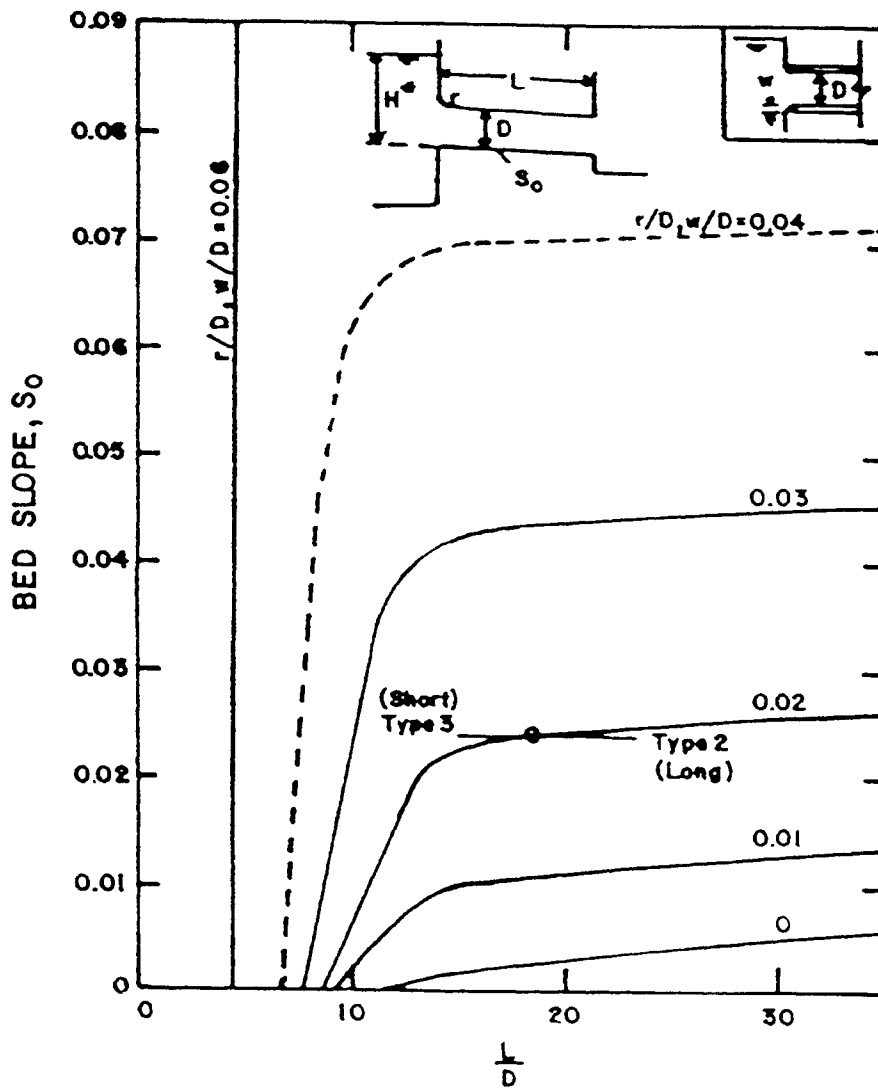


Figure 2.15: Criteria for hydraulically short and long concrete culverts. Type 3 is short and Type 2 is long (Carter, 1957).

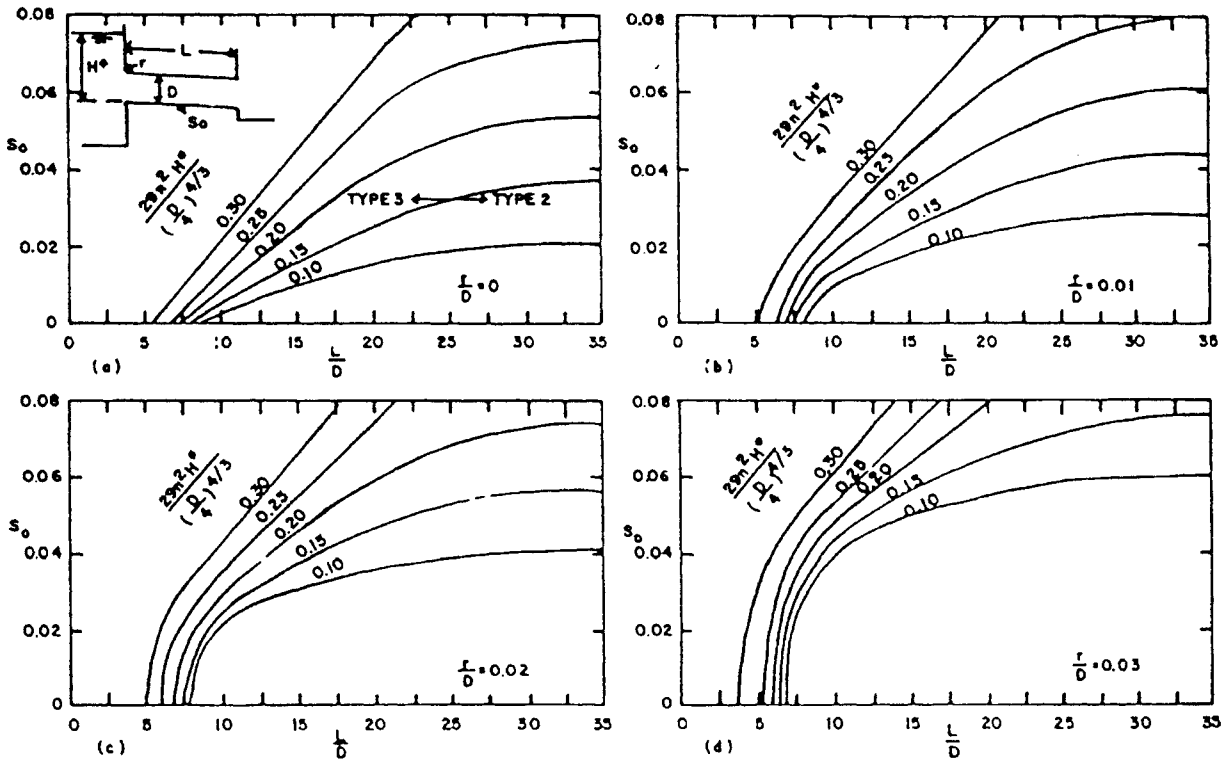


Figure 2.16: Criteria for hydraulically short and long culverts with rough corrugated pipes. Type 3 is short and Type 2 is long (Carter, 1957).

concrete pipes or Figure 2.16 for corrugated pipes and  $H > H^*$  with an unsubmerged outlet, the pipe will not flow full. The discharge can be determined with dimensionless plots developed for inlet control by Mavis (1942) as shown in Figure 2.17.

*Types 4-6 - Inlet Unsubmerged, Outlet Unsubmerged, Pipe not Flowing Full.* When neither the inlet nor the outlet are submerged, the pipe flows as an open channel. The discharge must be computed by means of a water surface flow profile starting with the depth of flow at the culvert outlet. The water surface profile is dependant upon the pipe slope, size, roughness, and entrance geometry to determine discharge (Haan et al., 1994 and Chow, 1959).

**Inlet Control.** Inlet controlled flow occurs when the discharge is only dependant upon the headwater and inlet geometry. As the headwater and discharge increase, the discharge will be controlled at the inlet until downstream factors such as slope, length, surface roughness, and outlet depth cause the pipe to flow full. Inlet control can be split into two categories: unsubmerged and submerged. When the inlet is unsubmerged one of the following two equations can be used to determine discharge (FHA, 1985):

$$\frac{HW_i}{D} = \frac{H_c}{D} + K \left( \frac{Q}{AD^{0.5}} \right)^M - 0.5S \quad (2.17)$$

or



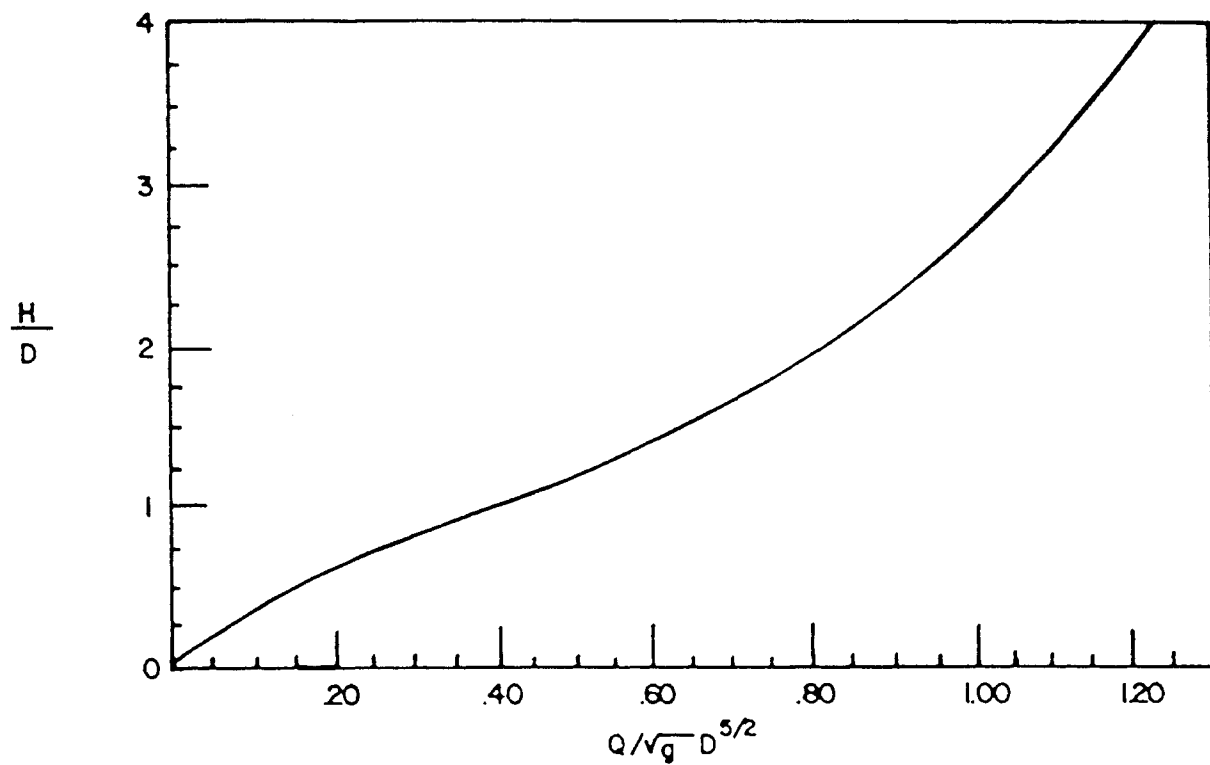


Figure 2.17: Stage-discharge relationship for a circular pipe with control at the inlet (Mavis, 1942).

$$\frac{HW_i}{D} = K \left( \frac{Q}{AD^{0.5}} \right)^M \quad (2.18)$$

where  $HW_i$  is the headwater depth in ft,  $D$  is the interior height of the culvert in ft,  $H_c$  is the specific head at critical depth,  $(d_c + V_c^2 / 2g)$ , in ft,  $Q$  is the discharge in  $\text{ft}^3/\text{sec}$ ,  $A$  is the cross sectional area of the culvert barrel in  $\text{ft}^2$ ,  $S$  is the culvert barrel slope in  $\text{ft}/\text{ft}$ , and  $K$  and  $M$  are constants. Both Equations 2.17 and 2.18 give reasonable predictions of unsubmerged inlet controlled flow (FHA, 1985). Equation 2.18 is utilized in the WEPP surface impoundment element because it has fewer terms and is easier to compute. When inlet is submerged the following expression can be utilized to determine the discharge (FHA, 1985):

$$\frac{HW_i}{D} = c \left( \frac{Q}{AD^{0.5}} \right)^2 + Y - 0.5S \quad (2.19)$$

where  $c$  and  $Y$  are constants. Table 2.3 lists values for  $K$ ,  $M$ ,  $c$ , and  $Y$  for a number of culvert shapes and inlet geometries.

**Outlet Control.** Outlet control occurs when the discharge is controlled by outlet conditions. Under these conditions, flow is dependant upon headwater depth, inlet geometry, tailwater depth, and culvert size, shape,

Table 2.3: Constants for inlet control culvert discharge equations (FHA, 1985).

Shape and Material	Inlet Description	Equation	K	M	c	Y
Circular Concrete	Square edge w/headwall	2.17	0.0098	2	0.0398	0.67
	Groove end w/headwall	2.17	0.0078	2	0.0292	0.74
	Groove end projecting	2.17	0.0045	2	0.0317	0.69
Circular CMP	Headwall	2.17	0.0078	2	0.0379	0.69
	Mitered to slope	2.17	0.021	1.35	0.0463	0.75
	Projecting	2.17	0.034	1.5	0.0553	0.54
Circular	Beveled ring, 45 deg. bevels	2.17	0.0018	2.5	0.03	0.74
	Beveled ring, 33.7 deg. bevels	2.17	0.0018	2.5	0.0243	0.83
Rectangular Box	45 deg. wingwall flare d = 0.043D	2.18	0.51	0.667	0.0309	0.8
	18 to 33.7 deg. wingwall flare d = 0.083D	2.18	0.486	0.667	0.0249	0.83
Rectangular Box	90 deg. headwall w/0.75" chamfers	2.18	0.515	0.667	0.0375	0.79
	90 deg. headwall w/45 deg. bevels	2.18	0.495	0.667	0.0314	0.82
	90 deg. headwall w/33.7 deg. bevels	2.18	0.486	0.667	0.0252	0.865
Rectangular Box	0.75" chamfers; 45 deg. skewed headwall	2.18	0.522	0.667	0.0402	0.73
	0.75" chamfers; 30 deg. skewed headwall	2.18	0.533	0.667	0.0425	0.705
	0.75" chamfers; 15 deg. skewed headwall	2.18	0.545	0.667	0.04505	0.68
	45 deg. bevels; 10 to 45 deg. skewed headwall	2.18	0.498	0.667	0.0327	0.75
Rectangular Box 0.75" chamfers	45 deg. non-offset wingwall flares	2.18	0.497	0.667	0.0339	0.803
	18.4 deg. non-offset wingwall flares	2.18	0.493	0.667	0.0361	0.806
	18.4 deg. non-offset wingwall flares; 30 deg. skewed barrel	2.18	0.495	0.667	0.0386	0.71
Rectangular Box Top Bevels	45 deg. wingwall flares - offset	2.18	0.497	0.667	0.0302	0.835
	33.7 deg. wingwall flares - offset	2.18	0.495	0.667	0.0252	0.881
	18.4 deg. wingwall flares - offset	2.18	0.493	0.667	0.0227	0.887
Circular	Smooth tapered inlet throat	2.18	0.534	0.555	0.0196	0.89
	Rough tapered inlet throat	2.18	0.519	0.64	0.0286	0.9
Elliptical Inlet Face	Tapered inlet - beveled edges	2.18	0.536	0.622	0.0368	0.83
	Tapered inlet - square edges	2.18	0.5035	0.719	0.0478	0.8
	Tapered inlet - thin edge projecting	2.18	0.547	0.8	0.0598	0.75
Rectangular	Tapered inlet throat	2.18	0.475	0.667	0.0179	0.97
Rectangular Concrete	Side tapered - less favorable edges	2.18	0.56	0.667	0.0466	0.85
	Side tapered - more favorable edges	2.18	0.56	0.667	0.0378	0.87
Rectangular Concrete	Slope tapered - less favorable edges	2.18	0.5	0.667	0.0466	0.65
	Slope tapered - more favorable edges	2.18	0.5	0.667	0.0378	0.71

slope, length, and roughness. Outlet controlled flow is considered to be full pipe flow and is computed with the pipe flow equation, Equation 2.8.

### **Emergency Spillways and Open Channels**

In many larger farm ponds and sedimentation basins, emergency spillways are used to route the excess runoff from very large storm events that cannot be routed through the principle spillway (drop inlet or culvert). This keeps the excess flow from over topping and breaching an earthen dam. Sometimes an open channel forms the only outlet structure. The discharge through an emergency spillway or an open channel is considered gradually varied flow. Gradually varied flow occurs when the gravitational forces driving the flow are not in equilibrium with the frictional forces resisting the flow due to changes in channel slope, roughness, or cross section. When the stage in the impoundment rises above the inlet stage of an emergency spillway or an open channel, runoff begins to flow through the channel. The flow initially experiences an entrance head loss as the water moves from a zero velocity to a velocity above zero. After this initial head loss, the flow depth gradually changes moving towards an equilibrium between the gravitational and frictional forces. In order to determine the discharge for a given head, a water surface flow profile is employed to determine the head required to drive a certain discharge.

Emergency spillways typically have three sections: (1) a sloped approach, (2) a flat crest and (3) a sloped exit as shown in Figure 2.18

(Barfield et al., 1981). If the exit slope is greater than the critical slope (slope at which flow is at critical depth), then flow passes through critical depth as it enters the sloped exit. The point at which the flow passes through critical depth is called the control section since the depth of flow defines the velocity at critical depth. If the exit slope is less than critical slope, no control section exists and the flow moves towards a subcritical normal depth. Emergency spillways can be constructed with or without a control section.

If a control section exists, the stage required to drive a particular flow is determined via a water surface flow profile routing starting at the control section. At the control section, the depth is known for a given discharge in a channel of known shape, slope, and roughness. If no control section exists, the water surface flow profile must start far enough down stream so that the flow has attained subcritical normal depth. The normal depth is known for a given discharge in a channel of known shape, slope, and roughness. In either case the water surface flow profile method is the same.

The steady state standard step method (Chow, 1959; Fogle and Barfield, 1992; and Haan et al., 1994) is a simple procedure for determining a water surface flow routing. The standard step method equates the total energy at two points on a channel starting with either the control section or a point far downstream where the flow has attained subcritical normal depth. The total energy at a known point can be determined with the following expression (Fogle and Barfield, 1992):

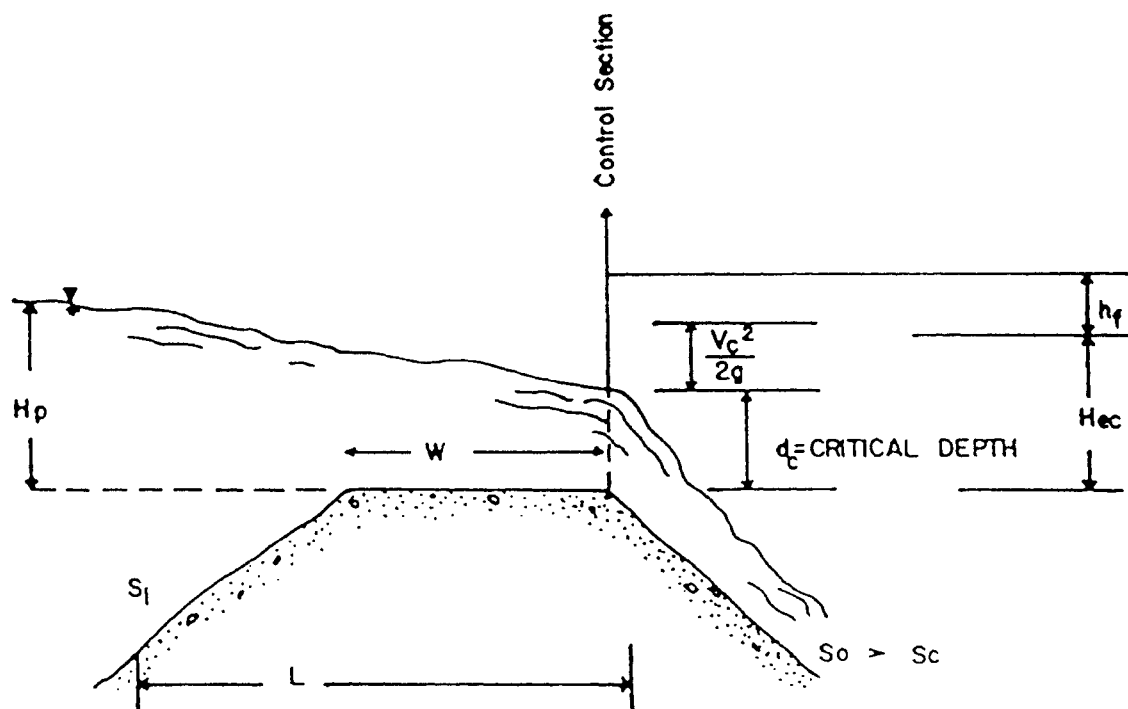


Figure 2.18: Broad Crested Spillway with a control section (Barfield et al., 1981).

$$h_i = d_i + Y_i + \frac{V_i^2}{2g} \quad (2.20)$$

where  $h_i$  is the total energy,  $d_i$  is the depth of flow,  $Y_i$  is the elevation of the bottom of the channel at point  $i$ , and  $V_i$  is the average cross sectional velocity. The total energy at the next point a distance  $\Delta X$  upstream ( $i + 1$ ) is related to point  $i$  by (Fogle and Barfield, 1992):

$$h_i = h_{i+1} + h_{f_{i+1}} \quad (2.21)$$

where  $h_{f_{i+1}}$  is the head loss due to friction over a distance  $\Delta X$ . Then the total energy at each point can be equated as follows (Fogle and Barfield, 1992):

$$h_i = d_i + Y_i + \frac{V_i^2}{2g} = d_{i+1} + Y_{i+1} + \frac{V_{i+1}^2}{2g} + h_{f_{i+1}} \quad (2.22)$$

The head loss due to friction  $h_{f_{i+1}}$  is related to the friction slope by (Fogle and Barfield, 1992):

$$h_{f_{i+1}} = S_{f_a} \Delta X + \frac{1}{2} (S_{f_i} + S_{f_{i+1}}) \Delta X \quad (2.23)$$

where  $S_{f_a}$  is the average friction slope on  $\Delta X$ ,  $\Delta X$  is the distance between point

$i$  and point  $i + 1$ ,  $S_{fi}$  is the friction slope at point  $i$ , and  $S_{fi+1}$  is the friction slope at point  $i + 1$ . The friction slope is computed from the following expression based on Manning's equation (Fogle and Barfield, 1992):

$$S_f = \left( \frac{nQ/A}{C_n R^{2/3}} \right)^2 \quad (2.24)$$

where  $n$  is Manning's roughness,  $A$  is the cross sectional area,  $Q$  is the flow rate,  $C_n$  is a constant (1.5 for english units or 1.0 for SI units), and  $R$  is the hydraulic radius. The hydraulic radius,  $R$ , is the ratio of the flow area to the wetted perimeter, or

$$R = \frac{A}{P} \quad (2.25)$$

Using an iterative process Equations 2.22 through 2.25 are solved simultaneously until convergence on the true value of  $h_{i+1}$  is attained. After  $h_{i+1}$  is determined, the iteration is repeated upstream to determine  $h_{i+2}$ ,  $h_{i+3}$ , . . . ,  $h_n$  until the flow profile is known all the way to the channel inlet (point- $n$ ).

Given the depth and velocity at the channel inlet, the water surface depth in the impoundment can be determined by adding the entrance head loss to the depth (SCS, 1986):



$$h_p = h_n + K_e \frac{V_n^2}{2g} \quad (2.26)$$

where  $h_p$  is the stage in the impoundment,  $h_n$  is the stage at the inlet of the outflow channel,  $K_e$  is the entrance loss coefficient (use 1.0 for free flowing entrances SCS, 1986), and  $V_n$  is the cross sectional velocity at the inlet of the outflow channel.

To determine the stage-discharge relationship for a given emergency spillway or open channel outlet structure the following procedure can be followed:

1. Assume an outflow rate.
2. Determine critical depth,  $y_c$ , for an emergency spillway with a control section or the subcritical normal depth far downstream for a outlet channel without a control section.
3. Utilize an iterative process with Equations 2.22 through 2.25 to solve for  $h_{i+1}$ ,  $h_{i+2}$ , . . . ,  $h_n$ .
4. Use Equation 2.26 to determine the stage in the impoundment required to drive the assumed flow.
5. Assume a new outflow rate and repeat steps 2-5.

This process should be repeated until the entire stage-discharge relationship is determined.

## Rock Fill Check Dams

Construction, mining, and silviculture operations need inexpensive temporary sediment traps. Porous rock fill check dams provide an inexpensive, easily constructed solution. A porous rock fill check dam is simply a pile of rocks obstructing the free flow of sediment laden water. Frequently a rock fill check dam is constructed with a coarse sand or fine gravel core in order to trap the most sediment and covered by a larger rip rap used to prevent washout. A schematic of a rock fill check dam appears in Figure 2.19.

Most of the work regarding flow through rock fill has occurred on a laboratory scale for low flows. Due to the difficulties in describing stone shapes and controlling flow, there have been relatively few *in situ* experiments. Much of the work in this area has been relating flow to head loss relationships for ground water flow and well problems. Stephenson (1979) related flow to head loss in porous granular media of uniform size for Reynolds numbers ranging from  $10^{-4}$  to  $10^4$ . He showed that head loss is proportional to the square of the flow velocity.

Stephenson (1979) reported a variation of the Darcy-Weisbach equation to determine flow in rock media of uniform diameter:

$$\frac{dH}{dl} = f \frac{1}{d} \frac{V_p^2}{2g} \quad (2.27)$$

where  $dH/dl$  is the gradient of head through the rock fill,  $f$  is the Darcy-Weisbach friction factor,  $d$  is the average diameter of the rock,  $V_p$  is the

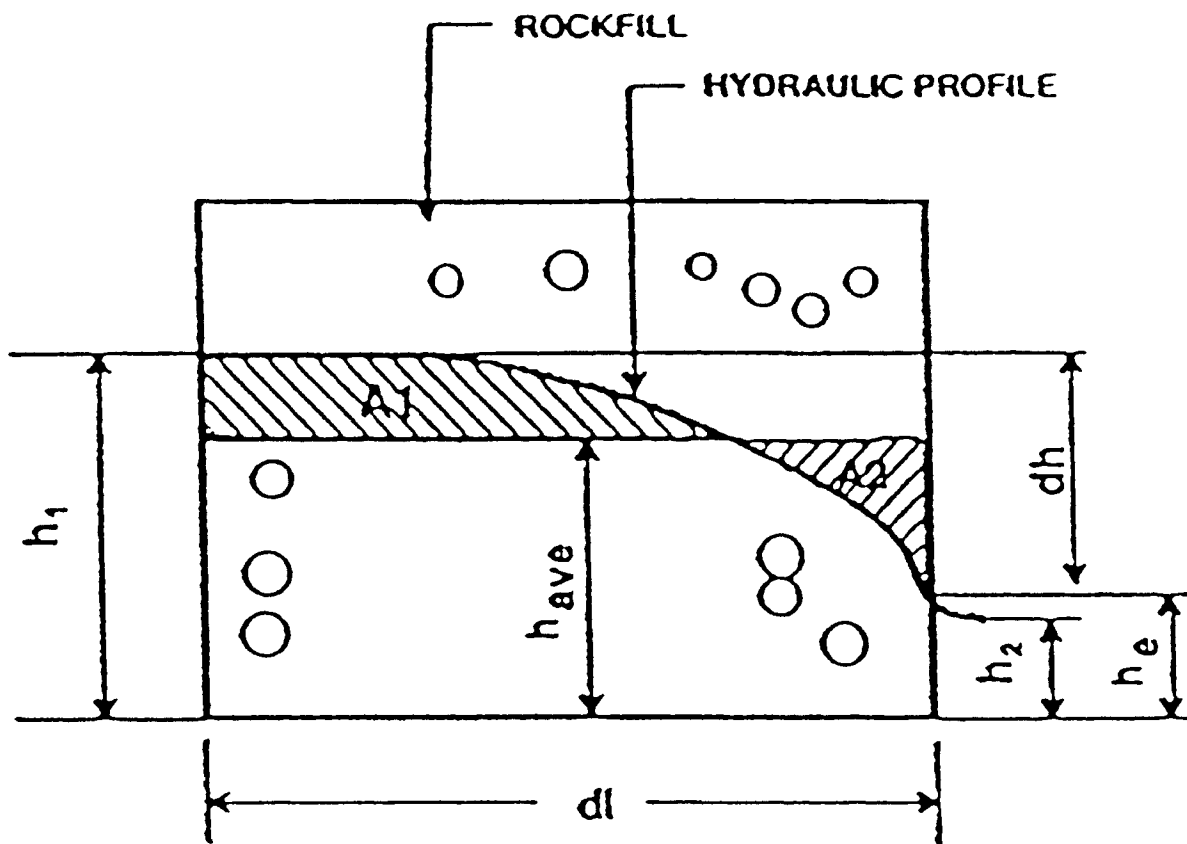


Figure 2.19: Schematic for flow in porous rock fill (after Haan et al., 1994).

velocity in the pores, and  $g$  is the acceleration of gravity. Stephenson (1979) assumed that the average diameter of the rock approximated the average pore size and further included the factor of 2 in the denominator of Equation 2.27. He also used a macro velocity instead of the pore velocity. The macro velocity (total flow rate divided by the area of flow) is related to the pore velocity by the porosity; or

$$V_p = \frac{V}{n} = \frac{Q/A}{n} \quad (2.28)$$

where  $V_p$  is the pore velocity,  $V$  is the macro velocity,  $n$  is the porosity,  $Q$  is the total flow rate, and  $A$  is the cross sectional area of flow. The Stephenson (1979) modified Darcy-Weisbach equation is:

$$\frac{dH}{dl} = f_k \frac{V^2}{d n^2 g} \quad (2.29)$$

where  $f_k$  is the modified friction factor. The modified friction factor can be determined by (Stephenson, 1979):

$$f_k = \frac{const}{Re} + f_t \quad (2.30)$$

where  $f_t$  is the friction factor for fully turbulent flow and  $Re$  is the Reynolds

number determined with:

$$Re = \frac{V d}{n v} \quad (2.31)$$

where  $v$  is the kinematic viscosity. Stephenson (1979) proposed the following values for  $f_s$ : 1 for smooth polished stones, 2 for semi-rounded stones, and 4 for angular stone.

In field applications rock fill is constructed with stones of varying sizes. Herrera (1989) and Herrera and Felton (1991) developed equations for the hydraulics of flow through rock fill of varying gradation using clear water. The standard deviation,  $\sigma$ , of the rock fill was used as a measure of gradation. The predicted head loss computed with the equations developed by Herrera (1989) and Herrera and Felton (1991) were compared to the results of 96 tests on 16 rock fill structures. The average error on the 96 tests was 8 percent.

The following equations were presented by Herrera (1989) to compute the flow through a rock fill structure:

1. Reynolds number determined by:

$$Re = \frac{(d - \sigma) V}{v n} \quad (2.32)$$

2. Friction factor determined by:

$$f_k = \frac{g d n^2 dh}{V^2 dl} \quad (2.33)$$

3. Friction factor - Reynolds number relationship determined by:

$$f_k = \frac{1600}{Re} + 3.83 \quad (2.34)$$

4. The  $h_2 - h_{ave}$  relationships determined by:

$$h_1 = h_2 + dh \quad (2.35)$$

and

$$h_{ave} = \frac{h_1 + h_2}{2} \quad (2.36)$$

where  $Re$  is the Reynolds number,  $d$  is the average rock diameter (m),  $n$  is the porosity of the rock fill,  $\sigma$  is the standard deviation of the rock size (m),  $\nu$  is the kinematic viscosity (m<sup>2</sup>/s),  $V$  is the average bulk velocity (m<sup>3</sup>/s/m<sup>2</sup>),  $f_k$  is the friction factor,  $dh$  is the static head drop as flow moves through the rock fill,  $dl$  is the flow length of the rock fill,  $g$  is the acceleration of gravity (m/s<sup>2</sup>),  $h_1$  is the upstream depth,  $h_2$  is the exit depth, and  $h_{ave}$  is the average depth of the water profile in the rock fill. Herrera (1989) suggested a value of 0.46 be used for porosity for typical rock fill. Figure 2.19 shows a schematic of the rock fill

problem.

To use the equations given above to yield flow velocity from head loss

Equations 2.33 and 2.34 are equated:

$$\frac{g d n^2}{V^2} \frac{dh}{dl} = \frac{1600}{(d - \sigma) V} + 3.83 \quad (2.37)$$

Collecting velocity terms Equation 2.37 becomes a traditional quadratic expression for V:

$$3.83 V^2 + \frac{1600 v n}{(d - \sigma)} V - g d n^2 \frac{dh}{dl} = 0 \quad (2.38)$$

Equation 2.38 can be solved for the velocity in terms of the known properties of the rock fill and the hydraulic gradient.

For a good, quick estimate of flow through a rock fill check dam, Haan et al. (1994) published a graphical adaptation of Equations 2.32 through 2.36. This graphical procedure uses the average diameter of the rock fill and the flow length to predict the coefficients used in the following power function relating head loss to flow (Haan et al., 1994):

$$\frac{dh}{dl} = a Q^b \quad (2.39)$$

where  $dh/dl$  is the head loss across the rock fill in m/m,  $Q$  is the flow rate per unit width through the rock fill in  $m^3/s/m$ , and  $a$  and  $b$  are coefficients. The

coefficients a and b are determined with the graphs presented in Figure 2.20 (Haan et al., 1994). The graphs presented in Figure 2.20 were prepared for the following conditions: a porosity of 0.46, a standard deviation of the rock fill diameter equal to 1/2 the average diameter, and a downstream depth of zero. If conditions are very different from those assumed, the results may not be accurate (Haan et al., 1994).

### **Filter Fence and Straw Bale Check Dams**

Check dams can also be constructed with straw bales or filter fence. Both straw bale and filter fence check dams provide inexpensive, easily constructed sediment trapping structures. A schematic of a straw bale check dam appears in Figure 2.21, and a schematic of a filter fence check dam appears in Figure 2.22 (Barfield et al., 1981). The discharge through a filter fence or straw bale check dam is dependant upon the porosity of the check dam, the flow stage, the cross sectional flow area, and the size distribution and concentration of incoming sediment.

Work in determining the stage discharge relationship for either filter fence or straw bales is very limited. Haan et al. (1994) recommends the use of a flow through velocity called the slurry flow rate to compute discharge. The slurry flow rate can be utilized to compute the flow through a straw bale or a filter fence check dam by assuming a rectangular cross sectional flow area (Haan et al., 1994; Fischer and Jarrett, 1984):



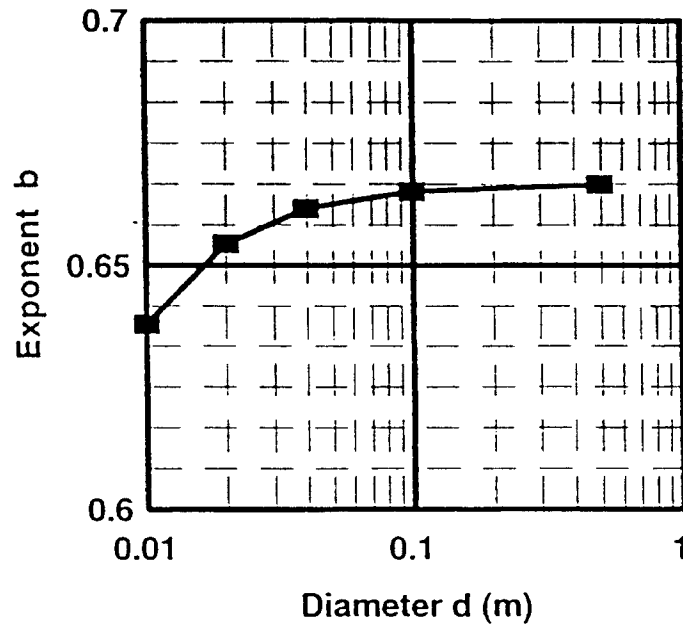
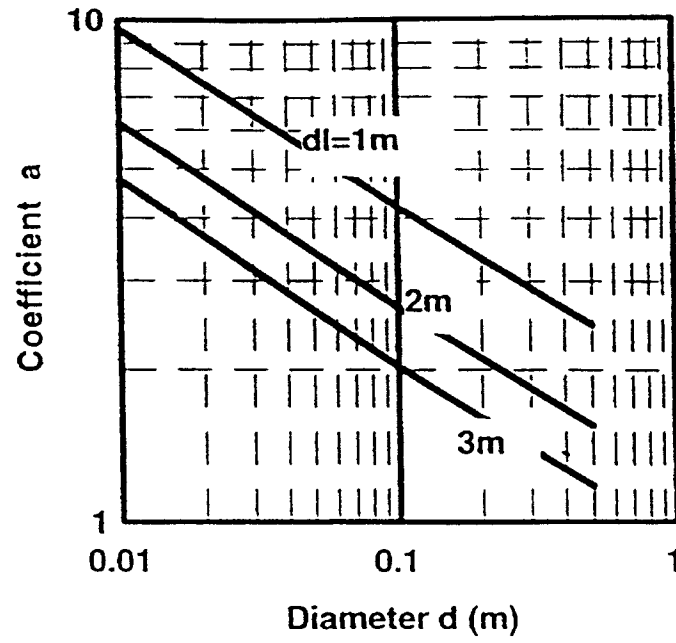


Figure 2.20: Coefficients for the rock fill stage-discharge power function (after Haan et al., 1994).

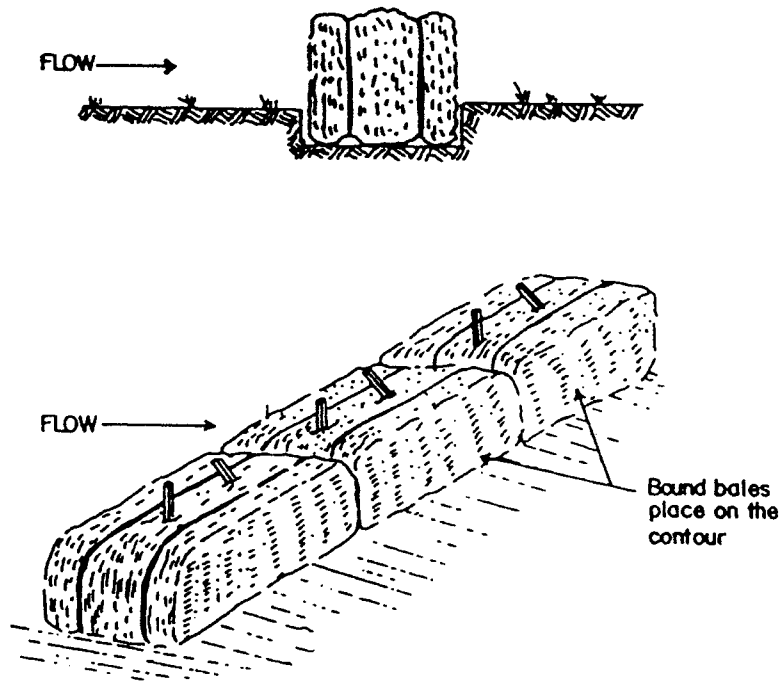


Figure 2.21: Straw bale check dam schematic (Barfield et al., 1981).

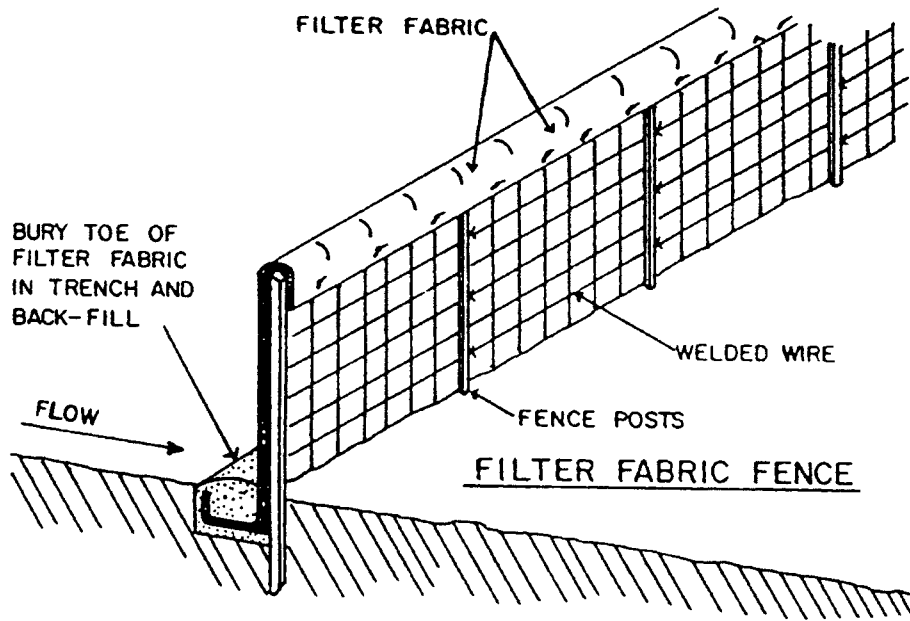


Figure 2.22: Filter fence check dam schematic (Barfield et al., 1981).

$$Q = V_{sl} b h \quad (2.40)$$

where  $Q$  is flow rate,  $V_{sl}$  is the slurry flow rate,  $b$  is the bottom width, and  $h$  is the stage. Several slurry flow rate values recommended by state regulatory agencies are listed in Table 2.4. Although recommended by several states, the value of 0.5 gpm/ft<sup>2</sup> for synthetic fabric is far below the values reported by Fisher and Jarrett (1984). Fisher and Jarrett (1984) report that slurry flow rates are dependant on the type of fabric used to construct the filter fence check dam, the Equivalent Opening Size (EOS), and sediment size distribution. If the sediment moving through the fabric is of the same size as the EOS, some of the sediment will get lodged into the holes in the fabric thereby altering the slurry flow rate. Thus, the slurry flow rate is dependant not only on the fabric, but the incoming size distribution. Fisher and Jarrett (1984) report that slurry flow rates are also dependant upon the flow orientation, thickness of the fabric, and upstream accumulation of sediment on the fabric.

Table 2.5 presents the results reported by Fisher and Jarrett (1984) for various fabrics tested with various sediments. Waynt (1980) reported slurry flow rates for 15 materials in the 0.3 gpm/ft<sup>2</sup> range which is far smaller than the values reported by Fisher and Jarrett (1984). However, the Waynt (1980) study and the Fisher and Jarrett (1984) study included different materials.

**Table 2.4: Slurry flow rates recommended by state regulatory agencies (Haan et al., 1994).**

Material	Slurry Flow Rate		Reference
	gpm/ft <sup>2</sup>	ft/sec	
Straw Bale	5.6	0.0125	VSWC, 1980*
Burlap (10 oz.)	2.4	0.0053	VSWC, 1980*
Synthetic Fabric	0.3	0.000674	VSWC, 1980* Maryland, 1983**
* Virginia Soil and Water Commission (1980).			
** Maryland Water Resources Administration (1983).			

Table 2.5: Slurry flow rates for various fabrics with different size distributions (Fisher and Jarrett, 1984).

Fabric	Slurry Flow Rates (gpm/ft <sup>2</sup> )			
	Clear Water	Sand	Coarse Silt	Silt-Clay
Cerex® 34	131	27	4.5	99
Cerex® 68	94	22	4.5	3
Supac® 139	111	21	10.5	75
Supac® 407	111	29	40.5	110
Typar® 64	37	12	33	44
Mirafi® 100	15	5	16.5	5

## Stage-Area Relationship

The hydraulic routing procedure employed in the WEPP impoundment element not only requires a stage-discharge relationship, but a stage-area relationship as well. Pondered area increases as stage increases. Haan and Johnson (1967) used the following power function relationship to relate pondered area to stage for several terrace impoundments in central Iowa:

$$A = aH^b \quad (2.41)$$

where  $A$  is pondered area,  $H$  is stage, and  $a$  and  $b$  are constants. Laflen (1972) used values of 1930, 2830, and 6870 for  $a$  with values of 1.29, 1.11, and 1.73 for the corresponding  $b$  value. Rochester and Busch (1974) used a value of 1.77 for  $b$ .

## Sedimentation

After runoff is routed through an impoundment, the WEPP impoundment element must determine how much of the incoming sediment settles out of suspension and how much leaves the impoundment. The effectiveness of a given impoundment at removing sediment from runoff is dependant upon many factors, including (Haan et al., 1994):

1. Physical characteristics of the sediment.
2. Hydraulic characteristics of the impoundment.
3. Inflow sediment graph.

4. Basin geometry.
5. Chemistry of the water and the sediment.

Thus, the impoundment element must take into account these factors and estimate how much sediment leaves the impoundment.

Daily sedimentologic inputs dictated by the WEPP convention include incoming sediment concentration, percent in each of five particle size classes defined by the CREAMS (Chemicals, Runoff, and Erosion from Agricultural Management Systems) model (USDA, 1980), and the mean particle size diameter for each of the five size classes. Given the hydraulic response of the impoundment and the incoming sedimentologic properties, the impoundment element determines the outgoing sediment concentration, the percent of effluent in each of the five particle size classes, and the mean particle diameter for each of the five size classes leaving the impoundment.

The performance of an impoundment can be measured by the trapping efficiency. Trapping efficiency provides a measure of the fraction of the incoming sediment that remains in an impoundment. Trapping efficiency is defined by the following expression:

$$TE = \frac{Mass_{in} - Mass_{out}}{Mass_{in}} \quad (2.42)$$

where TE is trapping efficiency,  $Mass_{in}$  is the total mass of sediment entering the impoundment, and  $Mass_{out}$  is the total mass leaving the impoundment.



The sedimentation section of the literature review begins by examining the relationship between particle size and settling velocity. Then it covers steady-state flow rate sedimentation models. Finally, models that deal with variable flow rates are examined.

### **Effect of Particle Size Distribution**

Particle settling velocity is the most important factor effecting pond performance, and is directly related to the particle size. Larger particles have less surface area per unit weight and settle faster than smaller particles. A particle falling at a steady-state or terminal velocity experiences drag forces that are in equilibrium with the force of gravity (Haan et al., 1994; Peavy et al., 1985; Barfield et al., 1981); or

$$C_D \left( \frac{\pi d^2}{4} \right) \left( \frac{\rho V_s^2}{2} \right) = \frac{\pi d^3}{6} (\rho_s - \rho) g \quad (2.43)$$

where  $C_D$  is the drag coefficient (functionally related to Reynold's number),  $d$  is the particle diameter,  $\rho_s$  is the particle density,  $\rho$  is the fluid density,  $V_s$  is the settling velocity, and  $g$  is the acceleration of gravity. Up to a Reynold's number of 0.5, Stokes showed that for a spherical particle the drag coefficient,  $C_D$ , is equal to:

$$C_D = \frac{24}{Re} \quad (2.44)$$

where  $Re$  is the Reynold's number given by:

$$Re = \frac{V_s d}{\nu} \quad (2.45)$$

where  $V_s$  is settling velocity,  $d$  is the diameter of the particle, and  $\nu$  is the kinematic viscosity. For the range of particles with settling Reynold's numbers up to 0.5, the settling velocity can be computed by combining Equations 2.43, 2.44, 2.45 into the following expression (Haan et al., 1994; Peavy et al., 1985; and Barfield et al., 1981):

$$V_s = \frac{1}{18} \frac{d^2 g}{\nu} (SG-1) \quad (2.46)$$

where  $SG$  is the specific gravity of the particles. For larger particles outside the Stokes range a settling velocity must be determined empirically. Figure 2.23 illustrates the relationship between settling velocity and particle size (Barfield et al., 1981).

Several factors influence the settling velocity of a particle. A non-spherical particle shape is accounted for by using an equivalent fall diameter (Graf, 1971; Simmons and Senturk, 1977). Aggregates are formed when several primary particles bond together. Aggregates have smaller specific gravities due to the pore space between the primary particles, but because they have many primary particles bound together, they typically have higher settling

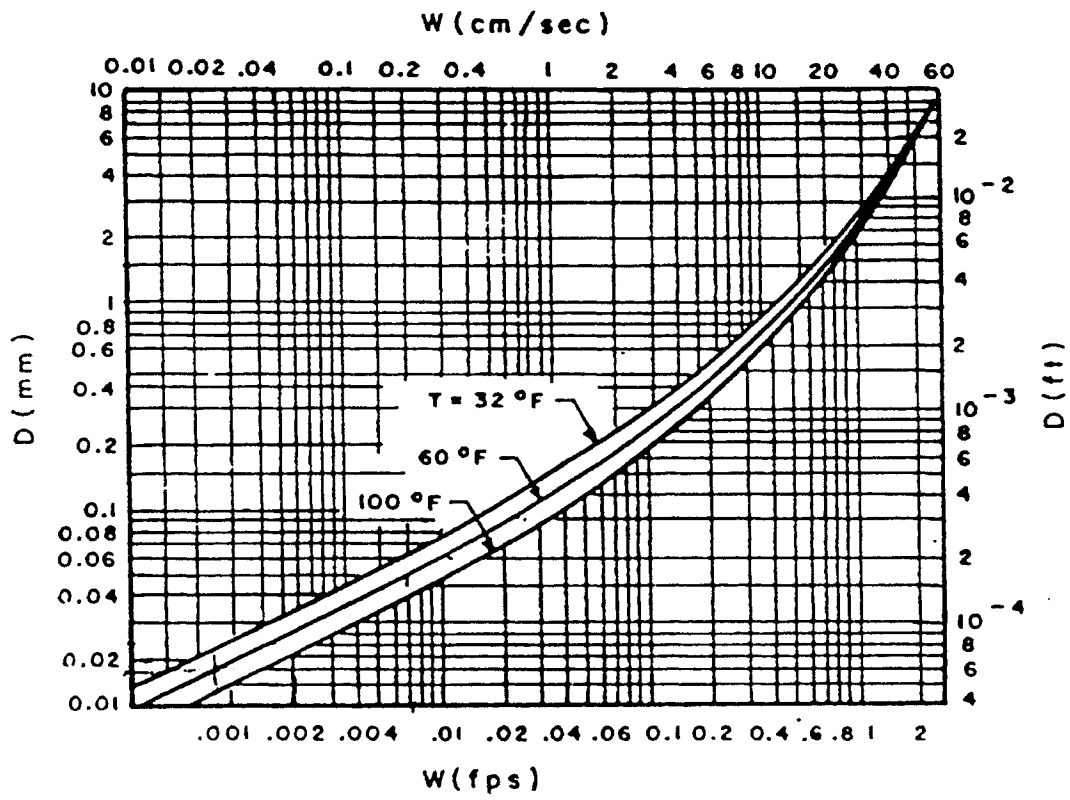


Figure 2.23: Sediment diameter vs. settling velocity in water assuming a specific gravity for sediment of 2.65 (Barfield et al., 1981).

velocities than primary particles. Turbulence helps to reduce the drag on a particle causing an increase in settling velocity. However, for smaller particles, turbulence also tends to increase diffusion, making deposition less likely (Graf, 1971).

### **Steady-State Flow - Overflow Rate Model - Quiescent Flow**

The overflow rate concept was developed by Camp (1946) to determine the trapping efficiency of an ideal basin with steady-state inflows and outflows using the particle settling velocity, flow rate, and basin area. The overflow rate model is based upon the following assumptions:

1. Steady-state inflow and outflow.
2. Rectangular reservoir.
3. No resuspension of sediment.
4. Quiescent flow.
5. Completely mixed inflow and outflow.
6. Discrete particle settling.

The overflow rate model is based upon the ratio of the settling velocity to the critical settling velocity. The critical settling velocity is defined as (Haan et al., 1994; Peavy et al., 1985; and Barfield et al., 1981):

$$V_c = \frac{D}{T} \quad (2.47)$$

where  $V_c$  is the critical settling velocity,  $D$  is the depth of the basin, and  $T$  is the

flow through or detention time. The critical settling velocity can also be defined in terms of the steady-state flow rate and the area of the water surface (Haan et al., 1994; Peavy et al., 1985; and Barfield et al., 1981):

$$V_c = \frac{D}{T} = \frac{D}{L/V} = \frac{DV}{L} = \frac{WDV}{LW} = \frac{Q}{A} \quad (2.48)$$

where L is the length of the basin, V is the flow through velocity, W is the width of the basin, Q is the steady-state flow rate, and A is the surface area. The critical settling velocity is also known as the overflow rate (Q/A).

The overflow rate concept defines the fraction trapped as the ratio of the settling velocity to the overflow rate (Haan et al., 1994; Peavy et al., 1985; and Barfield et al., 1981):

$$F = \frac{V_s}{V_c} \leq 1.0 \quad (2.49)$$

where F is the fraction of particles with a settling velocity of  $V_s$  trapped in the basin. All the particles with a settling velocity,  $V_s$ , greater than or equal to the overflow rate,  $V_c$ , will be trapped. A fraction of the particles with a settling velocity less than the overflow rate will settle out of suspension as defined in Equation 2.49. Figure 2.24 illustrates the overflow rate concept (Barfield et al., 1981).

To utilize the overflow rate concept for a distribution of sediment particle

sizes denoted by  $X$ , the total trapping efficiency is determined by integrating over all sizes (Haan et al., 1994; Peavy et al., 1985; and Barfield et al., 1981):

$$TE = \int_0^{\infty} F dx \quad (2.50)$$

Including the fact that the all of the particles with settling velocities greater than  $V_c$  settle out of suspension, Equation 2.50 becomes (Haan et al., 1994; Peavy et al., 1985; and Barfield et al., 1981):

$$TE = (1 - X_c) + \int_0^{X_c} \frac{V_s}{V_c} dx \approx (1 - X_c) + \sum_{i=1}^n \frac{V_{si}}{V_c} \Delta X_i \quad (2.51)$$

where  $X_c$  is the fraction of particles with a settling velocity less than  $V_c$  and  $\Delta X_i$  is fraction of particles represented by settling velocity  $V_{si}$ .

The amount of sediment discharged from the basin can be estimated with the overflow rate concept because the fraction of sediment discharged is (1 - the fraction trapped). The following expression yields an estimate of the fraction of sediment of size  $i$  discharged (Haan et al., 1994; Peavy et al., 1985; and Barfield et al., 1981):

$$\Delta FF_{o,i} = \frac{\left(1 - \frac{V_{si}}{V_c}\right) \Delta X_i M_s}{\sum \left(1 - \frac{V_{si}}{V_c}\right) \Delta X_i M_s} = \frac{\left(1 - \frac{V_{si}}{V_c}\right) \Delta X_i}{\sum \left(1 - \frac{V_{si}}{V_c}\right) \Delta X_i} \quad (2.52)$$

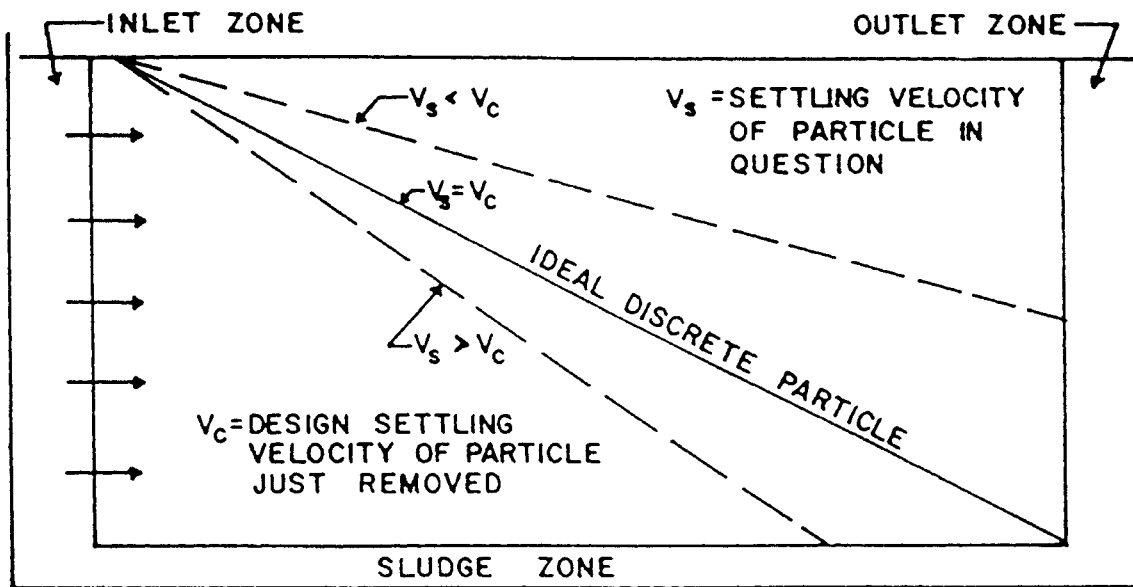


Figure 2.24: Illustration of the overflow rate concept in an ideal rectangular basin (Barfield et al., 1981).

where  $\Delta FF_{o,i}$  is the fraction of sediment of size  $i$  discharged and  $M_s$  is the total mass of sediment. The total mass of sediment smaller than size  $i$  is found by summing  $\Delta FF_{o,i}$  for all smaller particles and multiplying by total mass of sediment leaving the impoundment.

### **Steady-State Flow - Overflow Rate Model - Turbulent Flow**

Turbulence influences trapping in a basin by causing diffusion of particles from higher concentrations to lower concentrations. Dobbins (1944) concludes that turbulence will have a greater effect on larger particles due to upward transport because larger particles tend to be in higher concentrations towards the bottom of a basin. Figure 2.25 illustrates the effect of turbulence on the trapping efficiency of an ideal rectangular basin (Camp, 1946). The trapping efficiency is plotted against the Peclet number, which is an inverse measure of turbulence. Low Peclet numbers indicate very high turbulence and vice versa. The Peclet number is defined as follows:

$$Peclet\ Number = \frac{V_s D}{2\epsilon} \quad (2.53)$$

where  $V_s$  is the settling velocity,  $D$  is the basin depth,  $\epsilon$  is the turbulent diffusivity.

Chen (1975) defined a highly turbulent flow as one with a Peclet number of 0.01. He matched values of trapping efficiency for highly turbulent flow to Vetter's (1940) equation:



$$F = 1 - \exp\left(-\frac{V_s}{V_c}\right) \quad (2.54)$$

Figure 2.26 illustrates the difference between the trapping efficiency predicted for quiescent flow and highly turbulent flow.

The total trapping efficiency for highly turbulent flow can be determined by integrating Equation 2.64 over the entire particle size distribution:

$$TE = 1 - \int_0^1 \exp\left(-\frac{V_s}{V_c}\right) dx \approx 1 - \sum_0^1 \exp\left(-\frac{V_s}{V_c}\right) \Delta X_i \quad (2.55)$$

### Steady-State Flow - EPA Urban Methodology

The EPA methodology developed by Driscoll et al. (1986) accounts for trapping during storm flow (dynamic) conditions and quiescent settling between storms. During storm flow conditions, an empirical relationship based upon the overflow rate concept is utilized to predict trapping. During the no flow periods between storms a quiescent model is utilized to predict settling.

The following expression is utilized to predict trapping of a given particle under dynamic flow conditions (Driscoll et al., 1986):

$$F = 1 - \left(1 + \frac{1}{\beta} \frac{V_s}{V_c}\right)^{-\beta} \quad (2.56)$$

where  $F$  is the fraction trapped,  $V_s$  is the settling velocity,  $V_c$  is the overflow rate ( $Q/A$ ), and  $\beta$  is a turbulence or short circuiting parameter reflecting non-ideal performance of the pond. Recommended values for  $\beta$  are:

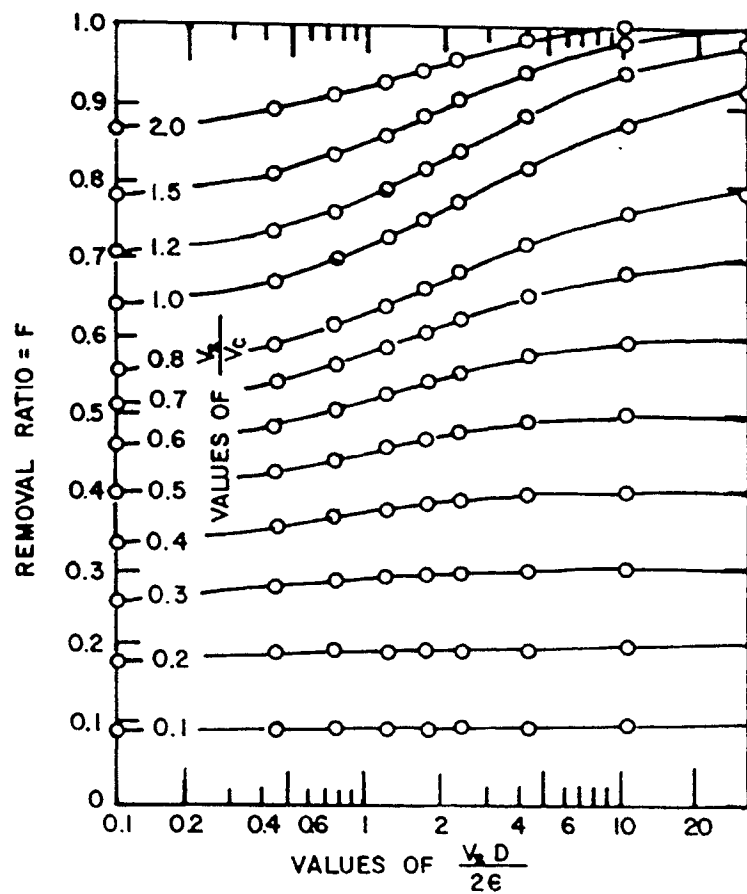


Figure 2.25: Trapping efficiency in a rectangular basin with turbulent steady-state flow (Camp, 1946).

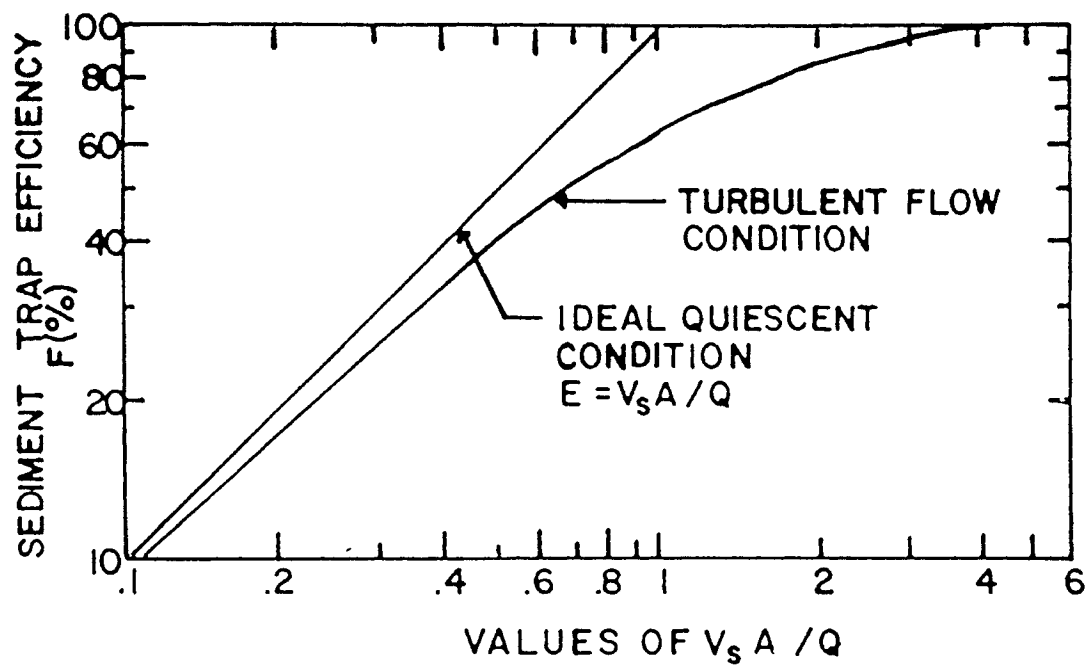


Figure 2.26: Trapping efficiency versus the ratio of settling velocity to overflow rate for a high turbulence model (Barfield et al., 1981; after Chen, 1975).

$\beta = 1$	very poor performance
$\beta = 2$	average performance
$\beta = 3$	good performance
$\beta > 5$	very good performance

For very small values of  $V_s/V_c$  with a  $\beta = 1$  Equation 2.56 is equal to the quiescent overflow rate equation, Equation 2.49. However, for large values of  $V_s/V_c$ , Equation 2.56 deviates greatly from Equation 2.49. For  $\beta = \infty$ , Equation 2.56 reduces to Vetter's (1940) equation for turbulent settling, Equation 2.54. Figure 2.27 presents a comparison of the EPA methodology to the overflow rate models (after Haan et al., 1994).

To predict long term trapping, the EPA methodology combines stochastically generated flows with Equation 2.56 for dynamic situations. Dynamic flows are characterized by a mean flow and a coefficient of variation of flow,  $CV_Q$ , with a gamma distribution. The total removal efficiency can be computed with the following equation based upon the assumption of a gamma distribution (Driscoll et al., 1986):

$$D_R = L_F \left( \frac{\frac{1}{CV_Q^2}}{\frac{1}{CV_Q^2} - \ln\left(\frac{E_m}{L_F}\right)} \right)^{\frac{1}{CV_Q^2} + 1} \quad (2.57)$$

where  $D_R$  is the long term removal fraction for dynamic flows,  $L_F$  is the removal

fraction for low flows,  $E_m$  is the mean storm removal fraction computed with Equation 2.56, and  $CV_Q$  is the coefficient of variation of flows. Figure 2.28 presents Equation 2.57 graphically.  $L_F$  and  $E_m$  must be determined for single storms. Driscoll et al. (1986) provide values of the necessary statistical parameters for different regions of the U.S. in Figure 2.29 and Table 2.6. Since the rainfall statistical parameters present in Table 2.6 are for large runoff producing storms and smaller storms that are not likely to produce runoff, the EPA suggests that to be conservative, designers should double flows.

Under quiescent no flow conditions Driscoll et al. (1986) recommended using the following expression for the settling rate:

$$Q_R = V_s A_Q \quad (2.58)$$

where  $Q_R$  is the quiescent removal rate and  $A_Q$  is the surface area during quiescent conditions. The average time between flow events is determined statistically. For the time between flow events, a removal ratio is defined as (Driscoll et al., 1986):

$$RR = \frac{T_{IA} Q_R}{Vol_R} \quad (2.59)$$

where  $RR$  is the removal rate,  $T_{IA}$  is the average time between storms, and  $Vol_R$  is the mean runoff volume.

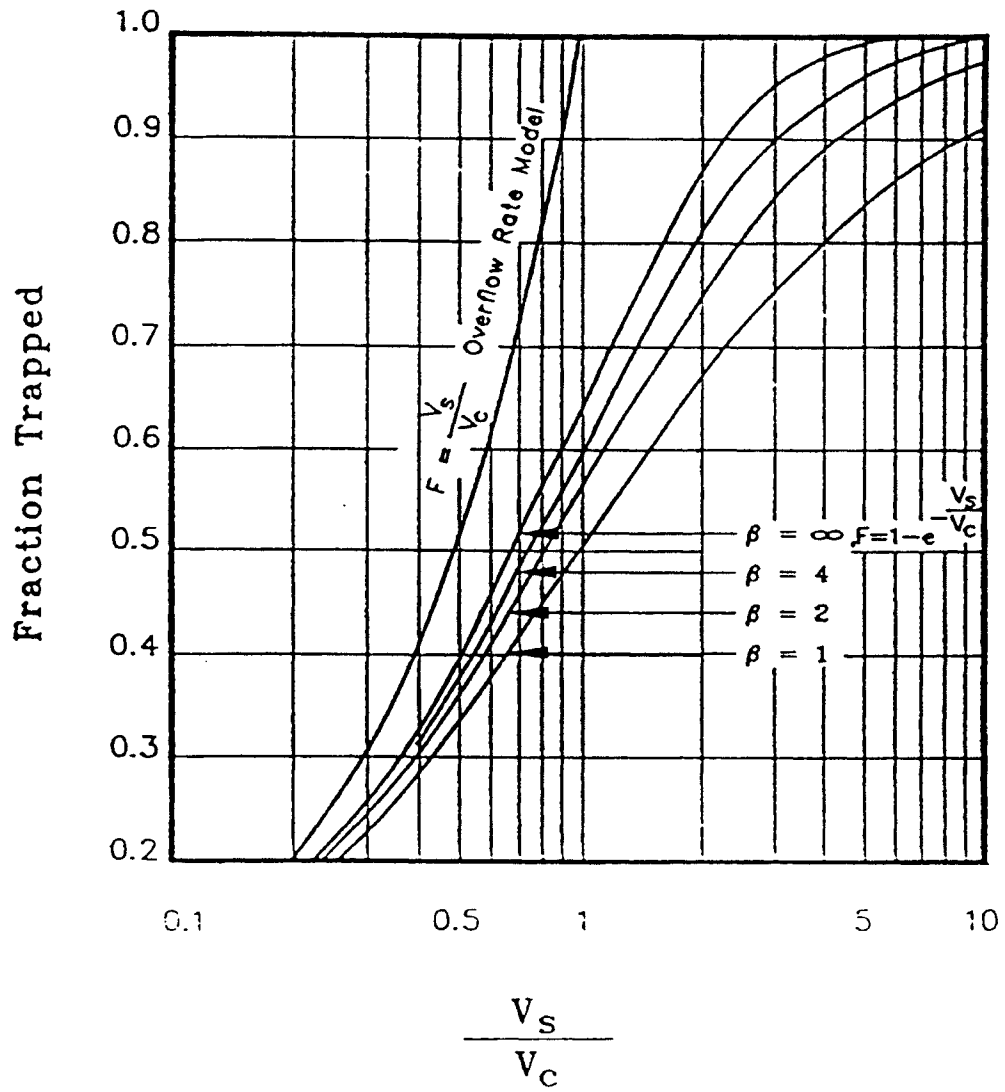


Figure 2.27: Comparison of the EPA and overflow rate models (after Haan et al., 1994).

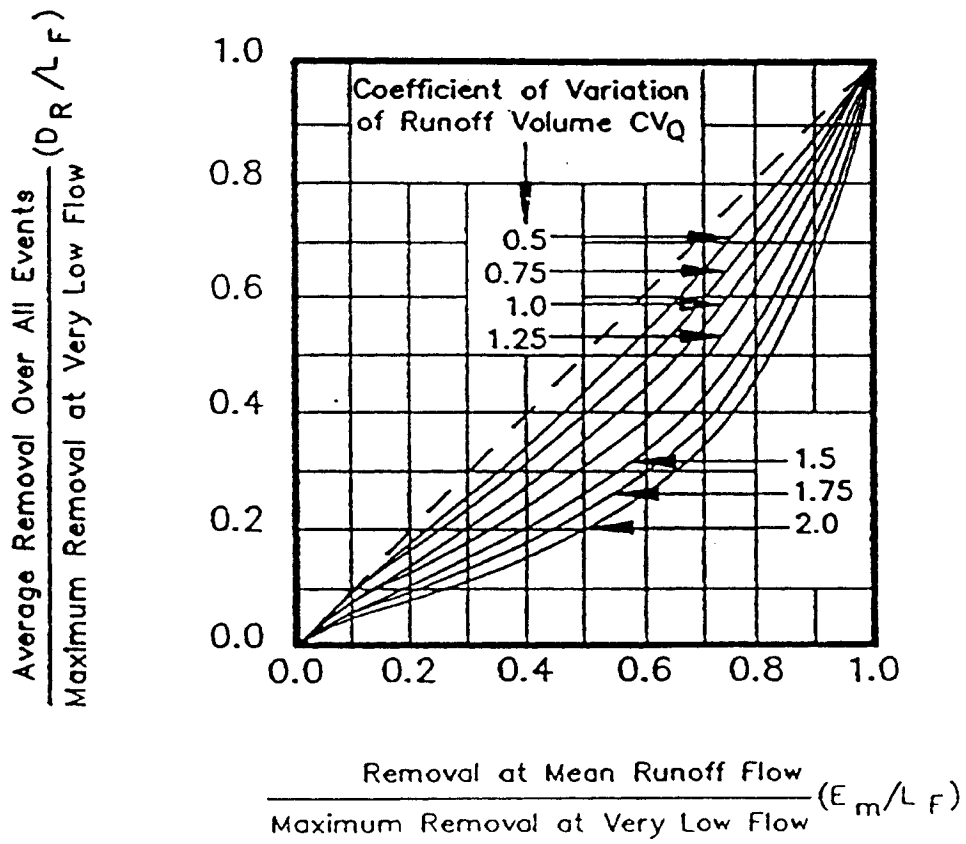


Figure 2.28: Long term sediment trapping in ponds under storm flow conditions (after Driscoll et al., 1986).

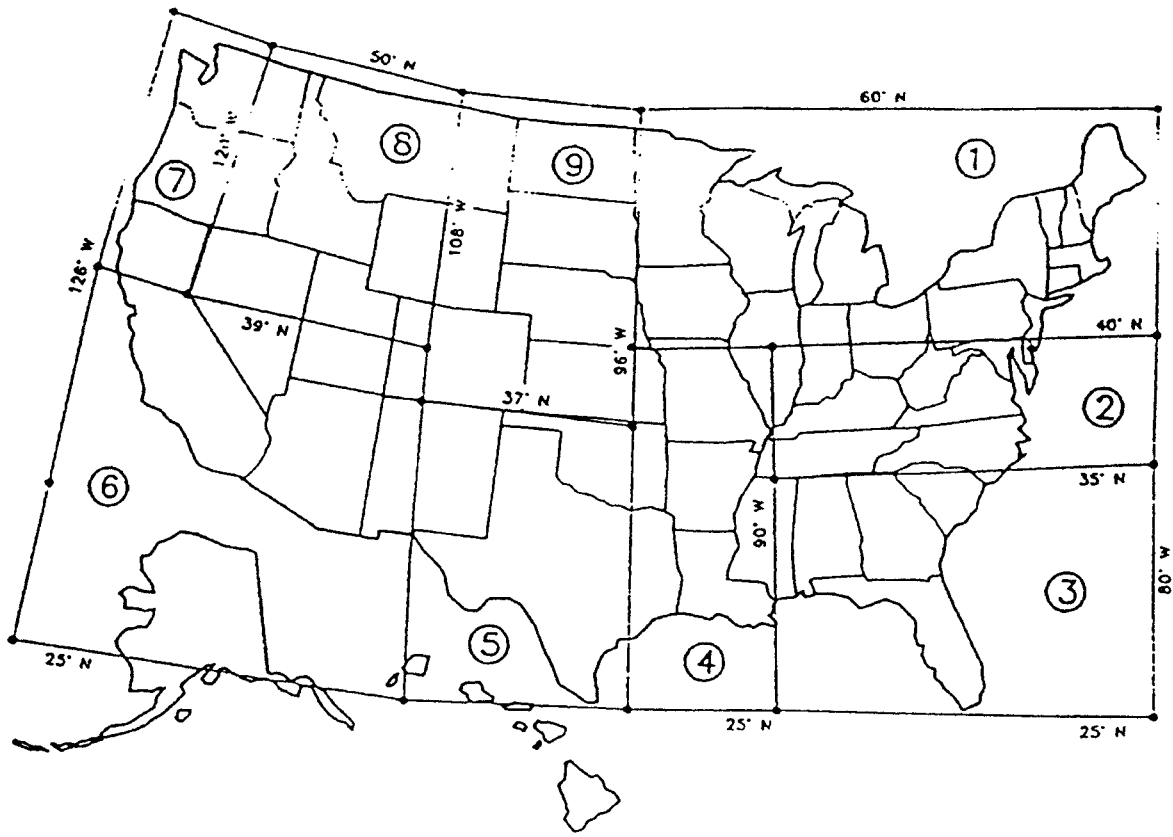


Figure 2.29: Regions for rainfall statistical parameters (after Driscoll et al., 1986).



Table 2.6: Rainfall statistical parameters (after Driscoll et al., 1986).

Zone	Period	Rainfall Statistics							
		Volume (in)		Intensity (iph)		Duration (Hr)		Interval (Hr)	
		Mean	C.V.	Mean	C.V.	Mean	C.V.	Mean	C.V.
1	Annual	0.28	1.46	0.051	1.31	5.8	1.05	73	1.07
	Summer	0.32	1.38	0.082	1.29	4.4	1.14	78	1.07
2	Annual	0.36	1.45	0.066	1.32	5.9	1.05	77	1.05
	Summer	0.40	1.47	0.101	1.37	4.2	1.09	77	1.08
3	Annual	0.49	1.47	0.102	1.28	6.2	1.22	89	1.05
	Summer	0.48	1.52	0.133	1.34	4.9	1.33	68	1.01
4	Annual	0.58	1.46	0.097	1.35	7.3	1.17	99	1.00
	Summer	0.52	1.54	0.122	1.35	5.2	1.29	87	1.06
5	Annual	0.33	1.74	0.080	1.37	4.0	1.07	108	1.41
	Summer	0.36	1.71	0.110	1.39	3.2	1.08	112	1.49
6	Annual	0.17	1.51	0.045	1.04	3.6	1.02	277	1.48
	Summer	0.17	1.61	0.080	1.16	2.6	1.01	425	1.26
7	Annual	0.48	1.61	0.024	0.84	20.0	1.23	101	1.21
	Summer	0.26	1.35	0.027	1.11	11.4	1.20	188	1.15
8	Annual	0.14	1.42	0.031	0.91	4.5	0.82	94	1.39
	Summer	0.14	1.51	0.041	1.13	2.8	0.80	125	1.41
9	Annual	0.15	1.77	.038	1.35	4.4	1.20	84	1.24
	Summer	0.10	1.74	.058	1.44	3.1	1.14	78	1.13

The storage volume under quiescent conditions is assumed to vary between storms. The effect of this variation is accounted for in two nomographs. First, in Figure 2.30, using the ratio of the empty storage volume to the mean runoff volume,  $Vol_B/Vol_R$ , and the removal rate,  $RR$ , calculated in Equation 2.59, the ratio of the effective storage volume to the mean runoff volume,  $Vol_E/Vol_R$ , is determined (Driscoll et al., 1986). Then, in Figure 2.31, the ratio of the effective storage volume to the mean runoff volume,  $Vol_E/Vol_R$ , is used with the coefficient of variation of flows,  $CV_R$ , to determine the long term fraction of sediment removed under quiescent conditions.

To determine the overall long term trapping efficiency, the long term dynamic trapping efficiency and the long term quiescent trapping efficiency must be combined. Driscoll et al. (1986) suggests the following simple relationship:

$$E_T = 1 - (1 - E_D)(1 - E_Q) \quad (2.60)$$

where  $E_T$  is the overall trapping efficiency,  $E_D$  is the long term dynamic trapping efficiency, and  $E_Q$  is the long term quiescent trapping efficiency.

#### **Variable Flow Rate - Modified Overflow Rate Models**

Steady-state flow rate models do well to predict settling in situations where inflows and outflows are steady-state such as in water and sewage treatment. However, in the agricultural setting for which WEPP is being developed, impoundments see a range of inflow and outflow volumes with variable flow rates.

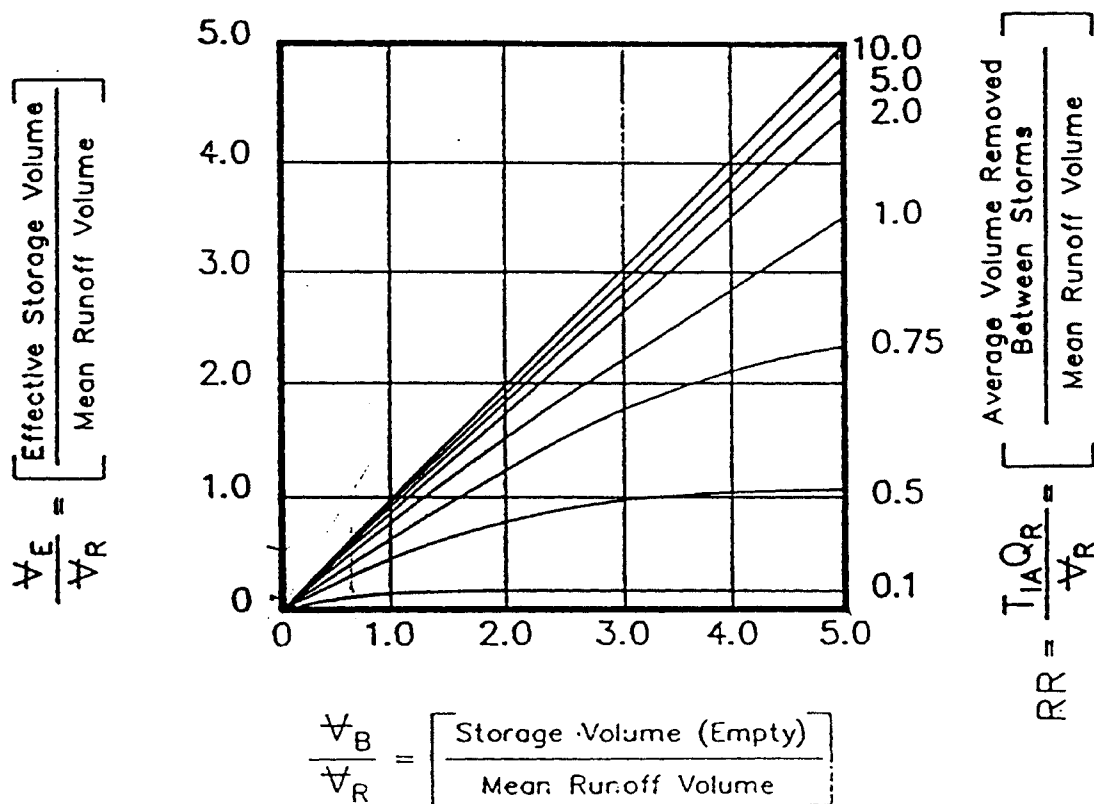


Figure 2.30: Ratio of the mean storage volume to the mean runoff volume (after Driscoll, 1986).

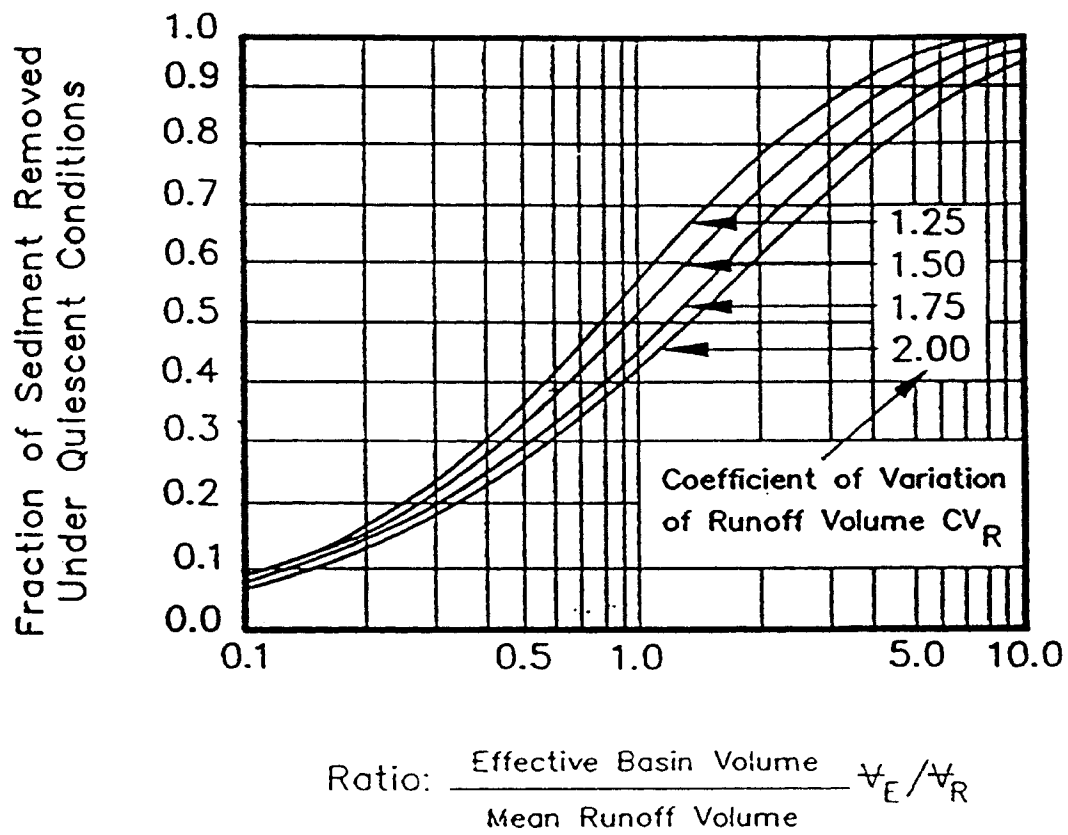


Figure 2.31: Long term removal ratio for impoundments under quiescent conditions between storms (after Driscoll, 1986).

To estimate trapping efficiency for impoundments experiencing variable flow rates, several researchers have attempted to apply the overflow rate concept. To apply the overflow rate concept in a varying flow rate situation, a flow rate and surface area must be chosen to define the overflow rate at several time intervals.

**Early EPA Model.** The EPA model developed by Hill (1976) applies a modification of the overflow rate concept to impoundments with variable flow rates. The EPA model (Hill, 1976) modifies the overflow rate definition given in Equation 2.48 by using the peak outflow rate for  $Q$ , using the water surface area at the inlet of the outflow structure, and including a factor of 1.2 to account for non-ideal settling. The overflow rate in the early EPA model is defined as follows (Hill, 1976):

$$V_c = \frac{1.2 Q_{po}}{A_{ris}} \quad (2.61)$$

where  $V_c$  is the overflow rate,  $Q_{po}$  is the peak outflow rate, and  $A_{ris}$  is the basin surface area at the outlet structure inlet. Using Equation 2.61 to define the overflow rate,  $V_c$ , the fraction trapped, overall trapping efficiency and outflow concentration are determined similar to the steady-state overflow rate method for quiescent settling (Equations 2.49 through 2.52).

**Tapp Method 1.** The Tapp Method 1 (Tapp et al., 1981) splits the outflow hydrograph into several intervals and utilizes a modified overflow rate

to determine the fraction trapped for each interval. The basin overflow rate for each interval is computed with (Tapp et al., 1981):

$$V_{ci} = \frac{C_{OR} Q_o}{A_i - C_A A_i} \quad (2.62)$$

where  $V_{ci}$  is the overflow rate for time interval  $i$ ,  $C_{OR}$  is a constant,  $A_i$  is the surface area for time interval  $i$ ,  $Q_o$  is the outflow corresponding to the stage at area,  $A_i$ , and  $C_A$  is the fraction of the surface area that does not contribute to settling. Using Equation 2.62 to define the overflow rate,  $V_c$ , the fraction trapped, overall trapping efficiency and outflow concentration for each outflow interval are determined similar to the steady-state overflow rate method for quiescent settling (Equations 2.49 through 2.52).

**Tapp Method 2.** The Tapp Method 2 (Tapp et al., 1981) is similar to Tapp Method 1 except that instead of using the surface area in the computation of the overflow rate, the settling depth and impoundment volume are used. Using the volume and settling depth is a more realistic approach for sediment ponds that have an irregular geometry as compared to assuming vertical side walls and using the surface area. The overflow rate for this method is defined by (Tapp et al., 1981):

$$V_{ci} = \frac{C'_{OR} Q_o D}{VOL - C_{VOL} VOL} \quad (2.63)$$

where  $V_{ci}$  is the overflow rate for time interval  $i$ ,  $C'_{OR}$  is a constant,  $Q_o$  is the outflow for interval  $i$ ,  $D$  is the settling depth,  $Vol$  is the of water in the basin,

and  $C_{v,d}$  is the fraction of the basin volume that does not contribute to settling. Using Equation 2.63 to define the overflow rate,  $V_o$ , the fraction trapped, overall trapping efficiency and outflow concentration for each outflow interval are determined similar to the steady-state overflow rate method for quiescent settling (Equations 2.49 through 2.52).

#### **Variable Flow Rate - Plug Flow Model**

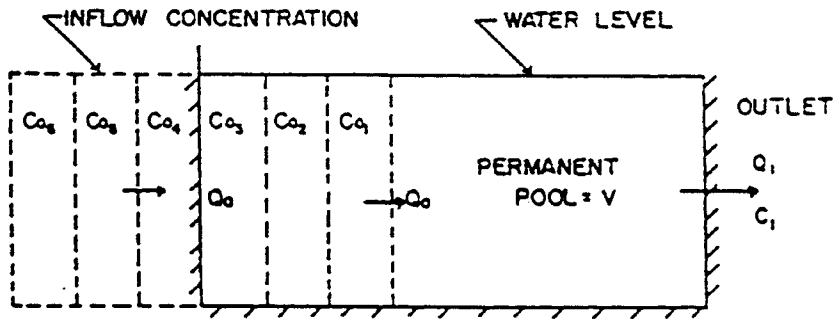
The variable flow rate models based upon the overflow rate concept presented above utilize a *de facto* plug flow concept. Plug flow assumes that the first "plug" of flow to enter a basin is the first "plug" of flow to leave a basin. Another model based upon the plug flow concept, the DEPOSITS (DEtention Performance of Sediments In Trap Structures) model was developed by Ward et al. (1977; 1979). The DEPOSITS model is more physically based than any of the variable flow rate models based upon the overflow rate concept presented above. The DEPOSITS model is incorporated in two widely used watershed erosion models: SEDIMOT II (Wilson et al., 1982) and SEDCAD (Warner and Schwab, 1992).

The plug flow concept assumes that flow that enters the impoundment first leaves the impoundment first, thus, it implicitly assumes no mixing between the plugs. Figure 2.32 presents an illustration of the plug flow concept (Wilson et al., 1982). The DEPOSITS model includes corrections for dead storage, short circuiting and turbulent flow. Dead storage is that portion of the impoundment that does not contribute to settling. Short circuiting is that

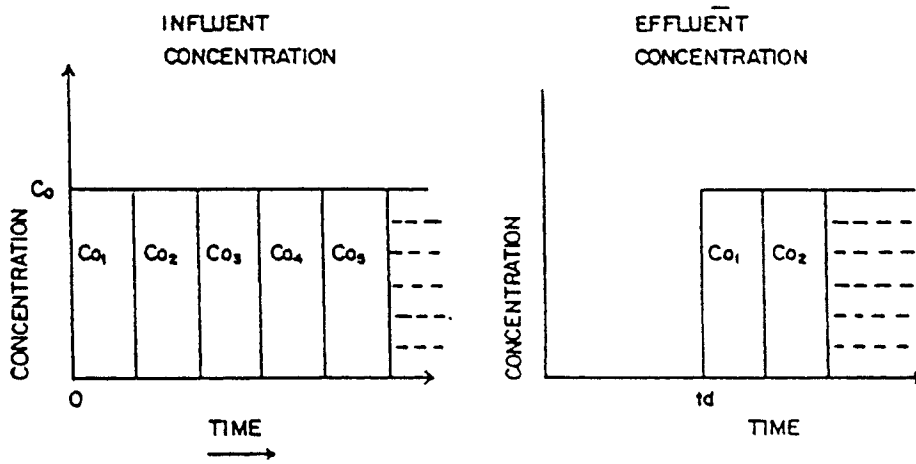
portion of the inflow that flows straight to the outflow structure, bypassing the impoundment altogether. Figure 2.33 illustrates the concepts of dead storage and short circuiting.

The computational procedures utilized in DEPOSITS are described in Haan et al. (1994); Wilson et al. (1982); and Ward et al. (1977; 1979). Flow routing in the DEPOSITS model is performed by a numerical adaptation of the PULS graphical routing procedure presented earlier in the hydraulic routing section of this literature review. The PULS routing procedure incorporated in DEPOSITS utilizes linear interpolation between the outflows and areas computed at the user entered stage points. Following the hydraulic routing, the inflow and outflow hydrographs are divided into plugs of equal volume as seen in Figure 2.34 (Wilson et al., 1982). The detention time for each plug is determined from the time lag between the plug at inflow and outflow. The average depth and surface area for the plug is determined. To determine the sedimentation that occurs during the residence time of the plug, the plug is divided into four vertical layers as seen in Figure 2.35 (Wilson et al., 1982). For a distribution of sediment entering the impoundment, the distribution is split up into intervals and settling velocities are computed with Stoke's law (Equations 2.43 through 2.46) for the mean diameter in each interval. Using the settling velocity, the residence time, and setting depth, the amount of sediment in each layer within each size distribution interval is determined via a mass balance computation. Particles are trapped when they reach the bottom



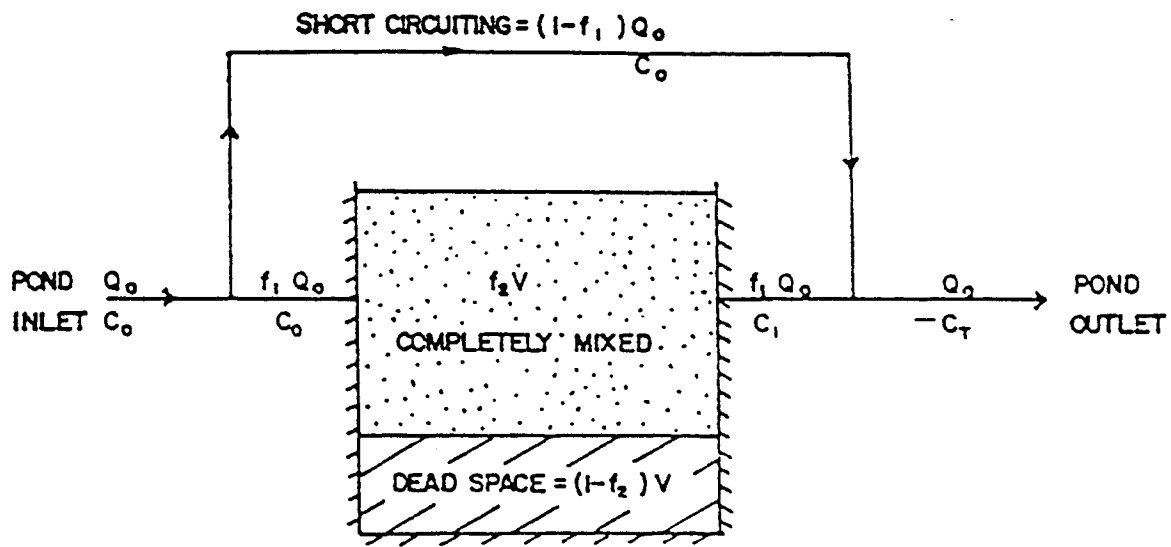


d) CONCEPTUALIZED VIEW OF A PLUG FLOW REACTOR



b) INFLUENT CONCENTRATION AND RESULTING EFFLUENT CONCENTRATION FOR A PLUG FLOW REACTOR

Figure 2.32: The plug flow concept (Wilson et al., 1982).



- $f_1$  - FRACTION OF DISCHARGE ENTERING CSTR
- $f_2$  - FRACTION OF REACTOR THAT IS ACTIVE

Figure 2.33: An impoundment with short-circuiting and dead storage (Wilson et al., 1982).

of the impoundment. The outflow concentration for each plug is the mass of sediment divided by the mass of water in the plug as it exits the impoundment.

#### **Variable Flow Rate - CSTRS Model**

Since the DEPOSITS model ignores mixing, the Continuous STirred Reactors in Series model was developed by Wilson and Barfield (1984) to consider mixing effects. The CSTRS model considers the mixing between plugs that occurs in a real world system that the DEPOSITS model ignores. In neglecting to model the mixing that occurs between plugs, the DEPOSITS model does not accurately predict timing or magnitudes of outflow sediment concentrations. The CSTRS model is also incorporated into SEDIMOT II (Wilson et al., 1982) and SEDCAD (Warner and Schwab, 1992).

The CSTRS model divides a pond into a series of continuously stirred reactors as seen in Figure 2.36 (Wilson and Barfield, 1985). Hydraulic routing is performed similarly to the DEPOSITS model. A mass balance is performed on each reactor:

$$Mass_{in} - Mass_{out} - Mass_{dep} = \Delta Mass \quad (2.64)$$

By definition, the effluent concentration for a continuously stirred reactor is equal to the concentration in the reactor. Put into flow and concentration terms, the mass balance becomes (Haan et al., 1994; Wilson and Barfield, 1984):

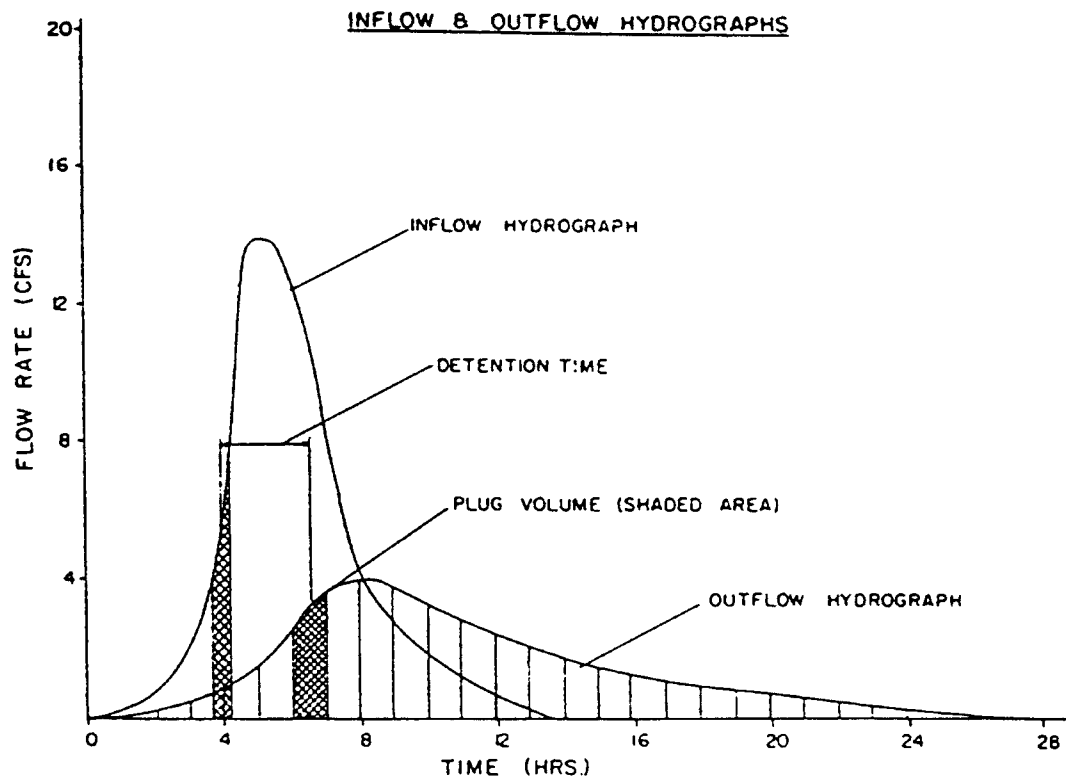


Figure 2.34: The inflow and outflow hydrographs split into plugs (Wilson et al., 1982).

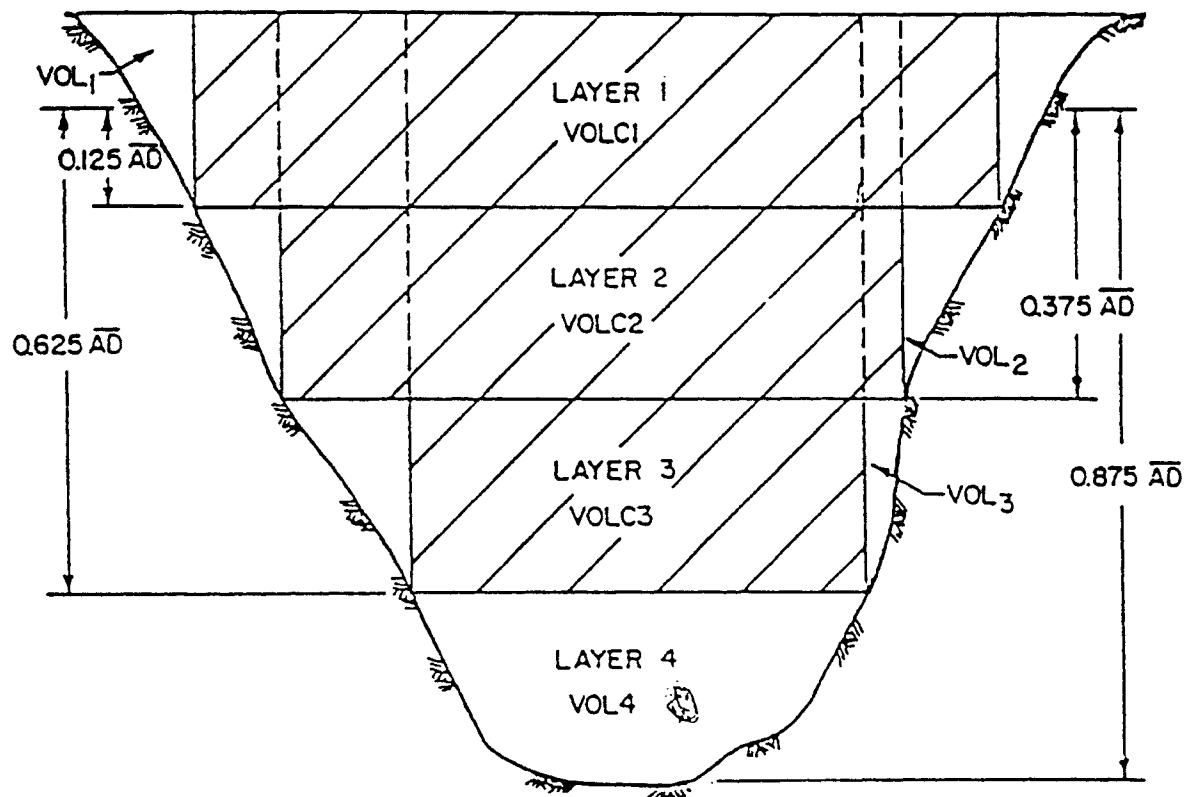


Figure 2.35: Layers for mass balance computations (Wilson et al., 1982).

$$Q_{i-1} C_{i-1} - Q_i C_i - DR_i = \frac{d(Vol_i C_i)}{dt} \quad (2.65)$$

where  $Q_{i-1}$  and  $C_{i-1}$  are the inflow rate and incoming sediment concentration,  $Q_i$  and  $C_i$  are the outflow rate and effluent sediment concentration,  $DR_i$  is the deposition rate of sediment in reactor  $i$ ,  $Vol_i$  is the volume of the reactor, and  $t$  is time.

Equation 2.65 is solved numerically to determine concentration in each reactor as a function of time (Wilson and Barfield, 1985). At the beginning of a time step, time =  $t$ , the concentration,  $C_{i,t}$ , and the volume,  $Vol_{i,t}$ , is known for all reactors,  $i = 1$  to  $n$ . Using a finite difference approximation, the concentration at the end of the time step,  $t + \Delta t$ , in the  $i$ th reactor is determined with (Wilson and Barfield, 1985):

$$C_{i,t+\Delta t} = \frac{\Delta t \left( Q_{i-1,avg} C_{i-1,avg} - \frac{(Q_{i,avg} C_{i,t})}{2} \right) - DEP_i + C_{i,t} Vol_{i,t}}{Vol_{i,t+\Delta t} + \Delta t \frac{Q_{i,avg}}{2}} \quad (2.66)$$

where  $\Delta t$  is the duration of the time increment used to route flow,  $Q_{i-1,avg} C_{i-1,avg}$  is the average sediment mass inflow rate,  $Q_{i,avg}$  is the average outflow rate,  $DEP_i$  is the mass of sediment deposited during the time step,  $C_{i,t}$  and  $C_{i,t+\Delta t}$  are the reactor concentrations at the beginning and end of the time step respectively,

NUMBER OF REACTORS =  $n$

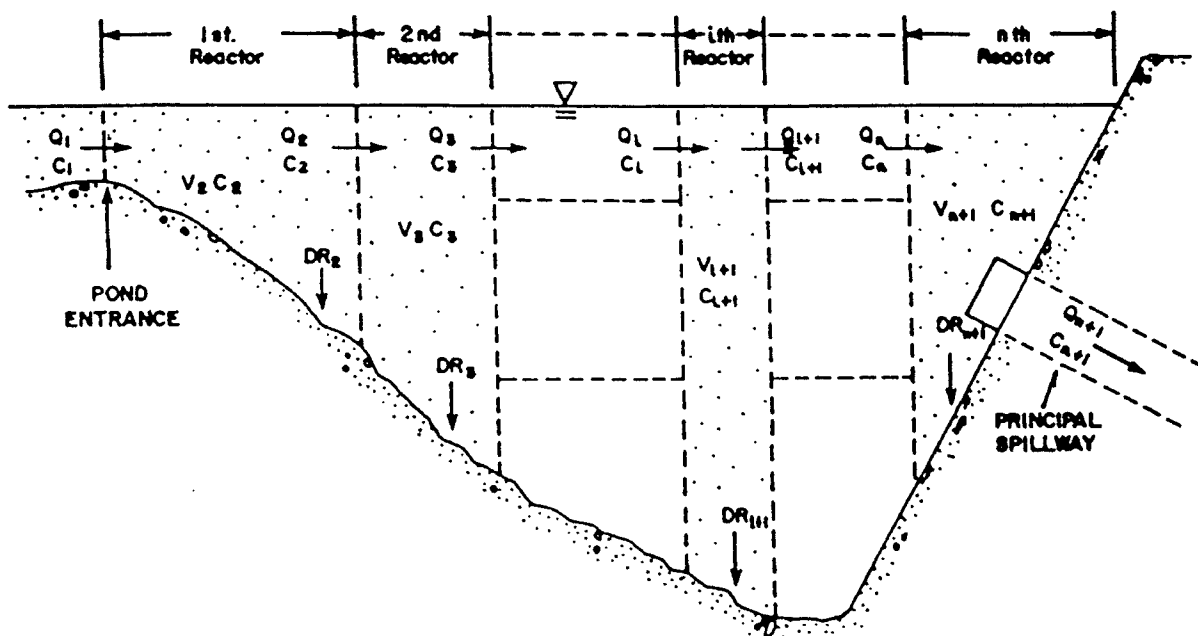


Figure 2.36: Pond divided into a series of CSTRS (Wilson and Barfield, 1985).

and  $Vol_{i,t}$  and  $Vol_{i,t+\Delta t}$  are the reactor volumes at the beginning and end of the time step, respectively.

Since each reactor is completely mixed, the effluent concentration is equal to the reactor concentration. The average sediment mass inflow rate,  $Q_{i-1,avg}C_{i-1,avg}$ , is known from the inflow hydrograph for the first reactor or the from the effluent of the previous reactor. The effluent and reactor concentration,  $C_{i,t}$ , is known from the previous time step. The average discharge,  $Q_{i,avg}$ , is determined by interpolating between the average inflow rate and outflow rate for the impoundment for the flow at reactor  $i$ :

$$Q_{i,avg} = Q_{0,avg} + (i - 1) \frac{Q_{n,avg} - Q_{0,avg}}{n} \quad (2.67)$$

where  $Q_{i,avg}$  is the average inflow rate for the  $i$ th reactor,  $Q_{0,avg}$  is the average flow rate at the inlet of the impoundment,  $Q_{n,avg}$  is the average discharge from the impoundment, and  $n$  is the number of reactors. The reactor volumes at the beginning and end of the time step are determined from the overall impoundment volume with:

$$Vol_{i,t} = \frac{(PV_t - DS)}{n} \quad (2.68)$$

where  $Vol_{i,t}$  is the volume of the  $i$ th reactor at time  $t$ ,  $PV_t$  is the pond volume at time  $t$ ,  $DS$  is the dead storage, and  $n$  is the number of reactors. The deposition



over the interval,  $DEP_i$ , is determined using the settling velocity for each interval in the particle size distribution as computed with Stoke's law (Equations 2.43 through 2.46), and the residence time for each inflow slug of sediment computed with a mass balance.

#### **Variable Flow Rate - BASIN Model**

The BASIN (Basin Analysis of Sediment laden INflow) model was developed by Wilson and Barfield (1985) as an improvement over the CSTRS model. The BASIN model includes an evaluation of bed scour and resuspension. Bed scour is estimated from a modification of the Einstein (1950) entrainment equation. Resuspension of scoured materials is predicted by including diffusion theory when analyzing settling in each reactor. The BASIN model divides an impoundment into a number of reactors in series and then further divides the reactors into a number of vertical layers as seen in Figure 2.37 (Wilson and Barfield, 1985).

Similar to the DEPOSITS and CSTRS models, hydraulic routing in the BASIN model is performed by a numerical adaptation of the PULS method. Details of the sedimentation procedures in the BASIN model have been presented by Wilson and Barfield (1985). First, the inflow size distribution is split into several particle size classes with the settling velocity computed with Stoke's law (Equations 2.43 through 2.46) for the median particle size defining the particle size class. Then, the impoundment is split into reactors and layers as seen in Figure 2.37. Each layer is assumed to be completely mixed

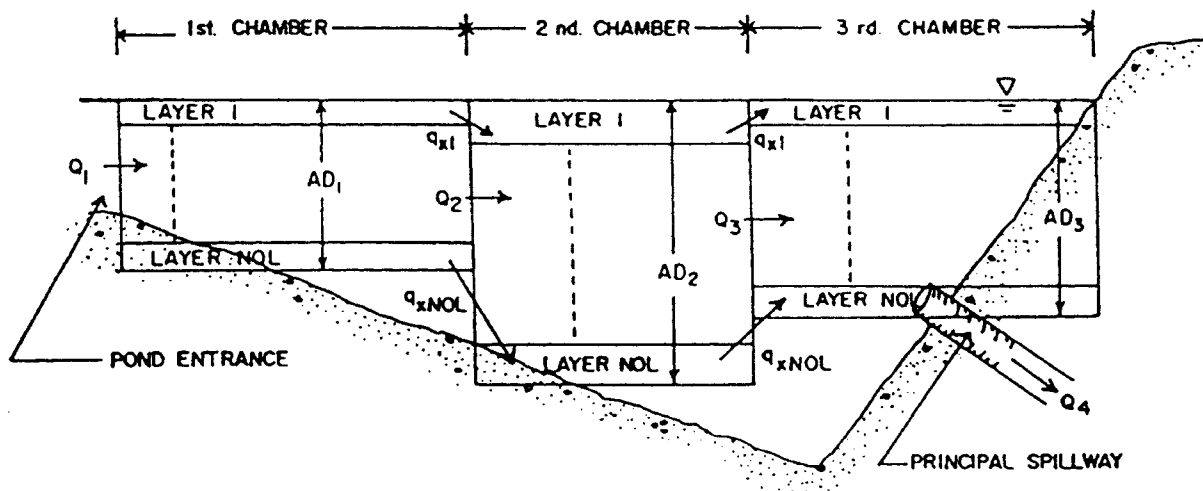


Figure 2.37: An impoundment split into reactors and vertical layers (Wilson and Barfield, 1985).

horizontally with vertical diffusion.

The following differential expression for concentration,  $C$ , is utilized to for any particle size class at any level  $z$  in reactor  $i$  (Wilson and Barfield, 1985):

$$\frac{\partial C}{\partial t} = \frac{Q_i U_f(z)}{Vol_{ei}} [C_p - C] + V_s \frac{\partial C}{\partial z} + \frac{\partial}{\partial z} \left( \epsilon \frac{\partial C}{\partial z} \right) \quad (2.69)$$

where  $C_p$  is the concentration entering the reactor from the previous reactor,  $Vol_{ei}$  is the effective volume of reactor  $i$  (reactor volume - dead storage),  $V_s$  is the settling velocity for the size class (positive in the  $-z$  direction),  $\epsilon$  is the turbulent diffusivity,  $Q_i$  is the inflow to reactor  $i$ ,  $U_f(z)$  is the fraction of flow through the reactor moving through a given layer. Wilson and Barfield (1985) should be consulted for a detailed account on how  $U_f(z)$  is determined. Equation 2.69 relates the change in concentration over time to the mass of sediment entering the layer, the amount of sediment settling out of the layer, and the amount of sediment diffusing into the layer.

#### Variable Flow Rate Models - Evaluation of Accuracy

The results obtained from the variable flow rate models presented here have all been compared to laboratory and field data. In general, the modified overflow rate models were no more accurate than the deposits model in predicting trapping efficiency (Haan et al., 1994). The DEPOSITS, CSTRS and BASINS models all did well in predicting trapping efficiencies (Wilson and Barfield, 1985). However, due to the assumption of plug flow, the DEPOSITS

model did not predict the shape of the effluent sediment graph correctly. The CSTRS and BASIN models both correctly predicted the shape of the effluent sediment graph (Wilson and Barfield, 1985).

## Chapter 3: Model Development

The first step in the development of the WEPP Surface Impoundment Element (WEPPSIE) is to understand WEPP and identify the requirements of its user. The Water Erosion Prediction Project, is a process oriented, continuous simulation model based upon state-of-art hydrologic and erosion theory. The goals of WEPP are to predict runoff and sediment yield for areas ranging from small field size plots to small watersheds. Projected users for WEPP include the Soil Conservation Service, Forest Service, Bureau of Land Management, and others involved in soil and water conservation and environmental planning and assessment [Foster et al., 1987]. These users will utilize WEPPSIE to determine the impact of a wide variety of impoundments on runoff and sediment yield.

User requirements dictate that the impoundment element utilized in WEPP must simulate several types of impoundments: farm ponds, terraces, culverts, filter fences, and check dams. In order to determine the impact of sediment laden runoff, the user needs to know:

1. Peak outflow rate and outflow volume.
2. Peak effluent sediment concentration and total sediment yield.
3. Time to fill an impoundment with sediment.

To meet the requirements of the user the WEPPSIE code includes five sections: a front end interface, daily input, hydraulic simulation, sedimentation simulation, and daily output. A flow chart illustrating how the WEPPSIE code is integrated

into the overall WEPP model is shown in Figure 3.1.

The front end interface is run once at the beginning of a WEPP simulation. Within the front end interface, the coefficients of continuous stage-discharge relationships are determined from information entered by the user describing each outflow structure present in a given impoundment. The user can enter information on one or more of the following possible structures:

1. Drop spillway.
2. Perforated riser.
3. Two sets of identical culverts.
4. Emergency spillway or open channel.
5. Rock fill check dam.
6. Filter fence or a straw bale check dam.

or the user also has the option of entering a discrete stage discharge relationship. For structures that are too hydraulically complex to allow for a direct solution of outflow for a given stage, the coefficients for continuous, directly solvable equations are developed using nonlinear regression. The coefficients for continuous stage-area and stage-length equations are also developed in the front end interface. The input section of WEPPSIE receives daily hydraulic inputs and sedimentologic inputs from the hillslope and channel components. Hydraulic inputs as defined by the WEPP convention consist of incoming storm volume and incoming flow rate using a rectangular hydrograph shape so the storm volume and flow rate form a

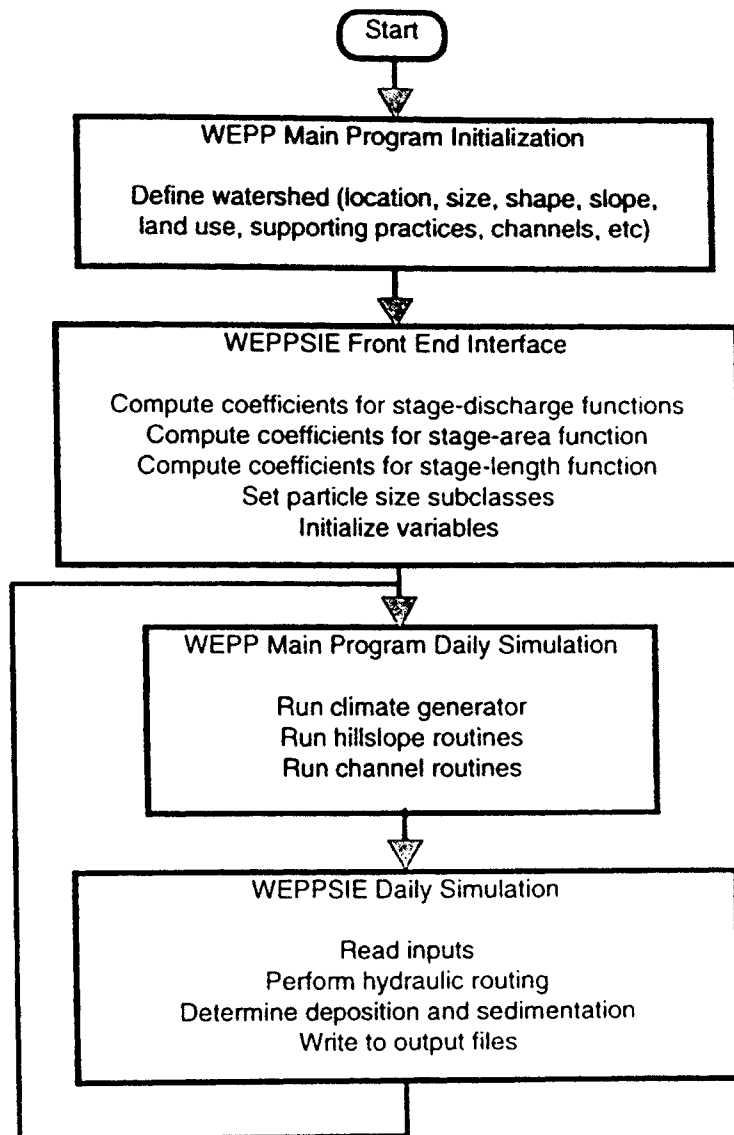


Figure 3.1: Flow chart for WEPPSIE.

rectangular hydrograph. Sedimentologic inputs include total suspended sediment concentration in each particle size class (clays, silts, sands, small aggregates, and large aggregates) with the size class divisions based upon the CREAMS criteria (Foster et al., 1985) and the median particle size diameter.

The hydraulic simulation section of the impoundment element performs a direct numerical integration of an expression of continuity. An adaptive time step which increases the time step when the inflow and outflow rates are relatively constant is utilized. A temporary file of the predicted outflow hydrograph including the time, stage and outflow at each time step included in the integration is created.

The sedimentation simulation section of the impoundment element determines the amount of sediment deposited and the outflow concentration for each time step. Deposition and effluent sediment concentration are predicted using conservation of mass and overflow rate concepts. Two calibration coefficients are included in the deposition procedures to account for impoundment geometry, hydraulic response, and stratification.

The output section creates output files for the user. Output files provide the user with daily information and yearly summaries. Information output to the user includes:

1. Peak inflow rate and inflow volume.
2. Peak outflow rate and outflow volume.
3. Peak stage and overtopping times.



4. Peak influent sediment concentration and influent sediment mass.
5. Peak effluent sediment concentration and total sediment discharge.
6. Break down of influent and effluent sediment mass by particle size class.
7. Time to fill an impoundment with sediment.

This model development chapter follows a format similar to the format of the literature review in Chapter 2. First, the hydraulic routing procedure is described. Then the stage-discharge and stage-area relationships developed in the front end interface that are necessary to perform the hydraulic routing are described in detail. Finally, the procedures used in determining the amount of sediment deposited in the impoundment and the amount of sediment leaving the impoundment are described.

## **Hydraulic Routing**

The WEPP Surface Impoundment Element (WEPPSIE) must function on several types of impoundments: farm ponds, terraces, culverts, filter fences, and check dams. Since WEPP is a continuous simulation model that runs on a daily basis, the impoundment element must also run as a continuous simulation model, updated on a daily basis. To determine the hydraulic routing for each day, the impoundment element utilizes the principle of continuity including functional stage-area and stage-discharge relationships. The hydraulic inputs and outputs for the impoundment element are defined by the WEPP convention as rectangular hydrographs formed by the peak inflow or outflow rate and the

incoming or exiting volume for each twenty-four hour period.

### Continuity Expression

The traditional expression of continuity is (Haan et al., 1994):

$$\frac{dVol}{dt} = Q_i - Q_o \quad (3.1)$$

where Vol is impoundment volume, t is time,  $Q_i$  is the inflow rate, and  $Q_o$  is outflow rate. If the volume is split into stage and area, and both sides of the continuity expression are divided by area, the expression becomes:

$$\frac{dh}{dt} = \frac{Q_i - Q_o}{A} \quad (3.2)$$

where h is stage and A is area. Equation 3.2 forms the basis for the hydraulic routing.

Since WEPP has a rectangular inflow hydrograph, the inflow in Equation 3.2 is constant. Thus, for any twenty-four hour period simulated, the inflow is at the constant peak inflow until the inflow volume has entered the impoundment, after which the inflow is zero.

The outflow,  $Q_o$ , in Equation 3.2 depends upon the type of outlet structure, and its dimensions. Given the type and size of the outlet structure, the outflow,  $Q_o$ , is functionally related to the difference between water surface stage and the inlet stage of the outlet structure called the driving head:

$$Q_o = f_{Q_o}(h) \quad (3.3)$$

The functional relationship is also dependant upon the water surface stage. In some impoundments, more than one outlet structure is utilized, as in the case of a traditional farm pond with a drop spillway and an emergency spillway. In this case, the functional relationship in Equation 3.3 takes one form when there is flow only through the drop spillway, and another form when there is also flow through the emergency spillway. In this thesis, an outflow regime is defined as the range of water surface stage in which the functional relationship in Equation 3.3 takes on a certain form. When the functional relationship in Equation 3.3 changes form, as in the case when flow changes from flowing only through a drop spillway to flowing through both a drop spillway and an emergency spillway, the flow is said to have transitioned from one outflow regime to another. A detailed discussion on how the outflow,  $Q_o$ , is determined for all of the possible outlet structures is presented in the Stage-Discharge Relationships section of this chapter.

The area,  $A$ , in Equation 3.2 is also related to the stage of the water surface, depending upon the topography of the impoundment.

$$A = f_A(h) \quad (3.4)$$

A detailed discussion on how the functional relationship between area and

stage is developed is presented in the Stage-Area Relationship section of this chapter.

Inserting Equations 3.3 and 3.4 into Equation 3.2 yields:

$$\frac{dh}{dt} = \frac{Q_i - f_o(h)}{f_\lambda(h)} \quad (3.5)$$

The continuity expression given in Equation 3.5 shows that the change in stage over time is entirely related to the inflow rate and two functional relationships to stage. The hydraulic routing procedure utilized by WEPPSIE involves performing a direct numerical integration of the continuity expression. To get a new stage point, given the current stage point, Equation 3.5 must be integrated over time with the proper stage-discharge relationship. From the new stage, the new outflow can be determined with the stage-discharge relationship. As the numerical integration proceeds over time, the outflow hydrograph is formed. The outflow hydrograph required by WEPP is formed solely by the peak outflow and the total outflow volume for a simulated twenty-four hour day. Equation 3.5 can be converted to a variable inflow by either using the breakpoint inflow or parameterizing the inflow hydrograph.

#### **Runge-Kutta Numerical Integration**

To integrate the continuity expression given in Equation 3.5, a classical fourth order Runge-Kutta numerical integration is employed which has been adapted from Press et al. (1986). For a given time step, the new head,  $h_{\text{new}}$ , is calculated from four separate estimates of  $dh/dt$ , the differential change in

stage with respect to time given in Equation 3.5. First  $dh/dt$  is evaluated at the current time and stage, at two trial midpoints, and then at a trial endpoint. This approach gives an error term on the order of  $\Delta t^5$ . The procedure is organized as follows to compute a new stage,  $h_{new}$ , from the current stage,  $h$ , the current time,  $t$ , and a time step,  $\Delta t$ :

$$\begin{aligned}
 \Delta h_1 &= \Delta t \left( \frac{dh}{dt} \right)_{(t, h)} \\
 \Delta h_2 &= \Delta t \left( \frac{dh}{dt} \right)_{(t + \frac{\Delta t}{2}, h + \frac{\Delta h_1}{2})} \\
 \Delta h_3 &= \Delta t \left( \frac{dh}{dt} \right)_{(t + \frac{\Delta t}{2}, h + \frac{\Delta h_1}{2})} \\
 \Delta h_4 &= \Delta t \left( \frac{dh}{dt} \right)_{(t + \Delta t, h + \Delta h_1)} \\
 h_{new} &= h + \frac{\Delta h_1}{6} + \frac{\Delta h_2}{3} + \frac{\Delta h_3}{3} + \frac{\Delta h_4}{6} + o(\Delta t^5)
 \end{aligned} \tag{3.6}$$

Figure 3.2 from Press et al. (1986) graphically illustrates the locations for which  $dh/dt$  is evaluated in the procedure.

### Adaptive Time Step

All computations begin at an initial time step referred to as the minimum time step. At the beginning and end of inflow, and when flow transitions from one outflow regime to another, the time step is set to the initial "minimum value." To increase the speed of the Runge-Kutta numerical integration procedure, an adaptive step size has also been incorporated from Press et al. [1986]. This adaptive step size procedure increases or decreases the time step,

$\Delta t$ , until the error in the prediction of  $h_{new}$  is just below a maximum acceptable error. First the new stage is computed by taking two successive time steps of  $\Delta t/2$ , then the new stage is computed by taking one time step of  $\Delta t$ . The difference between these two new stages is called the error. If the error is less than the specified maximum error,  $E_{max}$ , then the next time step is increased. If the error is less than a minimum error,  $E_{min}$ , then the next time step is four times greater than the current time step:

$$\Delta t_{next} = 4 \Delta t \quad (3.7)$$

If the error is between  $E_{min}$  and  $E_{max}$  then the next time step is increased relative to the current time step by (Press et al. 1986):

$$\Delta t_{next} = 0.9 \Delta t \left( \frac{error}{E_{max}} \right)^{-0.2} \quad (3.8)$$

If the error is greater than  $E_{max}$  then the current time step is decreased to (Press et al. 1986):

$$\Delta t = 0.9 \Delta t \left( \frac{error}{E_{max}} \right)^{-0.25} \quad (3.9)$$

and the computation of the new stage is attempted again from the beginning.

(Note: the exponents -0.20 and -0.25 in Equations 3.8 and 3.9 are correct.)

Currently,  $E_{max}$  is  $10^{-3}$  ft and  $E_{min}$  is  $6 \times 10^{-7}$  ft.

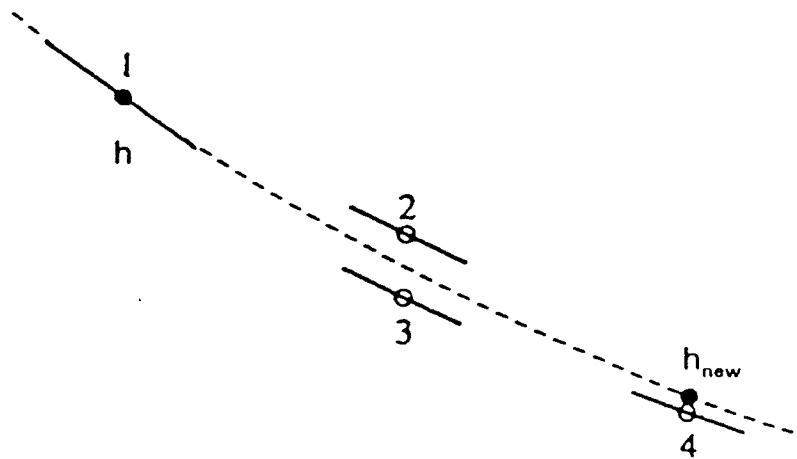


Figure 3.2: Illustration of Runge-Kutta integration (Press et al., 1986).

The new stage is also checked to be sure that it is within the same outflow regime. If the new stage indicates that the outflow regime has changed, the time step is decreased to an initial minimum time step and attempted again. At the beginning and end of inflow, the time step is also set equal to the initial minimum time step. Thus, at each point where the outflow function used in Equation 3.5 changes, the time step is set equal to the initial minimum time step. The adaptive step size begins to increase or decrease the time step from this initial minimum time step to develop the desired accuracy. Currently the minimum time step utilized ranges from 0.01 to 0.1 hr, at the users discretion.

### **Stage-Discharge Relationships**

Stage-discharge relationships are developed from information the user enters about each outflow structure incorporated into a given impoundment. To save time, the front end interface is utilized to develop coefficients for directly solvable continuous outflow functions for each possible outflow structure once at the beginning of a WEPP run. For structures such as: drop spillways, culverts, rock fill check dams, filter fence, and straw bale check continuous directly solvable stage-discharge functions can be developed directly from the dimensions of the outflow structure entered by the user. For structures with more complex stage-discharge relationships that require iterative solutions for the discharge for a given stage, regression equations are utilized as continuous directly solvable stage-discharge functions.



The WEPPSIE can function with any combination of the following outlet structures:

1. Drop spillway.
2. Perforated riser.
3. Two sets of identical culverts.
4. Emergency spillway or open channel.
5. Rock fill check dam.
6. Filter fence or a straw bale check dam.

or the user can enter a discrete stage-discharge relationship. Thus, the outflow function,  $f_{oo}(h)$ , used in the continuity expression, Equation 3.5, must be defined for the entire range of possible water surface stages for any combination of possible outlet structures. In order to cover all the possibilities,  $f_{oo}(h)$  is a summation of the outflow contributions from each possible outlet structure. If a structure is not present, or if the water surface stage is below the inlet of the structure, then the contribution of that outlet structure to the total outflow is zero. If there is flow through one or more outlet structures, the flows are summed to yield the total outflow.

Each of the possible outlet structures has at least two possible flow regimes, either no flow (when the structure is not present or the water surface stage is below the outlet structure stage) or flow (when there is outflow through the structure). The porous structures rock fill, filter fence, and straw bales; have three possible flow regimes: no flow, flow through the structure,

and flow overtopping the structure. Flow is said to transition from one flow regime to another. These transitions occur at specific water surface stages for each structure. Thus, as the water surface stage rises or falls through a transition, the outflow function,  $f_{o_o}(h)$ , must change.

If more than one outlet structure is present, the transitions for each structure must be combined together. Consider the case of a large farm pond with a culvert outlet for small flows, a drop spillway for large storms, and an emergency spillway to prevent breaching of the dam as illustrated in Figure 3.3. Each structure has a transition from no flow to flow at a different stage. The overall outflow function,  $f_{o_o}(h)$ , must reflect all three transitions as seen in Figure 3.4.

At the beginning of the WEPP simulation the front end interface subroutine is executed. This routine develops the stage-discharge relationship for all the possible structures. The user enters data on which structures are present and their dimensions. From this information the front end interface develops the stage-discharge relationship for all possible water surface stages.

Equations used in developing the stage-discharge relationships are discussed in the following sections. Where appropriate, equations in the literature review referred to without repeating the equation here.

### **Drop Spillway**

A drop spillway is a common outflow structure used in farm ponds and sediment detention basins. It consists of a vertical riser connected to a

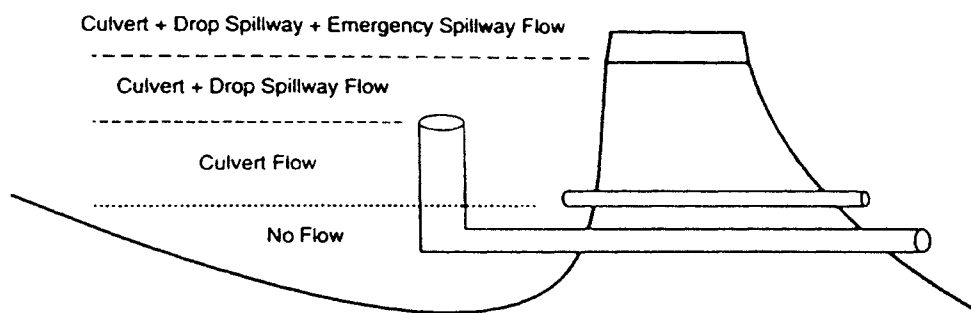


Figure 3.3: Schematic of an impoundment with multiple outlet structures.

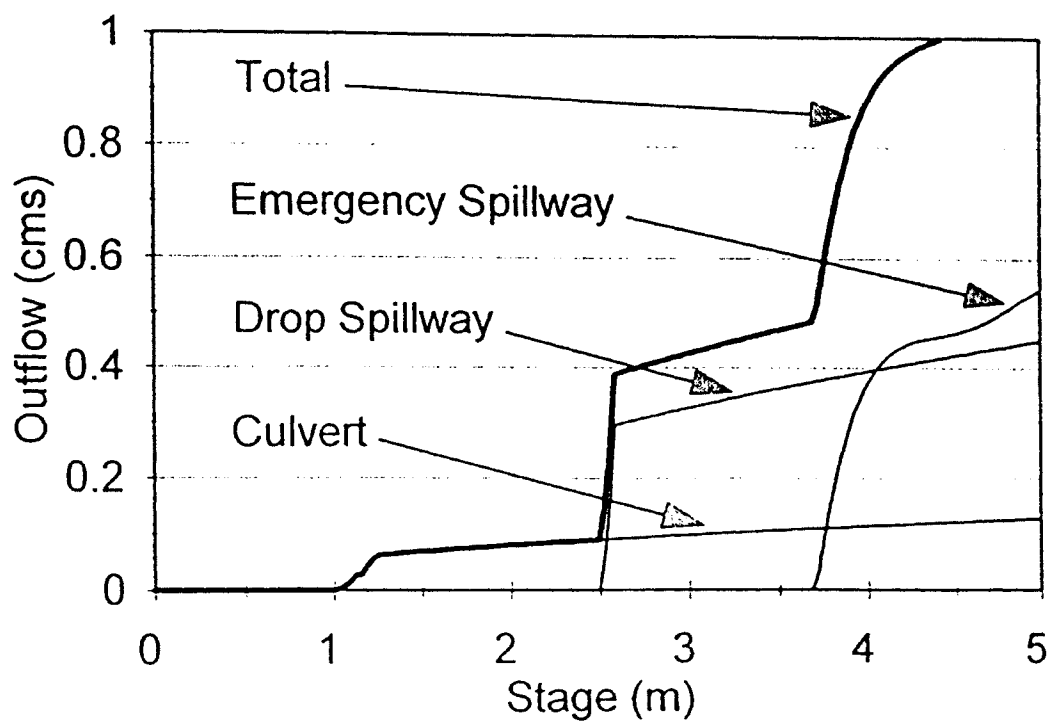


Figure 3.4: Stage-discharge relationship for individual structures and all structures combined including transitions between flow regimes.

horizontal or near horizontal barrel as scene in Figures 2.6 through 2.10. The drop spillway has two possible outflow regimes; no flow and flow. If the water surface stage is below the stage of the riser opening, the outflow is zero.

Flow through a drop spillway occurs when the water surface stage is above the riser inlet. The outflow rate is determined by assuming weir flow, orifice flow, and pipe flow control. The outflow rate is the minimum of the three possible controlling flows.

Weir flow is computed with Equation 2.6. Orifice flow is determined according to Equation 2.7. Pipe flow is computed with Equation 2.8. Flow through the drop spillway is the minimum of the three possible controlling flows:

$$Q_{drop\ spillway} = MIN(Q_{weir}, Q_{orifice}, Q_{pipe}) \quad (3.10)$$

### Perforated Riser

Perforated risers are often used as outlet structures for terrace systems. A perforated riser is similar to a drop inlet in that both employ a riser that empties into a subsurface conduit. The perforated riser includes slots along the riser to allow complete drainage of the terrace, and a bottom orifice plate to limit flow to the subsurface conduit located below the slots. The perforated riser has three possible outflow regimes: no flow, flow through the side slots, and flow submerging the perforated riser. If the water surface stage is below the stage of the bottom of the slots, the outflow is zero.

When the water surface stage moves above the stage at the bottom of the slots, water begins to flow through the riser. Flow can be controlled by either the slots (slot flow), the orifice plate located below the slots (orifice flow), or by the subsurface conduit flowing in full pipe flow (pipe flow). The outflow rate is determined by computing the slot flow, orifice flow, and the pipe flow and taking the minimum controlling flow.

For stages between the stage at the bottom of the slots and the stage at which the riser becomes submerged the outflow is determined according to the McEnroe et al. (1988) procedure described in the Literature Review section. The discharge is computed by solving for the flow through the bottom orifice plate given by Equation 2.11 simultaneously with one of Equations 2.12 through 2.16 which give the flow through the slots to yield the outflow for a given stage. When the water surface is above the stage of the riser inlet there is flow entering the riser as well as the slots. To account for this increase in flow, the flow over the riser is added to the flow through the slots. Flow entering over the riser is controlled by either weir flow or orifice flow. Weir controlled flow over the riser inlet is computed with Equation 2.6; orifice controlled flow through the riser inlet is computed with Equation 2.7. The minimum flow is added to the flow through the slots computed with one of Equations 2.14, 2.15, or 2.16.

Computing flow through the slots using the McEnroe et al. (1988) procedure is far too time consuming for the number of time steps taken in a

twenty year daily simulation. Thus, a regression relationship was developed to compute flow through the slots using stage-discharge points computed according to the McEnroe et al. (1988) procedure described in Chapter 2. One hundred stage-discharge points were run on each of the ten perforated risers utilized in developing the regression relationship. The perforated risers included a range of bottom orifice to riser flow area ratios with the bottom orifice plate located at two different depths below the slots. Several possible regression equations were used to fit the ten stage-discharge relationships. The following functional relationship between driving head and outflow was chosen because it had the best average  $r^2$  of 0.991:

$$Q_o = \frac{1}{A_{PR} + \frac{B_{PR}}{H^{1.5}}} \quad (3.11)$$

where  $Q_o$  is the outflow,  $H$  is the driving head (water surface stage - stage of the bottom of the slots), and  $A_{PR}$  and  $B_{PR}$  are regression coefficients.

When a perforated riser is utilized, a stage-discharge relationship including 20 to 100 points is computed according to the McEnroe et al. (1988) procedure in the front end interface. This stage-discharge relationship is used with the regression routines (Press et al., 1986) to yield unique coefficients,  $A_{PR}$  and  $B_{PR}$ , used in Equation 3.11 for the perforated riser dimensions entered by the user.

Flow through the slots is determined with Equation 3.11. To determine

with Equation 2.18. To determine flow with a submerged inlet, Equation 2.19 is utilized. Table 2.3 lists the coefficients used in Equations 2.18 and 2.19 for several types of culverts. Full pipe flow is determined according to Equation 2.8. The contribution to the total outflow by a culvert is minimum controlling flow:

$$Q_{culvert} = MIN(Q_{unsubmerged}, Q_{submerged}, Q_{pipe}) \quad (3.13)$$

In practice it is common for engineers to use two or more identical culverts to route channels under roadways. It is also possible for engineers to utilize two culverts of different shapes, sizes, or at different elevations. To accommodate these situations, the impoundment element allows the user to specify two different sets of any number of identical culverts.

#### **Emergency Spillways and Open Channels**

In many larger farm ponds and sedimentation basins, emergency spillways are used to route the excess runoff from very large storm events that cannot be routed through the principle spillway in order to keep the excess flow from over toping and breaching an earthen dam. Sometimes an open channel forms the only outlet structure. Emergency spillways and open channel outlet structures have two possible flow regimes; either no flow or flow. If the water surface stage is below the stage of the open channel inlet the outflow is zero.

When the water surface stage in the impoundment rises above the channel inlet, water begins to flow through the outlet channel out of the



impoundment. To determine the outflow for a given stage, a flow profile must be computed utilizing the steady-state standard step method (Fogle and Barfield, 1992; Chow, 1959). For the number of time steps included in a twenty year daily simulation, this is far too time consuming. To save time, flow through an open channel is determined with a fourth-order polynomial expression.

The coefficients of the fourth-order polynomial expression are computed in the front end interface. First, the stage is determined for 20 to 100 discharges using the steady-state standard step method of Fogle and Barfield (1992) as described by steps 1 to 5 and Equations 2.20 to 2.26 in the emergency spillway/open channel section of Literature Review section. Then the 20 to 100 stage-discharge points are used with a regression routine (Press et al., 1986) to determine the coefficients of the following fourth order polynomial:

$$Q_{open\ channel} = A + BH + CH^2 + DH^3 + EH^4 \quad (3.14)$$

where H is the driving head (water surface stage - stage of the open channel inlet) and A, B, C, D, and E are coefficients determined by the regression routine.

### Rock Fill Check Dams

Construction, mining, and silviculture operations need inexpensive temporary sediment traps. Porous rock fill check dams provide an inexpensive, easily constructed solution. A porous rock fill check dam is simply a pile of

rocks obstructing the free flow of sediment laden water. Frequently a rock fill check dam is constructed with a coarse sand or fine gravel core in order to trap the most sediment and covered by a larger rip-rap used to prevent washout. A porous rock fill check dam has three possible outflow regimes; no flow, flow through the rock, or flow overtopping the structure and flow through the rock fill. If the water surface stage is below the stage of the rock fill inlet the outflow is zero.

Flow begins when the water surface stage rises above the stage of the rock fill inlet. Flow through the rock fill is determined using a numerical adaptation of the graphical method developed by Haan et al. (1994). Equation 2.39 can be rearranged to yield the following expression for flow through rock fill:

$$Q_{rock\ fill} = wd_{rf} \left( \frac{dH}{a\ dl} \right)^{1/b} \quad (3.15)$$

where  $wd_{rf}$  is the width of the rock fill,  $dH$  is the head loss through the rock fill,  $dl$  is the length of the rock fill, and  $a$  and  $b$  are coefficients (see Figure 2.18). Coefficient  $a$  is determined by either interpolation or extrapolation between the curves in Figure 2.18 using the size of the rocks and the flow length, given in a numerical form as (Haan et al., 1994):

$$\begin{aligned}
\ln_{RF} = 0.5 \text{ m} & \quad a = 3.04185 \text{ dia}_{RF}^{-0.34677} \\
\ln_{RF} = 1.0 \text{ m} & \quad a = 1.91041 \text{ dia}_{RF}^{-0.34935} \\
\ln_{RF} = 2.0 \text{ m} & \quad a = 1.19637 \text{ dia}_{RF}^{-0.35422} \\
\ln_{RF} = 3.0 \text{ m} & \quad a = 0.90990 \text{ dia}_{RF}^{-0.35705}
\end{aligned} \tag{3.16}$$

Coefficient  $b$  is determined using the size of the rocks and the curve in Figure 2.18; given in a numerical form as (Haan et al., 1994):

$$b = \frac{1}{1.50056 - 0.0001317 \frac{\log(\text{dia}_{RF})}{\text{dia}_{RF}}} \tag{3.17}$$

When flow overtops the rock fill, the flow over the rock fill is modeled as a broad crested weir and added to the flow through the rock fill (Haan et al., 1994):

$$Q_{rock \text{ fill}} = wd_{rf} \left( \left( \frac{dH}{a \, dl} \right)^{1/b} + 3.087 (H - H_{ot})^{1.5} \right) \tag{3.18}$$

where 3.087 is the broad crested weir coefficient and  $H_{ot}$  is the stage that the rock fill is overtopped.

#### Filter Fence and Straw Bale Check Dams

Check dams can also be constructed with straw bales or filter fence. Both straw bale and filter fence check dams provide inexpensive, easily constructed sediment trapping structures. The discharge through a filter fence

or straw bale check dam is dependant upon the porosity of the check dam, the flow stage, the cross-sectional flow area, and the size distribution and concentration of incoming sediment. A filter fence or straw bale check dam has three possible outflow regimes: no flow, flow through the filter, or flow overtopping the structure and flow through it. *Although WEPPSIE will compute flow overtopping a filter fence or a straw bale check dam, in reality most filter fence or straw bale check dams will wash out under such large flows.* If the water surface stage is below the stage of the filter fence or straw bales inlet the outflow is zero.

Flow begins when the water surface stage rises above the stage of the check dam inlet. The outflow through a filter fence or straw bale is computed using a slurry flow rate according to Equation 2.40. Tables 2.4 and 2.5 list slurry flow rates for straw bales and several filter fence fabrics.

When flow overtops a filter fence, the flow over the top of the filter fence is modeled as a sharp crested weir and added to the flow through the filter fence given in Equation 2.40:

$$Q_{filter\ fence} = wd_{ff} \left( V_{sl} (H - H_{ff}) + \left( 3.27 + \frac{0.4}{(H_{ot} - H_{ff})} \right) (H - H_{ot})^{1.5} \right) \quad (3.19)$$

where  $wd_{ff}$  is the width of the filter fence,  $V_{sl}$  is the slurry flow rate,  $H$  is the water surface stage,  $H_{ff}$  is the inlet stage,  $H_{ot}$  is the overtop stage.

When flow overtops a straw bale check dam, the flow over the top of the

straw bales is modeled as a broad crested weir and added to the flow through the straw bales given in Equation 2.40:

$$Q_{straw\ bale} = wd_{sb}(V_{sl} (H - H_{sb}) + 3.087 (H - H_{ot})^{1.5}) \quad (3.20)$$

where  $wd_{sb}$  is the width of the straw bales,  $V_{sl}$  is the slurry flow rate,  $H$  is the water surface stage,  $H_{sb}$  is the inlet stage,  $H_{ot}$  is the overtop stage.

When the flow overtops a filter fence or a straw bale check dam, the structure will probably wash out. Filter fence and straw bale check dams are designed to filter low flows and should not see water surface stages greater than 0.2 to 0.4 m. WEPPSIE assumes that proper maintenance is utilized to promptly repair any damaged check dam. When choosing slurry flow rates the user should consider the effects of sediment laden water and clogging which usually result in lower slurry flow rates as compare to clear water.

#### **User Defined Stage-Discharge Relationship**

A user defined stage discharge relationship is utilized a structure is encountered that is not included in the user interface. When using a user defined stage-discharge relationship, two flow regimes are possible. When the water surface stage is below the user defined stage at which flow starts, the outflow is zero. When the water surface stage is above the stage at which flow starts, flow is computed according to the fourth-order polynomial given in Equation 3.14.

To determine the coefficients of Equation 3.14, the user enters as many

stage-discharge points as possible (at least 15). Regression routines (Press et al., 1986) are then utilized to determine the coefficients in Equation 3.14. Fifteen points are recommended to ensure that the stage-discharge relationship predicted by the fourth-order regression has no unexpected dips. Further, those fifteen points should be fairly evenly spaced within the range of possible stages.

To save computational time, the user defined stage-discharge relationship utilizes the same fourth-order polynomial function used for emergency spillway/open channel flow. Thus, the user is limited to using either points from a user defined stage-discharge relationship or points determined with the emergency spillway/open channel flow water surface profile routine in determining the coefficients for the fourth order polynomial.

#### **Overall Outflow Expression**

The total outflow is simply the summation of the outflow contribution of every possible structure making it possible to have any combination of the possible outflow structures on a given impoundment (see Figures 3.3 and 3.4). If a structure is not present or the water surface stage is below an outlet structure's inlet stage, it's contribution to the total outflow is zero. If the water surface stage is above an outlet structure's inlet stage, it contributes to the total outflow. The total outflow is determined by summing the contributions of each possible outlet structure considering the relationship of the stage to the transition stages for each of the possible outlet structures. The total outflow is determined with the following expression:

$$\begin{aligned}
Q_{total} = & Q_{drop\ spillway} \\
& + Q_{perforated\ riser} \\
& + Q_{culvert\ set\ 1} \\
& + Q_{culvert\ set\ 2} & (3.21) \\
& + Q_{emergency\ spillway,\ open\ channel,\ user\ defined} \\
& + Q_{rock\ fill} \\
& + Q_{filter\ fence,\ straw\ bale}
\end{aligned}$$

## Stage-Area Relationship

The stage-area relationship,  $f_A(h)$ , utilized in the continuity expression, Equation 3.5, is in the form of a power function as recommended by Lafien (1972), Haan and Johnson (1967), and Rochester and Busch (1974). The functional relationship between area and stage is given in the following expression:

$$A = f_A(h) = a + bh^c \quad (3.22)$$

where  $h$  is the stage and  $a$ ,  $b$ , and  $c$  are coefficients. To determine the coefficients in Equation 3.22, the user enters as many stage-area points as possible (at least 10), and regression routines (Press et al., 1986) are used to determine the coefficients  $a$ ,  $b$ , and  $c$ . Ten points are recommended to ensure that the stage-area relationship predicted by the power function provides a reasonable estimation of the actual stage-area relationship.

## Evaporation and Infiltration

On a daily basis the impoundment stage is adjusted for evaporation and infiltration losses. Evaporative losses are computed from the potential evapotranspiration, PET, computed elsewhere in the WEPP code according to (Kohler et al., 1955):

$$Evap = 0.7 PET \quad (3.23)$$

The coefficient of 0.7 was given by Kohler et al. (1955) for small lakes and ponds.

Infiltration losses are computed from the saturated hydraulic conductivity,  $K_{sat}$ , of the draining layer below the impoundment, or

$$Infil = K_{sat} T \quad (3.24)$$

where T is 24 hours. The  $K_{sat}$  (m/hr) utilized in Equation 3.22 is the saturated hydraulic conductivity of the layer draining the impoundment. For impoundments with a homogenous subsurface, the layer with the lowest  $K_{sat}$  is considered the limiting layer, and its  $K_{sat}$  is used. For impoundments with a heterogeneous subsurface, such as when a sandy soil is above a clay base, the  $K_{sat}$  for the sandy soil is utilized because it is the draining layer. Engineering judgement is required on the part of the user to choose a reasonable value of  $K_{sat}$  for a given situation.



At the end of each day the stage is adjusted for evaporation and infiltration according to:

$$h_{new} = h - Evap - Infil \quad (3.25)$$

## **Sedimentation**

The hydraulic simulation section of the impoundment element performs a direct numerical integration of an expression of continuity. A temporary file of the predicted outflow hydrograph including the time, stage and outflow at each time step included in the integration is created. The sedimentation simulation section of the impoundment element determines the amount of sediment deposited and the outflow concentration for each time step. Deposition and effluent sediment concentration are predicted using conservation of mass and overflow rate concepts. When outflow ends, settling in the permanent pool is determined using quiescent settling theory.

Sedimentologic inputs dictated by the WEPP convention include total inflow suspended sediment concentration, percent in each size class (clays, silts, sands, small aggregates, and large aggregates) with the size class divisions based upon the CREAMS criteria (Foster et al., 1985), and the mean particle size diameter,  $d_{50}$ , for each size class. The WEPP Surface Impoundment Element must return outputs similar to the inputs for further routing through a watershed. The impoundment element also outputs a detailed analysis of incoming and effluent sediment amounts and concentrations for each particle

size class.

The goal of the sedimentation algorithm is to determine the sediment concentration exiting the impoundment at the end of each time step taken in the hydraulic simulation. One approach to this problem would have been to use an existing validated prediction model such as DEPOSITS (Ward et al., 1979), CSTRS (Wilson and Barfield, 1984), or BASIN (Wilson and Barfield, 1985). The computational requirements of these models are, however, too time consuming to use for daily simulations over a twenty year time period on the large variety of impoundment shapes, sizes, and outflow structures that will be encountered by the WEPP user. Thus, a simpler algorithm is needed that predicts values reasonably close to those more complex procedures. In this thesis, the CSTRS model of Wilson and Barfield (1984) was chosen over the other models as the standard of comparison due to its prediction accuracy, ability to evaluate the effects of mixing, and simplicity of inputs.

### Conservation of Mass

The simplified sedimentation algorithm developed for the WEPP impoundment element is based upon the principle of conservation of mass, as applied to a single continuously stirred reactor or:

$$\frac{dM}{dt} = Q_i C_i - Q_o C_o - Dep \quad (3.26)$$

where  $dM/dt$  is the change in total mass in the impoundment over time,  $Q_i$  is

inflow rate,  $Q_o$  is the outflow rate,  $C_i$  is the incoming sediment concentration,  $C_o$  is the outgoing sediment concentration, and  $Dep$  is the deposition. The mass of sediment in the impoundment,  $M$ , is equal to  $C_{avg} Vol$  where  $C_{avg}$  is the average concentration in the impoundment and  $Vol$  is the volume of the impoundment. Based on the assumption that the pond can be represented as a single continuously stirred reactor, then the average concentration is equal to the outflow concentration,  $C_o$ . Using dye tracers, Griffin et al., (1985) showed that two continuous stirred reactors in series (CSTRS) were the optimum model to represent small ponds; however, the data also showed that one continuously stirred reactor was a reasonable representation (Griffin, 1983). Using the assumption that the impoundment can be represented as a single continuous stirred reactor, the mass in suspension in the impoundment,  $M$ , is equal to  $C_o Vol$ . Through a series of mathematical manipulations, Equation 3.26 can be solved numerically to determine the outgoing sediment concentration at the end of a given time step, or

$$C_{on} = \frac{Q_i C_i \Delta t - Dep \Delta t + C_o \left[ \frac{Vol + Vol_n}{2} - \frac{Q_i \Delta t}{2} \right]}{\left[ \frac{Vol + Vol_n}{2} - \frac{Q_i \Delta t}{2} \right]} \quad (3.27)$$

where  $C_{on}$  is the outgoing sediment concentration at the end of the time step,  $\Delta t$  is the length of the time step,  $C_o$  is outgoing sediment concentration at the beginning of the time step,  $Vol$  and  $Vol_n$  are the volume of the pond at the

beginning and end of the time step, respectively, and the rest of the terms are as defined for Equation 3.26. The accuracy of Equation 3.27 is dependant upon an accurate determination of deposition since the other terms are known from the hydraulic simulation or the previous time step.

To represent sedimentation more accurately the five sediment size classes are split into several subclasses and Equation 3.27 is utilized to determine a  $C_{on}$  for each subclass. At the beginning of the simulation, the number of subclasses for each particle size class ranging from two to ten is defined by the user. In the user interface section of the routines, each size class is evenly divided into the user defined number of subclasses based upon the logarithmic particle size range. The daily input of sediment in each particle size class is divided into the portion in each size subclass using the log mean particle size diameter for the size class as seen in Figure 3.5. Throughout the entire simulation, the concentration of sediment in each particle size subclass is maintained. Runs were made with two to ten particle size subclasses. Little improvement in accuracy was noted with more than six particle size subclasses, and considering the simplifying assumptions going into the WEPP convention, two to four particle size subclasses provides sufficient accuracy.

### **Deposition**

When the impoundment is experiencing flow conditions, the determination of the amount of sediment deposited for each particle subclass is based upon an analogy to the overflow rate concept (Barfield et al. 1981).

The overflow rate concept states that deposition is linearly related to the ratio of the ideal settling velocity of the sediment particle to the overflow rate, defined as:

$$V_c = \frac{Q_o}{A} \quad (3.28)$$

where  $V_c$  is the overflow rate,  $Q_o$  is the outflow rate, and  $A$  is the impoundment area (assumed constant). The particle settling velocity,  $V_s$ , is determined from discrete settling theory using Stoke's law for small silts and clays or empirical data for large particles. If  $V_c$  is less than  $V_s$  then 100% of the suspended sediment settles out of suspension. If  $V_c$  is greater than  $V_s$ , then the ratio,  $V_s/V_c$ , of the suspended sediment settles out of suspension (Haan et al., 1994). The overflow rate concept can also be expressed in terms of detention times,

$$V_c = \frac{H}{t_p} = \frac{\text{settling depth}}{\text{detention time}} \quad (3.29)$$

The settling velocity can be idealized as

$$V_s = \frac{H}{t_{D100}} = \frac{\text{settling depth}}{\text{detention time for 100\% deposition}} \quad (3.30)$$

Thus,  $V_s/V_c$  can be conceptualized as

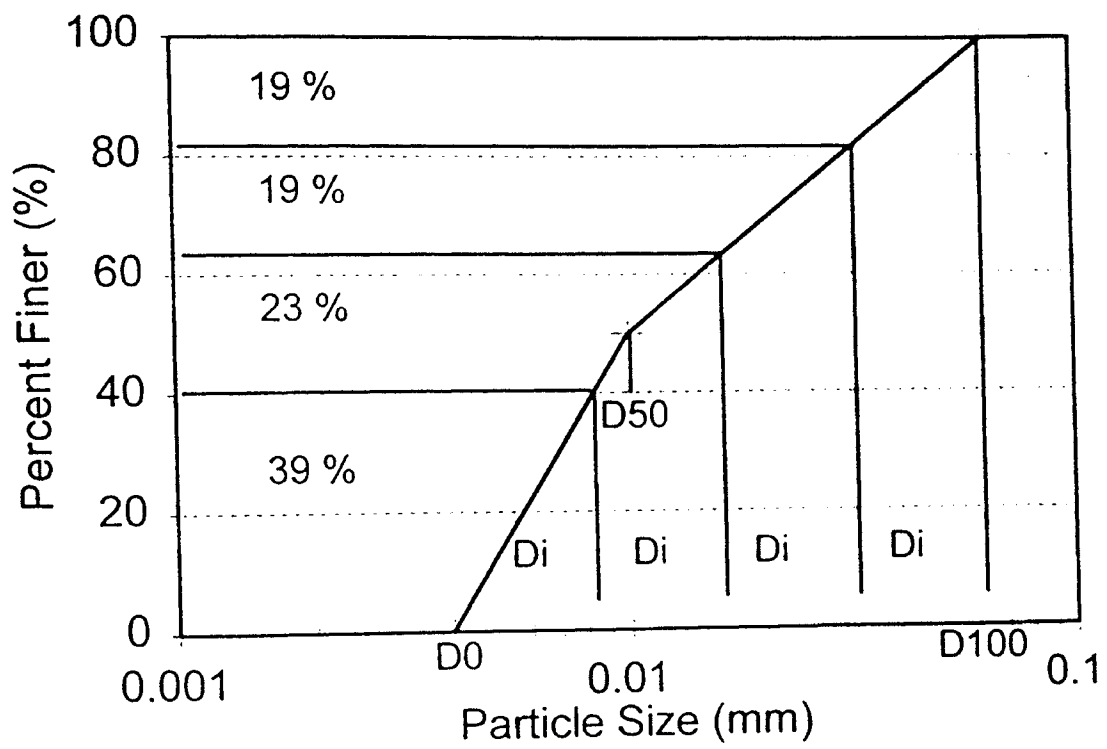


Figure 3.5: Division of a particle size distribution into four subclasses.

$$\frac{V_s}{V_c} = \frac{\frac{H}{t_{D100}}}{\frac{H}{t_D}} = \frac{t_D}{t_{D100}} \quad (3.31)$$

which is the ratio of the actual detention time to the detention time required for 100% of the sediment to settle out of suspension. The deposition routine in the WEPP impoundment element utilizes Equation 3.31.

For each time step, the deposition routine begins with the computation of the detention times. The actual detention time is based upon the ratio of the impoundment volume to the outflow rate:

$$t_D = \frac{(c_t (1 - DS) Vol)}{Q_o} \quad (3.32)$$

where  $t_D$  is detention time,  $c_t$  is an empirical parameter to account for impoundment geometry, hydraulic response, and stratification of the suspended sediment, DS is the dead storage (the portion of the pond area that does not contribute to settling) (Griffin et al., 1985), Vol is the average impoundment volume over the time step, and  $Q_o$  is the average outflow rate over the time step. The detention time required for 100% of the suspended sediment to settle out of suspension is computed from the average impoundment depth (volume / area) and the settling velocity, or:

$$t_{D100} = \frac{(1 - DS) \frac{Vol}{A}}{V_s} \quad (3.33)$$

where  $t_{D100}$  is the detention time required for 100% of the suspended sediment to settle out of suspension under quiescent conditions,  $A$  is the average impoundment area over the time step, and  $V_s$  is the settling velocity for the given sediment particle size. Since the impoundment element utilizes five sediment size classes and up to ten subclasses for each size class all with unique settling velocities,  $t_{D100}$  must be computed for each particle size subclass.

In the computation of both  $t_D$  and  $t_{D100}$ , the concept of dead storage is utilized. According to Griffin et al. (1985), dead storage is related to the ratio of impoundment length (in the flow direction) to impoundment width. Long impoundments with length to width ratios greater than two have approximately 15% dead storage on average while short impoundments with length to width ratios less than two have more dead storage, approximately 25% on average (Griffin et al., 1985). The impoundment length is determined with a power function, or

$$L = a_L + b_L H^{c_L} \quad (3.34)$$

where  $L$  is the impoundment length,  $H$  is the water surface stage, and  $a_L$ ,  $b_L$ , and  $c_L$  are the power function coefficients. The power function in Equation



3.34 is developed in the front end interface section of the program from a number of stage-length points entered by the user. The equation is similar to the stage-area power function. The width is determined by dividing the area by the length. For length to width ratios less than two, the dead storage is set equal to 0.25; For length to width ratios greater than two, the dead storage is set equal to 0.15 based on the Griffin et al. (1985) studies.

Once the detention times are determined, the actual deposition occurring within each size subclass during the times step,  $\Delta t$  must be determined. Two different deposition rate expressions are used, depending on the time period during the runoff event. Figure 3.6 illustrates the times during which each deposition expression is applied. One expression is used throughout the duration of the inflow hydrograph, based upon the inflow rate and incoming sediment concentration, or:

$$Dep = \left( \frac{t_D}{t_{D100}} \right) Q_i C_i \Delta t \quad (3.35)$$

where Dep is the deposition rate,  $t_D/t_{D100}$  is the ratio of the actual detention time to the detention time required for 100% of the suspended sediment to settle out of suspension (maximum of 1.0),  $Q_i$  is the inflow rate,  $C_i$  is the incoming sediment concentration, and  $\Delta t$  is the duration of the time step.  $Q_i C_i \Delta t$  is the inflow mass of sediment during the time period, and  $t_D/t_{D100}$  represents the fraction of the inflow mass trapped.

After inflow ceases, the deposition rate is determined with the sediment concentration in the pond and the particle settling velocity, or:

$$Dep = c_d \left( \frac{t_D}{t_{D100}} \right) C_o V_s A \Delta t \quad (3.36)$$

where Dep is the deposition rate,  $c_d$  is a parameter to account for impoundment geometry, hydraulic response, and stratification of the suspended sediment,  $C_o$  is the outgoing sediment concentration at the beginning of the time step,  $V_s$  is the particle settling velocity, and A is the average area of the impoundment over the time step.  $C_o V_s A \Delta t$  is the fraction of mass in the impoundment that would settle out if the concentration in the impoundment were uniform, and  $c_d(t_D/t_{D100})$  is the fraction that corrects for non-uniformity. Once the deposition is determined, it is used in Equation 3.27 to determine the effluent sediment concentration for each particle size subclass. This sediment concentration then becomes the sediment concentration at the beginning of the next time step and the process is repeated to "march" through the hydrograph.

This method to determine deposition includes two calibration coefficients,  $c_t$  and  $c_d$ . These coefficients are utilized to account for the effects of impoundment geometry, hydraulic response, and stratification. Regression equations that utilize hydraulic and geometric parameters known from the hydraulic simulation performed before the sedimentation routines begin are used to estimate  $c_t$  and  $c_d$ . These regression coefficients were developed from a data

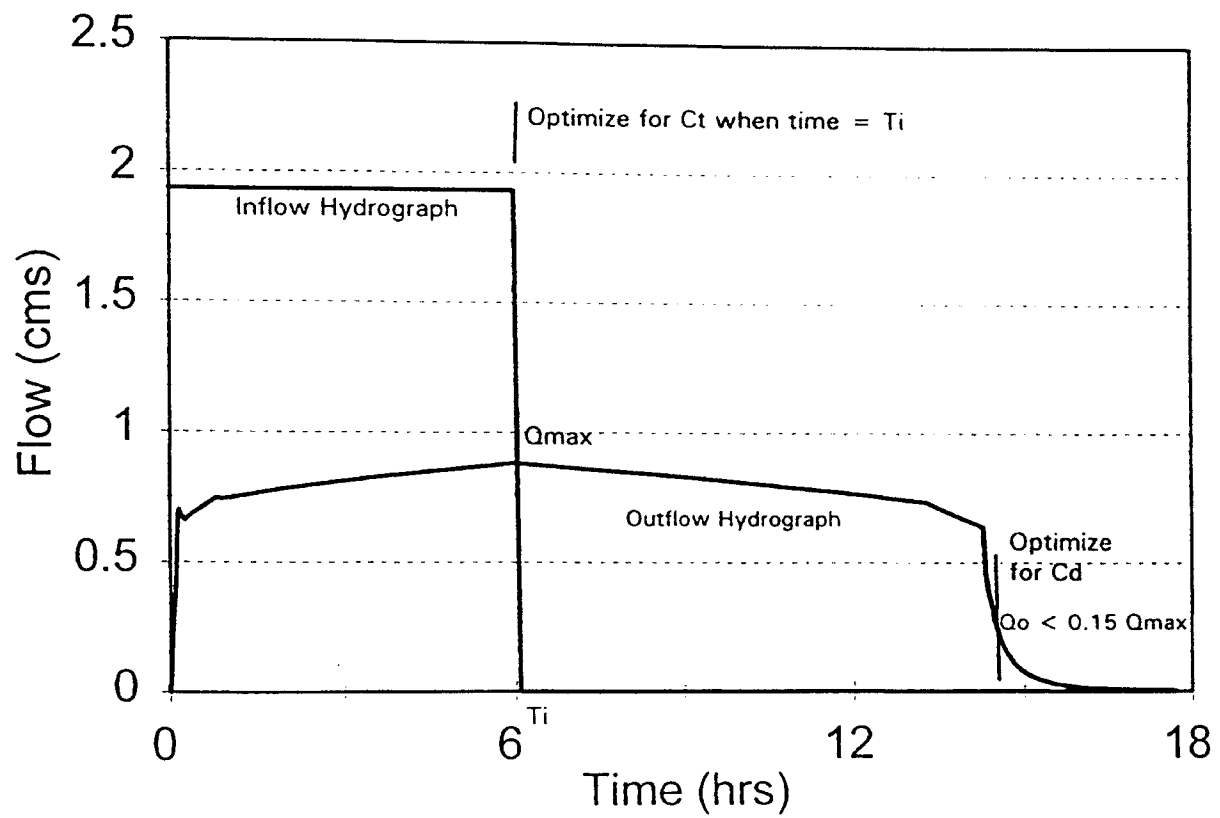


Figure 3.6: Locations in time for which each deposition statement is used (Lindley et al., 1993).

base generated with the CSTRS model. The Calibration Coefficients chapter of this thesis discusses the development of the regression equations in detail.

### Quiescent Settling During No Flow Conditions

After the water surface stage falls below the inlet stage of the lowest outlet structure, the only outflows are due to evaporation and infiltration and the impoundment experiences quiescent settling. To determine settling for each day during periods of no flow, quiescent settling theory is utilized. First, the depth of the interface between clear water and sediment laden water is determined for each particle size subclass with the settling velocity for the subclass as follows:

$$H_{set} = H - V_s T \quad (3.34)$$

where  $H_{set}$  is the depth of the interface,  $V_s$  is the settling velocity, and  $T$  is the duration of no flow conditions (number of days with no flow). When the depth of the interface is known, the area,  $A_{set}$ , of the impoundment at the interface depth and volume,  $Vol_{set}$ , of the impoundment below the interface depth are computed. The concentration of sediment in the sediment laden portion of the impoundment volume,  $C_{set}$ , is determined using the ratio of impoundment volume,  $Vol$ , to the sediment laden volume of the impoundment,  $Vol_{set}$ , and the overall concentration of sediment in the impoundment,  $C_o$ , or

$$C_{set} = C_o \left( \frac{Vol}{Vol_{set}} \right) \quad (3.35)$$

The total deposition for the particle size subclass is computed using the concentration of sediment in the sediment laden portion of the impoundment,  $C_{set}$ , the area at the sediment laden interface,  $A_{set}$ , the settling velocity,  $V_s$ , and the duration of a day,  $T$ , as follows:

$$DEP = MIN( ( C_{set} V_s A_{set} T ) , ( C_{set} Vol_{set} ) ) \quad (3.36)$$

The total deposition cannot be greater than the total amount of sediment in the impoundment, hence the use of the minimum function in Equation 3.36. The new particle size subclass concentration,  $C_{on}$ , is computed from the concentration at the beginning of the day,  $C_o$ , and the impoundment volume,  $Vol$ , or

$$C_{on} = \frac{C_o Vol - DEP}{Vol} \quad (3.37)$$

## Chapter 4: Calibration Coefficients

The accuracy of the sedimentation algorithms depends upon the values used for the calibration coefficients,  $c_t$  and  $c_d$ . Since the sedimentation algorithms utilize a single continuously stirred reactor and neglect the effects of stratification, the calibration coefficients are used to adjust the sediment graph for the effects of impoundment geometry, hydraulic response, and stratification. Ideally the calibration coefficients should be estimated from independent variables that are readily available from the impoundment geometry and the hydraulic routing for the 24 hour period.

Two sets of estimation models have been developed for each of the five CREAMS (Foster et al., 1987) particle size classes: (1) a set for small impoundments with little to no permanent pool and (2) a set for larger impoundments with a permanent pool. In order to develop the estimation models, results from the WEPP routines were compared to the results from the CSTRS model (Wilson and Barfield, 1984). The CSTRS model was chosen as a standard for comparison since it accounts for the effects of impoundment geometry, hydraulic response, and stratification. Further, the CSTRS model has been validated against empirical data. Comparisons were made for each of the five particle size classes run with twenty storms on each of ten small impoundments and ten large impoundments to yield optimal values of  $c_t$  and  $c_d$ . SAS (SAS, 1984) regression procedures were used to develop acceptable

estimation models. Hydraulic routing in the Water Erosion Prediction Project Surface Impoundment Element, WEPPSIE, is computed prior to sediment routing, hence, hydraulic parameters for a given storm are available for sediment routing. Therefore, independent variables for the  $c_t$  and  $c_d$  estimation models were selected from the geometry of the impoundment and the hydraulic routing.

#### **Optimal values of $c_t$ and $c_d$**

To produce an accurate outgoing sediment graph, the sedimentation algorithm described above must have appropriate values of the deposition parameters that account for impoundment geometry, hydraulic response, and stratification of the suspended sediment ( $c_t$  and  $c_d$ ). To determine these optimal  $c_t$  and  $c_d$  values, WEPPSIE was optimized against the Continuous STirred Reactors in Series (CSTRS) model (Wilson and Barfield, 1984) which is used in SEDIMOT II [Wilson et al., 1982] and SEDCAD (Warner and Schwab, 1992). Both models were run with inputs created for identical impoundments with identical inflow hydrographs and sediment graphs.

The WEPPSIE was optimized at two points on the outflow hydrograph as seen in Figure 4.1. First, an optimal  $c_t$  value was determined when the inflow ceased, which is the time equal to the duration of the inflow hydrograph. Optimization for  $c_t$  was conducted at the end of the inflow hydrograph since during the period of inflow, only the  $c_t$  calibration coefficient is utilized in the computation of deposition. Then using the optimal value for  $c_t$ , an optimal

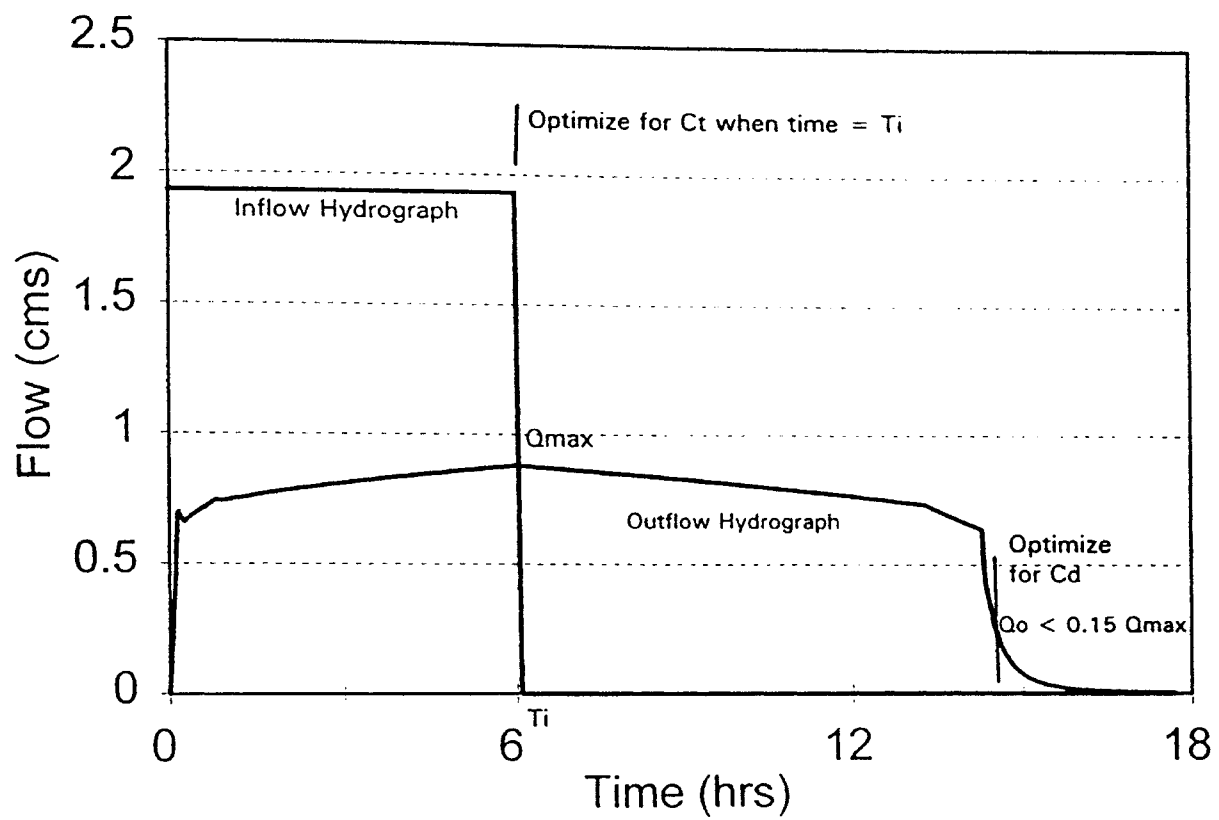


Figure 4.1: Locations in time for which optimizations took place (Lindley et al., 1993).



value for  $c_d$  was determined when the outflow rate fell below 15% of the maximum outflow rate. This point in time was chosen since it represents a time when because most of the inflow volume has moved through the pond. Values were considered optimal when the value of  $c_t$  or  $c_d$  (to three or four decimal places) produced a minimum error between the total outgoing sediment predicted by CSTRS and WEPPSIE, where error is defined as

$$Error = ABS \left( \frac{Mass\ sed\ out_{CSTRS} - Mass\ sed\ out_{WEPP}}{Mass\ sed\ out_{CSTRS}} \right) \quad (4.1)$$

Optimized values for  $c_t$  and  $c_d$  were determined for a variety of impoundment sizes and outflow structures using twenty storms for each size class. Impoundments were grouped by size. Small impoundments included check dams or terraces with no permanent pool and large impoundments included farm ponds with a permanent pool. The small impoundments included a filter fence check dam, a straw bale check dam, three rock fill check dams, and five terraces with perforated riser outlets. The ten small impoundments ranged in volume from 38 to 7325 m<sup>3</sup> which is typical for small impoundments that may be modelled by WEPP. Each of the ten small impoundments was run with 20 storms for each of the five sediment size classes. The twenty storms ranged in volume from 1 to 39 times the impoundment volume with the average being four times the impoundment volume. The storm sizes were chosen to be typical of the storm sizes that might occur in a WEPP simulation. The small

impoundment areas, volumes, and outflow structures are presented in Table 4.1. In order to cover the range of possible stages between zero and one meter and to prevent excessive overtopping, inflow hydrographs were defined by a flow rate and a duration. The inflow rates for small impoundments were based upon the maximum outflow,  $Q_{\text{max}}$ , computed at a water surface stage of 0.61 m. Following the WEPP convention, inflow hydrographs were rectangular. The inflow hydrographs used with the small impoundments are described in Table 4.2.

The large impoundments were farm ponds with an 2.4 m deep permanent pool. The 2.4 m permanent pool was chosen to be typical of farm ponds in the field. The ten large impoundments used drop spillway outlets and ranged in volume from 2837 to 67,832 m<sup>3</sup>. Each of the large impoundments was also run with twenty storms for each of the five sediment size classes. To be typical of the conditions experienced in the field, the twenty storms ranged in volume from 25% of the impoundment volume to 20 times the impoundment volume. Each of the ten large impoundments had outflow structures sized such that the largest storm would drain the impoundment in 70 to 125 hours, thus providing a range of hydraulic responses. Five runs were made with identical hydrographs for each size class. Thus, 2000 optimized values of  $c_t$  and  $c_d$  were determined, 400 for each sediment size class with 200 values for large impoundments and 200 for small impoundments. Table 4.3 lists the area and volume computed at a four meter depth and the outflow structure for each large

impoundment utilized in the optimization. Table 4.4 lists the range of storm sizes used with the large impoundments upon which  $c_t$  and  $c_d$  were optimized.

### Statistical Analysis

Once the 2000 optimized values of  $c_t$  and  $c_d$  were determined, the next step was to develop reliable estimation models for  $c_t$  and  $c_d$  based on impoundment geometry and hydraulic routing. Table 4.5 lists the hydraulic and geometric parameters computed for each of the 2000 sets of data. The parameters listed in Table 4.5 were chosen because they are all indirectly related to settling in an impoundment. Emphasis was placed on using normalized variables in the estimation models, if possible.

Volume parameters and the ratio of the maximum impoundment volume to the volume of inflow were chosen because they provide a measure of impoundment geometry and hydraulic response. Overflow rate parameters provide a measure of detention time. In an ideal quiescent settling basin, fraction trapped is directly related to the ratio of settling velocity to the overflow rate. Stage parameters and dimensionless stage ratios were included because stratification is related to stage.

Extensive attempts were made to find  $c_t$  and  $c_d$  estimation models for each particle size class that would work well for both large and small impoundments. However, using separate models for large and small impoundments yielded far better predictions of sediment yield. The following procedure was used to find estimation models for both small and large

Table 4.1: Description of small impoundments used in the optimization runs (areas and volumes computed at a stage of 0.5 m). Impoundment sizes were chosen to be typical of the impoundment sizes encountered in a watershed simulated by WEPP.

Area (m <sup>2</sup> )	Volume (m <sup>3</sup> )	Outlet Structure
500	93	Filter Fence
3000	550	Straw Bales
500	93	Rock Fill
4500	925	Rock Fill
32500	7325	Rock Fill
789	174	Perforated Riser
1311	312	Perforated Riser
2071	385	Perforated Riser
381	70	Perforated Riser
225	38	Perforated Riser

Table 4.2: Description of inflow hydrographs utilized in the small impoundment optimization runs ( $Q_{omax}$  is the outflow at a depth of 0.61 m). Hydrograph flows were chosen to prevent excessive overtopping, and to be typical of the flows encountered in a watershed simulated by WEPP.

Flow Rate	Hydrograph Duration
0.25 $Q_{omax}$	6, 9, 12, & 15 hrs.
0.50 $Q_{omax}$	6, 9, 12, & 15 hrs.
0.75 $Q_{omax}$	6, 9, 12, & 15 hrs.
1.00 $Q_{omax}$	6, 9, 12, & 15 hrs.
1.25 $Q_{omax}$	6, 9, 12, & 15 hrs.

Table 4.3: Description of large impoundments used in the optimization runs (areas and volumes computed at a stage of 4.0 m). Impoundment sizes were chosen to be typical of the impoundment sizes encountered in a watershed simulated by WEPP.

Area (m <sup>2</sup> )	Volume (m <sup>3</sup> )	Riser Diameter (m)	Barrel Diameter (m)
949	2,837	0.46	0.30
2,103	5,797	0.46	0.30
4,362	10,976	0.46	0.30
4,473	11,346	0.91	0.46
10,068	24,296	1.22	0.61
10,068	24,296	0.91	0.46
21,007	48,839	1.83	0.91
21,007	48,839	1.22	0.61
29,166	68,448	1.83	0.91
29,166	68,448	1.22	0.61

Table 4.4: Description of inflow hydrographs utilized in the large impoundment optimization runs. Hydrograph volumes were to be typical of the flows encountered in a watershed simulated by WEPP.

Storm Volume / Pond Volume	Hydrograph Durations
0.25	6 hrs & 9 hrs
0.5	6 hrs & 9 hrs
1	6 hrs & 9 hrs
2	6 hrs & 9 hrs
3	6 hrs & 9 hrs
5	12 hrs & 15 hrs
8	12 hrs & 15 hrs
12	12 hrs & 15 hrs
16	12 hrs & 15 hrs
20	12 hrs & 15 hrs

Table 4.5: Variables considered for inclusion in  $c_t$  and  $c_d$  estimation models.

Variable	Definition
VI	Volume of the inflow storm event.
VPI	Volume of the pond at the average stage, HI, (averaged over the duration of the inflow hydrograph).
VMX	Volume of the pond at the maximum stage.
VMXVI	$VMX / VI$ . Ratio of the volume of the pond at the maximum stage to the volume of the inflow storm event.
AR	Area of the pond at the riser.
AI	Area of the pond at the average stage (averaged over the duration of the inflow hydrograph).
QO	Outflow corresponding to the average stage, HI, (averaged over the duration of the inflow hydrograph).
VS	Particle settling velocity (from Stokes law or empirical data).
QOAIVS	$(QO / AI) / VS$ ; ratio of the overflow rate to the settling velocity.
QOARVS	$(QO / AR) / VS$ ; ratio of the overflow rate to the settling velocity.
QOAIVSE	$(1 - \exp(-((QO / AI) / VS)))$ .
QOQI	$QO /$ average inflow rate.
HI	The average stage (averaged over the duration of the inflow hydrograph).
HR	The stage of the riser.
HIHR	$(HI - HR) / HI$ .



impoundments. Since separate  $c_t$  and  $c_d$  estimation models for each particle size class were developed for both small and large impoundments. Each estimation model was based upon 200 optimized runs for each particle size class.

Following the computation of the parameters listed in Table 4.5, a correlation matrix was run on the 200 values of the above parameters for the silt particle size class. All of the parameters included in Table 4.5 are based on impoundment geometry and hydraulic routing. Since identical inflow hydrographs were used for each size class, the hydraulic routing was similar for each particle size class; therefore, the values of the parameters listed in Table 4.5 are also similar. Since the parameters listed in Table 4.5 are similar for each particle size class, the correlation matrix for the silt particle size class is identical to the correlation matrix for any of the other size classes. A high correlation between two parameters is an indication that the two parameters are explaining a similar variance in the data. In choosing an estimation model it was decided that parameters with a high correlation should not be included based on recommendations from Haan (1977).

After computing the correlation matrix, the next step was to determine the best estimation models for  $c_t$  and  $c_d$  for each size class on the basis of maximum  $r^2$ . The SAS-REG-R-SQUARE (SAS, 1984) procedure was utilized to determine the  $r^2$  for every possible 1, 2, and 3 variable model from a given set of  $n$  possible independent variables. For the clay size particles, deposition is

not very sensitive to the value of  $c_d$  used in WEPPSIE, making a reliable determination of an optimal  $c_d$  impossible. Therefore,  $c_d$  for clays was simply assumed to be 1.0 for large impoundments, thus eliminating its effect on the determination of deposition. For small impoundments the mean optimal value of 4.07 was used for  $c_d$ . However, utilizing a  $c_d$  value of one or ten has little effect on the predicted total sediment yield.

The output from the SAS-REG-R-SQUARE (SAS, 1984) procedure was then examined to find possible 1, 2 and 3 independent variable estimation models for  $c_t$  and  $c_d$  for each size class. Possible models were those that had maximum correlation among the independent variables below 0.7. The 0.7 cutoff can be considered relatively conservative. Haan (1977) recommends a cutoff of between 0.7 and 0.9. Detailed statistics for each of the possible models was run using the SAS-REG/CORR (SAS, 1984) procedure.

From the detailed statistics on the possible estimation models, a final or "best" estimation model for  $c_t$  and  $c_d$  for each size class was chosen based on the following criteria:

1. High  $r^2$ .
2. High model F value indicating a very significant estimation model.
3. Low sum of squares on error and mean square error.
4. Low correlation among the parameter estimates.
5. Parameter estimates that provide reasonable estimations throughout the range of possible inputs.

6. Normally distributed residuals.

The order shown here was not followed rigorously, each criteria was considered important in choosing the final estimation model. The final or "best" estimation model for  $c_t$  and  $c_d$  for each size class is presented in Tables 4.6 and 4.6, with the models developed for small impoundments presented Table 4.6 and the models developed for large impoundments presented in Table 4.7.

When inspecting the statistics on the  $c_t$  and  $c_d$  estimation models, two observations can be made. First, on the basis of  $r^2$  and root mean square error, the estimation models for  $c_t$  appear to be statistically better than the estimation models for  $c_d$ . This is because the effects of impoundment geometry, hydraulic response, and stratification are more pronounced after the peak outflow is reached. Trying to model such complex effects with a single linear modification parameter such as  $c_d$  is a large simplification of the natural system. Further, the independent parameters computed from the impoundment geometry and hydraulic response used to estimate  $c_d$  are only somewhat correlated to  $c_d$  or the effects it is accounting for.

The second observation is that in general the estimation models for the silt and small aggregate size classes are statistically better than the estimation models for the clay, sand, and large aggregate size classes. For sands and large aggregates, this is due to the fact that nearly 100 % of sands and large aggregates settle out of suspension in most impoundments making settling for sands and large aggregates not very sensitive to the values of  $c_t$  and  $c_d$ , and

Table 4.6: Small impoundment models.

Particle Size Class	Estimation Model	$r^2$	Mean	RMSE	Correlation
Clay	$c_t = 0.040 + 0.011(QOAIVS)$	0.37	0.115	0.177	NA
Silt	$c_t = 0.014 + 0.110(QOQI)^2$	0.77	0.042	0.016	NA
Sm. Agg.	$c_t = 0.015 + 0.127(QOQI)^2$	0.80	0.047	0.017	NA
Sand	$c_t = 0.006 + 0.255(QOAIVS)$	0.45	0.009	0.006	NA
Lg. Agg.	$c_t = 0.006 + 12.59(QOAIVS)$	0.77	0.011	0.006	NA
Clay	$c_d = 4.07$	NA	4.07	NA	NA
Silt	$c_d = 0.755 + 1.305(VMXVI) + 0.132(VPI)$	0.39	1.72	0.76	0.05
Sm. Agg.	$c_d = 0.466 + 2.753(VMXVI) + 0.058(VMX)$	0.56	2.21	0.74	0.11
Sand	$c_d = 0.632(QOAIVS)$	NA	0.006	0.014	NA
Lg. Agg.	$c_d = 41.67(QOAIVS) + 0.005(HI)$	NA	0.020	0.028	NA

<sup>1</sup> Terms are defined in Table 4.5.

Table 4.7: Large impoundment models.

Particle Size Class	Estimation Model	$r^2$	Mean	RMSE	Correlation
Clay	$c_t = 0.101 + 0.049(QOAIVS) + 0.118(HIHR)$	0.78	0.071	0.019	0.21
Silt	$c_t = 0.002 + 0.125(QOQI)$	0.76	0.071	0.020	NA
Sm. Agg.	$c_t = -0.040 + 0.193(QOQI) + 0.041(VMXVI)$	0.76	0.098	0.033	0.12
Sand	$c_t = 0.004 + 3.105(QOAIVSE) - 0.005(HIHR)$	0.95	0.018	0.002	0.19
Lg. Agg.	$c_t = 0.008 + 12.44(QOAIVSE) - 0.012(HIHR)$	0.92	0.029	0.005	0.19
Clay	$c_d = 1.0$	NA	2.11	NA	NA
Silt	$c_d = 0.002(VMX) + 3.831(HIHR)$	NA	1.74	0.85	0.71
Sm. Agg.	$c_d = 0.004(VMX) + 3.124(HIHR)$	NA	1.68	0.13	0.71
Sand	$c_d = -0.075 + 17.71(QOARVS) - 0.0002(VI)$	0.38	0.06	0.14	0.37
Lg. Agg.	$c_d = -0.576 + 172.4(QOARVS) + 0.359(VMXVI)$	0.53	0.33	0.35	0.57

<sup>1</sup> Terms are defined in Table 4.5.

finding optimal values of  $c_t$  and  $c_d$  difficult. For clays, little to no clay particles settle out of suspension in most impoundments making settling for clays very insensitive to values of  $c_t$  and  $c_d$ . Silts and small aggregates, alternatively, are very sensitive to the values of  $c_t$  and  $c_d$ , making the optimized data set less erratic and more correlated to the possible input parameters.

The silt data set was used to develop the estimation model for clay particles in large impoundments presented in Table 4.7. The best estimation model based upon the optimization data for the clay particles occasionally provided estimations of  $c_t$  that were too high, resulting in unreasonably high deposition. Thus, the silt data set was used with the QOAIVS variable in developing the above model to provide more reasonable estimations of  $c_t$ . Since QOAIVS variable is the ratio of the overflow rate to the settling velocity, using the settling velocity adjusts the silt model for the clay size class.

Although many of the models presented in Tables 4.6 and 4.7 do not appear to have good ratios of the dependant mean value to the mean square error, or good  $r^2$  values, WEPPSIE does a better of predicting trapping efficiency when using the models presented. Much of the statistical variation listed in Tables 4.6 and 4.7 is due to a one or two severe outliers.

#### **Comparison to CSTRS database**

The sedimentation algorithms presented in the Model Development (Chapter 3), including the calibration coefficient estimation models presented in this chapter, are utilized in WEPPSIE to predict an effluent sediment graph.

To determine the overall ability of WEPPSIE to predict deposition and effluent sediment concentration, a comparison between the WEPPSIE results and the CSTRS results was made using an independently generated data set. Both the estimation models presented above and mean values of  $c_t$  and  $c_d$  were used. The comparison included both small impoundments without permanent pools and larger impoundments with permanent pools. To generate an independent data set, both the small and large impoundment geometries were changed from those used in the 2000 optimization runs. Table 4.8 presents a description of the nine small impoundments, and Table 4.9 contains a description of the 10 large impoundments utilized for comparison. Comparison runs were made for twenty inflow hydrographs for each particle size class. As in the optimization runs, impoundment sizes and the relative storm sizes were chosen to be typical of the sizes encountered in watersheds modelled by WEPP. Thus, 1800 new runs were made to compare the resulting trapping efficiencies obtained with WEPPSIE containing the  $c_t$  and  $c_d$  estimation models to the trapping efficiencies obtained with the CSTRS model, and 1800 new runs were made comparing the trapping efficiencies obtained with WEPPSIE containing the mean values of  $c_t$  and  $c_d$  to the trapping efficiencies obtained with the CSTRS model.

The comparisons were made directly on the difference in trapping efficiency between the WEPPSIE results and the CSTRS results. Trapping efficiency was determined with:

Table 4.8: Description of small impoundments used in the comparison runs (areas and volumes computed at a stage of 0.5 m). Sizes typical of the range encountered in watersheds simulated by WEPP.

Area (m <sup>2</sup> )	Volume (m <sup>3</sup> )	Outlet Structure
633	117	Filter Fence
2438	444	Straw Bales
8250	1703	Rock Fill
25500	6015	Rock Fill
380	84	Perforated Riser
1774	422	Perforated Riser
2674	497	Perforated Riser
235	43	Perforated Riser
400	68	Perforated Riser



Table 4.9: Description of large impoundments used in the comparison runs (areas and volumes computed at a stage of 4.0 m). Sizes typical of the range encountered in watersheds simulated by WEPP.

Area (m <sup>2</sup> )	Volume (m <sup>3</sup> )	Riser Diameter (m)	Barrel Diameter (m)
1,016	3,083	0.46	0.30
2,016	5,550	0.46	0.30
4,138	10,606	0.46	0.30
4,697	10,483	0.91	0.46
10,459	25,283	1.22	0.61
10,459	25,283	0.91	0.46
21,647	48,222	1.83	0.91
21,647	48,222	1.22	0.61
28,443	66,845	1.83	0.91
28,443	66,845	1.22	0.61

$$TE = \frac{\text{Mass Sediment}_{in} - \text{Mass Sediment}_{out}}{\text{Mass Sediment}_{in}} \quad (4.22)$$

where TE is the trapping efficiency,  $\text{Mass Sediment}_{in}$  is the total amount of sediment entering the impoundment and  $\text{Mass Sediment}_{out}$  is the total amount of sediment exiting the impoundment. The difference in trapping efficiency predicted by WEPPSIE and the CSTRS model was determined with:

$$TE_{\text{difference}} = \text{ABS} (TE_{\text{CSTRS}} - TE_{\text{WEPP}}) \quad (4.23)$$

where  $TE_{\text{difference}}$  is the difference in the trapping efficiencies,  $TE_{\text{CSTRS}}$  and  $TE_{\text{WEPP}}$  are the trapping efficiencies determined with the CSTRS model and WEPPSIE respectively.

Three different estimation methods for  $c_i$  and  $c_d$  were used in WEPPSIE:

1. The estimation models as presented above were used.
2. Mean values of  $c_i$  and  $c_d$  computed from the optimization runs for small impoundments were used for comparison runs on small impoundments, and mean values of  $c_i$  and  $c_d$  computed from the optimization runs for large impoundments were used for comparison runs on large impoundments.
3. Overall mean values of  $c_i$  and  $c_d$  computed from the optimization runs for both small impoundments and large impoundments were

used for comparison runs on both large and small impoundments.

Results of the comparison for small impoundments are presented in Tables 4.10, 4.11, and 4.12. Table 4.10 presents the small impoundment results when using the estimation models presented above in WEPPSIE. Table 4.11 presents the results when using the average  $c_t$  and  $c_d$  values computed from small impoundment optimization data in WEPPSIE; and Table 4.12 presents results when using the average  $c_t$  and  $c_d$  values computed from small and large impoundment optimization data in WEPPSIE. Figures 4.2 and 4.3 illustrate how the differences in trapping efficiencies vary with the ratio of storm volume to a fixed pond volume when using the specific estimation models for each size class.

The results for small impoundments presented in Tables 4.10, 4.11, and 4.12 indicate that using the estimation models for  $c_t$  and  $c_d$  (scenario 1) in WEPPSIE provides the best trapping efficiency predictions. When using the estimation models in the WEPPSIE algorithms, WEPPSIE predicts an average trapping efficiency difference within 0.1 % for sand particles to 5.8 % for small aggregates as compared to the results from the CSTRS model. Table 4.11 shows the loss of accuracy that occurs when the average values of  $c_t$  and  $c_d$  computed from the small impoundment optimization data (scenario 2) were used in WEPPSIE; the average difference in trapping efficiency predicted with WEPPSIE ranged from 2.4 % for large aggregates to 12.0 % for clay particles as compared to the CSTRS results. Further loss of accuracy occurs when the

Table 4.10: Results on small impoundments using the estimation models presented above.

ABS(TEcstrs - TEwepp) (TEcstrs - TEwepp)			
CLAY	4.92%	-4.26%	MEAN
	4.45%	5.09%	STD
	19.20%	8.71%	MAX
SILT	3.35%	1.85%	MEAN
	2.95%	4.06%	STD
	11.73%	11.73%	MAX
SM AGG	6.19%	5.46%	MEAN
	3.98%	4.94%	STD
	16.18%	16.18%	MAX
SAND	0.09%	-0.04%	MEAN
	0.17%	0.19%	STD
	0.88%	0.88%	MAX
LG AGG	0.23%	-0.15%	MEAN
	0.30%	0.35%	STD
	1.14%	0.78%	MAX

Table 4.11: Results on small impoundments using the mean values of  $c_t$  and  $c_d$  computed with the optimization data for small impoundments.

ABS(TEcstrs - TEwepp) (TEcstrs - TEwepp)			
CLAY	11.96%	-11.89%	MEAN
	9.75%	9.84%	STD
	36.28%	2.09%	MAX
SILT	6.38%	1.69%	MEAN
	6.48%	8.94%	STD
	28.83%	28.83%	MAX
SM AGG	6.76%	-0.25%	MEAN
	5.15%	8.49%	STD
	25.90%	25.90%	MAX
SAND	2.70%	2.64%	MEAN
	7.95%	7.97%	STD
	28.52%	28.52%	MAX
LG AGG	2.38%	2.18%	MEAN
	6.38%	6.45%	STD
	23.76%	23.76%	MAX

Table 4.12: Results on small impoundments using the mean values of  $c_t$  and  $c_d$  computed with the optimization data for both small and large impoundments.

ABS(TEcstrs - TEwepp) (TEcstrs - TEwepp)			
CLAY	47.11%	-47.11%	MEAN
	20.14%	20.14%	STD
	72.19%	-3.18%	MAX
SILT	5.86%	-2.09%	MEAN
	3.84%	6.69%	STD
	21.88%	21.88%	MAX
SM AGG	7.77%	-5.37%	MEAN
	4.59%	7.25%	STD
	19.73%	19.73%	MAX
SAND	1.47%	1.40%	MEAN
	4.30%	4.32%	STD
	15.83%	15.83%	MAX
LG AGG	1.25%	1.00%	MEAN
	3.33%	3.41%	STD
	12.29%	12.29%	MAX

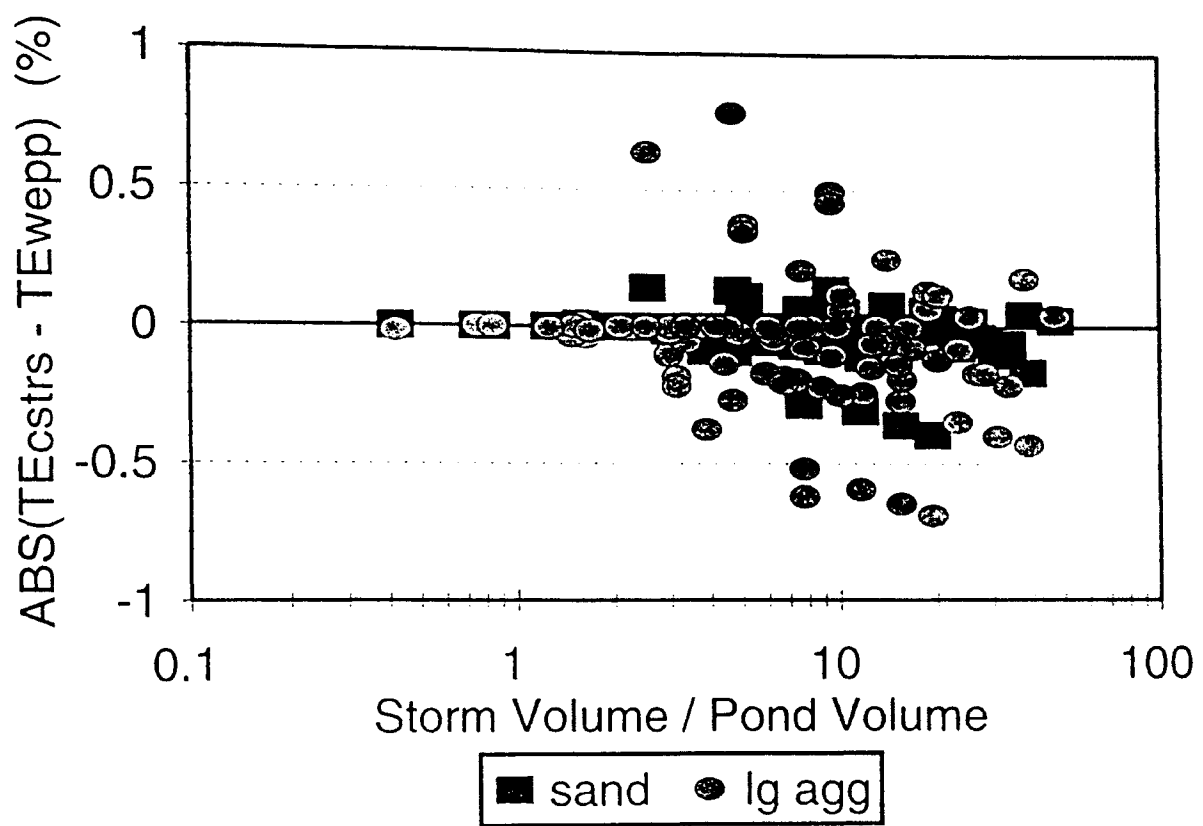


Figure 4.3: Trapping efficiency difference between the WEPPSIE and CSTRS predictions for small impoundments when using the estimation models computed for small impoundments.

overall average values of  $c_t$  and  $c_d$  computed from small and large impoundment optimization data (scenario 3) are used in WEPPSIE. The average difference in trapping efficiency as shown in Table 4.9, for this scenario, ranged from 1.5 % for large aggregates to 47.1 % for clay particles.

Results for large impoundments are presented in Tables 4.13, 4.14, and 4.15. Table 4.13 presents the large impoundment results when using the estimation models presented above in WEPPSIE (scenario 1). Table 4.14 presents the results when using the average  $c_t$  and  $c_d$  values computed from large impoundment optimization data in WEPPSIE (scenario 2); and Table 4.15 presents results when using the average  $c_t$  and  $c_d$  values computed from small and large impoundment optimization data in WEPPSIE (scenario 3). Figures 4.4 and 4.5 illustrate how the differences in trapping efficiencies vary with the ratio of storm volume to a fixed pond volume when using the specific estimation models for each size class.

The results for large impoundments presented in Tables 4.13, 4.14, and 4.15 indicate that using the estimation models for  $c_t$  and  $c_d$  presented above in WEPPSIE provide the best trapping efficiency predictions. When using the estimation models in the WEPPSIE algorithms, WEPPSIE predicts an average trapping efficiency difference ranging from 0.6 % for large aggregates to 4.0 % for clay particles as compared to the results from the CSTRS model. Table 4.14 shows the loss of accuracy that occurs when the average values of  $c_t$  and  $c_d$  computed from the large impoundment optimization data were used in



Table 4.13: Results on large impoundments using the estimation models presented above.

ABS(TEcstrs - TEwepp) (TEcstrs - TEwepp)			
CLAY	4.01%	-4.54%	MEAN
	3.64%	3.69%	STD
	12.64%	2.83%	MAX
SILT	3.09%	-1.31%	MEAN
	2.50%	3.75%	STD
	12.64%	6.94%	MAX
SM AGG	3.93%	-3.51%	MEAN
	2.98%	3.46%	STD
	14.40%	3.47%	MAX
SAND	0.84%	0.53%	MEAN
	0.94%	1.14%	STD
	6.67%	5.37%	MAX
LG AGG	0.62%	0.21%	MEAN
	0.58%	0.82%	STD
	3.26%	1.73%	MAX

Table 4.14: Results on large impoundments using the mean values of  $c_t$  and  $c_d$  computed with the optimization data for large impoundments.

ABS(TEcstrs - TEwepp) (TEcstrs - TEwepp)			
CLAY	9.20%	-7.92%	MEAN
	7.24%	8.62%	STD
	28.20%	9.31%	MAX
SILT	4.74%	-3.19%	MEAN
	4.43%	5.64%	STD
	18.39%	10.32%	MAX
SM AGG	6.26%	-5.28%	MEAN
	5.18%	6.18%	STD
	21.13%	6.08%	MAX
SAND	2.33%	1.88%	MEAN
	3.20%	3.49%	STD
	14.00%	14.00%	MAX
LG AGG	1.69%	0.92%	MEAN
	1.80%	2.29%	STD
	10.45%	10.45%	MAX

Table 4.15: Results on large impoundments using the mean values of  $c_t$  and  $c_d$  computed with the optimization data for both small and large impoundments.

ABS(TEcstrs - TEwepp) (TEcstrs - TEwepp)			
CLAY	6.02%	-2.84%	MEAN
	4.21%	6.78%	STD
	16.34%	12.79%	MAX
SILT	4.42%	-0.50%	MEAN
	3.56%	5.65%	STD
	15.87%	13.16%	MAX
SM AGG	5.04%	-2.62%	MEAN
	4.37%	6.13%	STD
	18.79%	8.51%	MAX
SAND	4.60%	4.31%	MEAN
	5.33%	5.56%	STD
	20.66%	20.66%	MAX
LG AGG	3.51%	3.16%	MEAN
	3.61%	3.92%	STD
	15.63%	15.63%	MAX

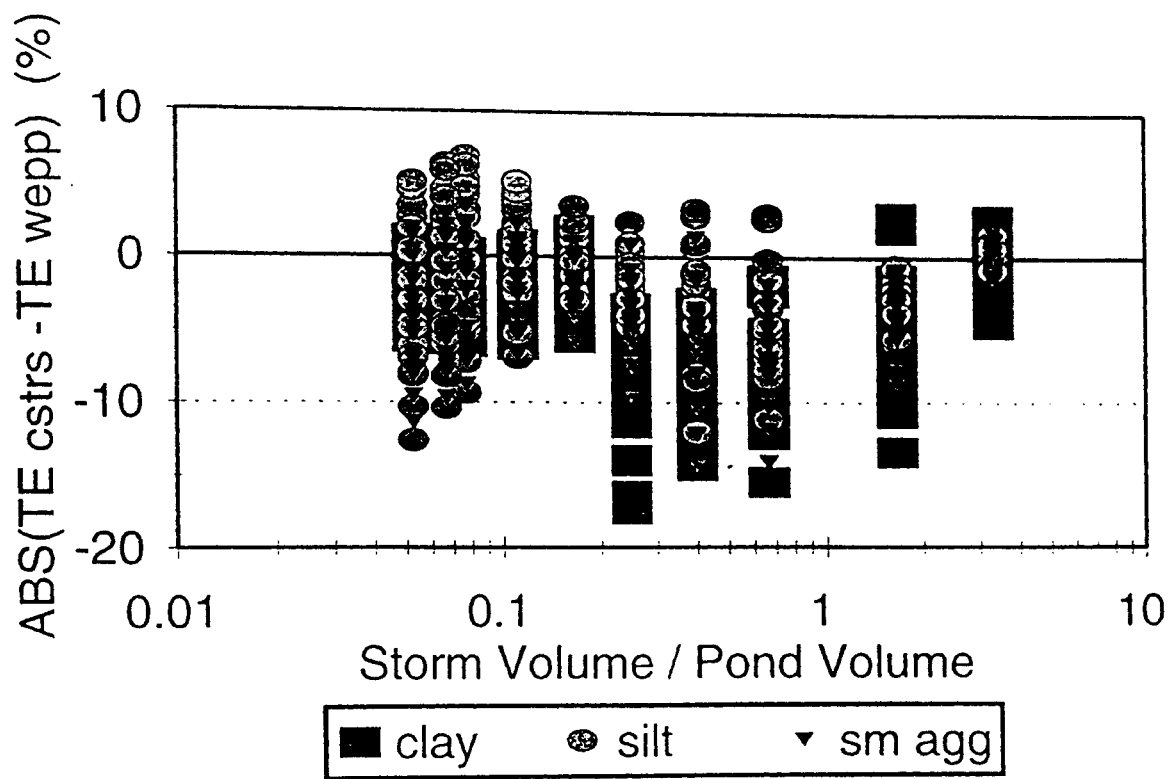


Figure 4.4: Trapping efficiency difference between the WEPPSIE and CSTRS predictions for large impoundments when using the estimation models computed for large impoundments.

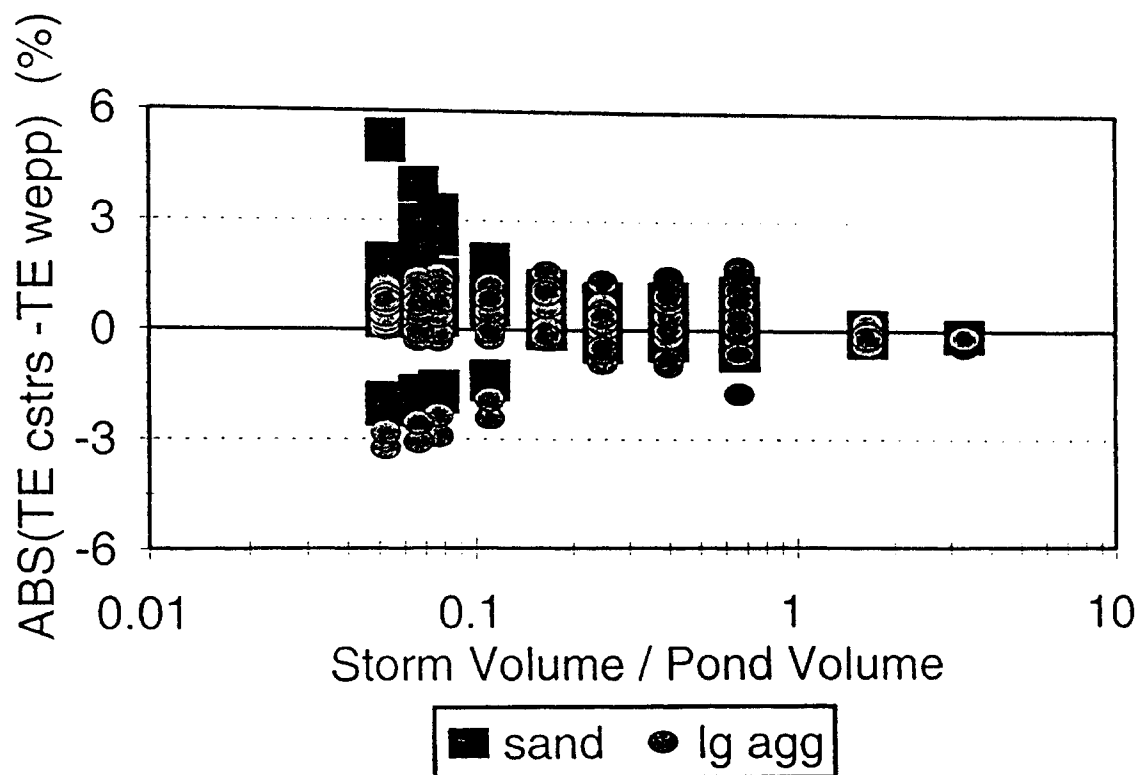


Figure 4.5: Trapping efficiency difference between the WEPPSIE and CSTRS predictions for large impoundments when using the estimation models computed for large impoundments.

WEPPSIE. The average difference in trapping efficiency predicted with WEPPSIE for this scenario ranged from 1.7 % for large aggregates to 9.2 % for clay particles as compared to the CSTRS results. The average trapping difference is similar when the average values of  $c_t$  and  $c_d$  computed from small and large impoundment optimization data are used in WEPPSIE. Table 4.15 shows the average difference in trapping efficiency predicted by WEPPSIE ranged from 3.5 % for large aggregates to 6.0 % for clay particles.

Using the estimation models presented in Tables 4.6 and 4.7 results in predicted trapping efficiencies that average within 0.1 % to 5.8 % of the trapping efficiencies predicted by the CSTRS model. Using the estimation models provided better predictions than using mean values for  $c_t$  and  $c_d$ . Further, even a difference of 5.8 % in predicted trapping efficiency is well within the WEPP criteria which is shooting for a ten percent observed minus predicted limit. Therefore, the estimation models provide an improvement over using mean values and provide predictions that are within the WEPP limitations. The reader should note that for clay particles, The trapping efficiency predicted by WEPPSIE was consistently higher than the trapping efficiency predicted by CSTRS, this should be taken into account when making decisions with the results from WEPPSIE.

## **Chapter 5: Validation**

Validation is important because it lends credibility to the algorithms and code that make up the WEPP Surface Impoundment Element (WEPPSIE). First, the hydraulic routing procedure is validated for 50 simulations against the PULS routing method that is incorporated in SEDIMOT (Wilson et al., 1982) and SEDCAD (Warner and Schwab., 1992). Then the stage-discharge relationships which have been modified for inclusion in the impoundment element are validated. Specifically, the regression relationships utilized for perforated risers and open channel outlets, and the numerical simplification of the Herrera (1989) method for determining flow through rock fill check dams are validated. The stage-discharge relationships utilized for drop spillways, culverts, filter fence check dams, and straw bale check dams have all enjoyed wide spread use, and all have been validated previously in the literature (see Chapter 2). Finally, the sedimentation algorithms are validated against a large data base created with the CSTRS (Wilson and Barfield, 1984) model and several empirical data sets collected on model ponds.

### **Hydraulic Routing**

The predicted outflow hydrographs for WEPPSIE have been compared to the resulting outflow hydrographs produced by the PULS routing method incorporated in the CSTRS model. A total of 50 simulations were used (Table 5.1). All the inflow hydrographs had a 6 hour duration which is typical of the

watersheds simulated by WEPP, although the duration is not important for the rectangular hydrographs. Two typical outflow hydrograph comparisons appear in Figures 5.1 and 5.2. The peak outflow predicted by WEPPSIE is compared to the peak outflow predicted by PULS routing method in Figure 5.3. The results are visually very favorable.

As mentioned in Chapter 2, the numerical adaption of the PULS routing method included in the CSTRS model utilizes linear interpolation of stage-area-discharge values between discrete stage points. To minimize errors resulting from such an interpolation, at least fifteen stage-area-discharge points were entered into the CSTRS model. Particular emphasis was placed on using many points in the regions of the stage-discharge relationship in which the discharge was changing quickly. As discussed in the Chapter 3, WEPPSIE utilizes continuous functions to predict area and discharge as functions of stage.

The excellent agreement in Figures 5.1, 5.2, and 5.3 indicates that the impoundment element performs hydraulic routing at an accuracy comparable to the hydraulic routing component used in the CSTRS model. In Figure 5.2 the CSTRS prediction appears to have a slight numerical error on the increasing section of the predicted outflow hydrograph, resulting in the slight deviations seen in Figure 5.3.

The outflow hydrographs for two of the ponds have been compared to the outflow hydrographs produced by the CSTRS model when only five stage-area-discharge points were utilized into the hydraulic routing procedure included



Table 5.1: Summary of input data used for validation of the hydraulic routing.

Pond Volume (m <sup>3</sup> )	Runoff Volume (m <sup>3</sup> )	Riser Size (m)	Barrel Size (m)
3,823	987 - 11,347	0.91	0.46
7,770	1,973 - 23,309	1.22	0.61
15,663	3,947 - 47,112	1.83	0.91
15,663	3,947 - 47,112	0.91	0.46
34,286	8,510 - 102,733	1.83	1.22
34,286	8,510 - 102,733	0.91	0.46
69,682	17,390 - 208,921	2.74	1.83
69,682	17,390 - 208,921	0.91	0.46
97,307	24,296 - 291,922	4.57	2.74
97,307	24,296 - 291,922	0.91	0.46

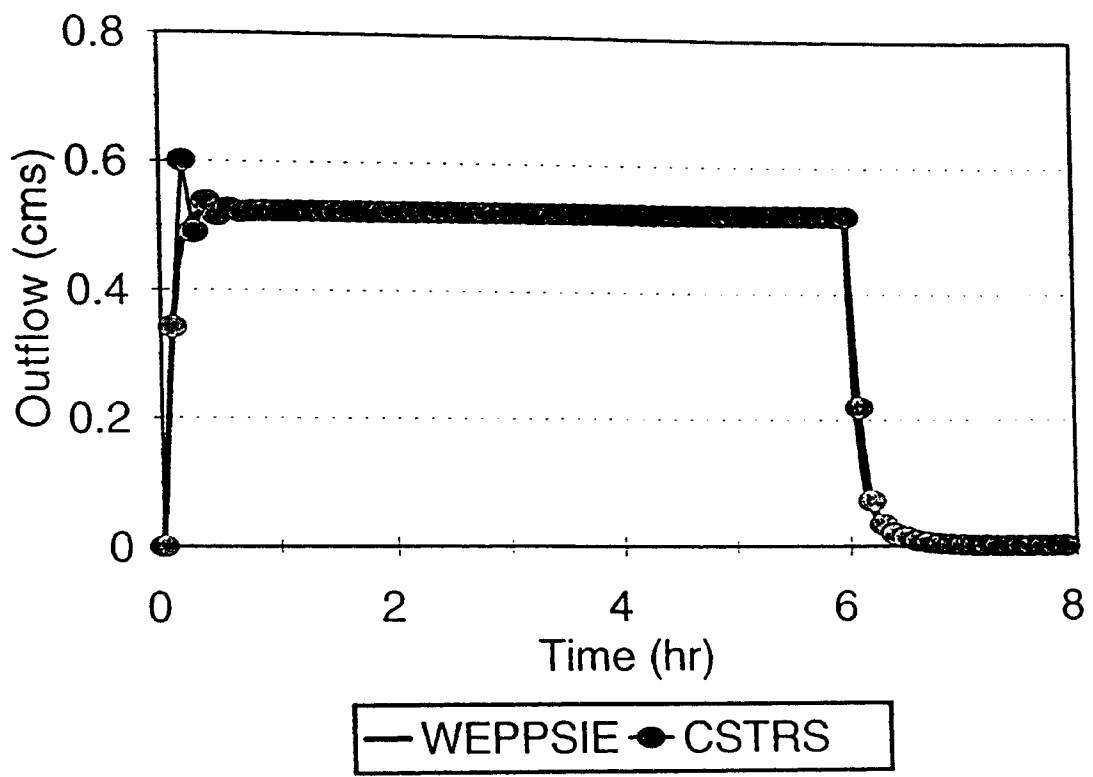


Figure 5.1: Outflow hydrograph comparison for the 7770 m<sup>3</sup> pond.

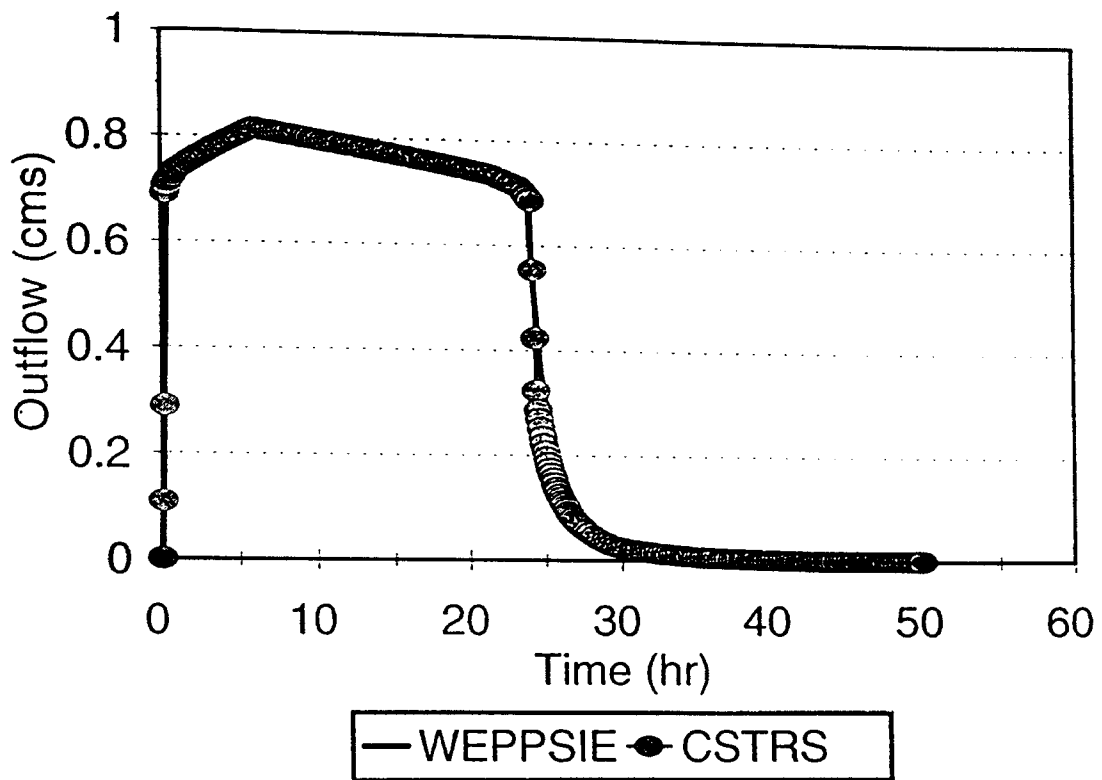


Figure 5.2: Outflow hydrograph comparison for a 15,663 m<sup>3</sup> pond.

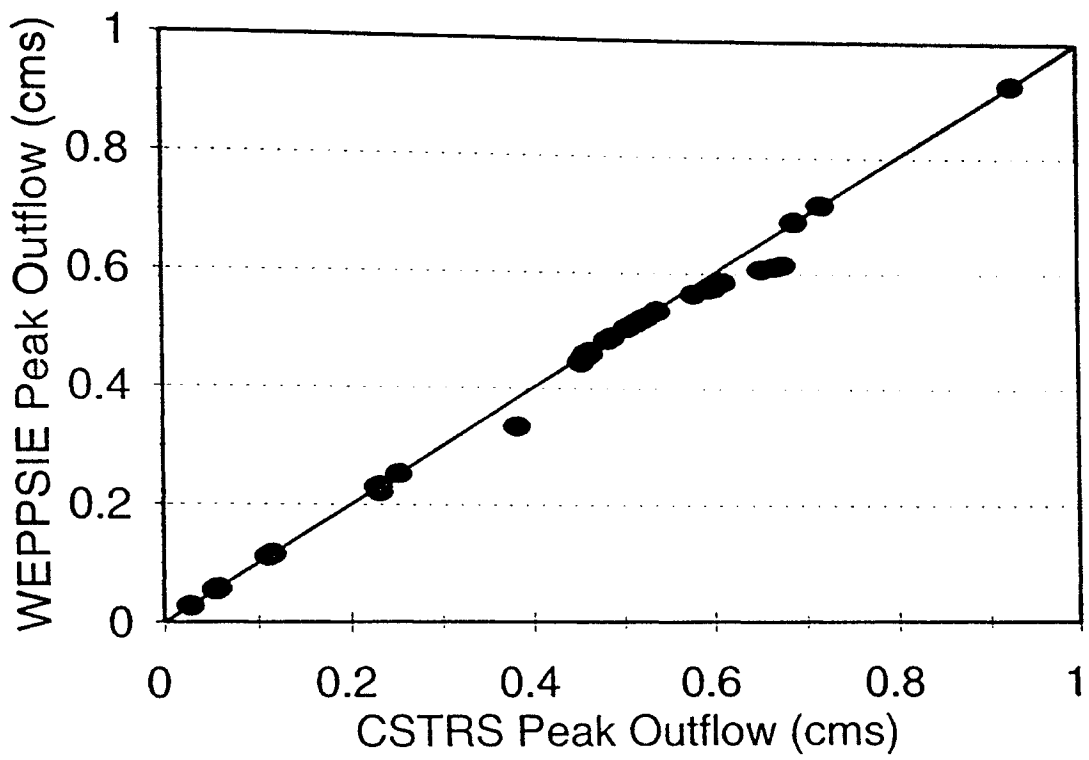


Figure 5.3: Comparison of peak outflows for the 10 impoundments presented in Table 5.1.

in CSTRS. These outflow hydrograph comparisons appear in Figures 5.4 and 5.5, illustrating the errors that occur from linear interpolation.

The hydraulic routing in WEPPSIE has advantages over the PULS hydraulic routing included in the CSTRS model. First, the adaptive time step allows the hydraulic routing in WEPPSIE to perform much faster than the PULS routing method. The adaptive time step utilized in WEPPSIE will increase the time step to several hours without sacrificing accuracy when the inflow and outflow rates are relatively constant. Secondly, the hydraulic routing in the WEPP impoundment element can potentially perform far more accurately than the hydraulic routing included in the CSTRS model. This results from continuous outflow functions used in basic WEPPSIE routing procedure. Conversely, the numerical adaption of the PULS routing procedure included in the CSTRS model linearly interpolates between the outflows computed at the stage points entered by the user. Figures 5.4 and 5.5 illustrate that the outflow hydrograph drifted from the true outflow hydrograph when only five stage points are entered by the user.

### **Stage-Discharge Relationships**

The previous section shows that, given the correct stage-discharge relationship, the hydraulic routing procedure in the WEPPSIE performs at least as well as the PULS hydraulic routing procedure included in the CSTRS model. The stage-discharge relationships included in WEPPSIE for drop spillways, culverts, filter fence check dams, and straw bale check dams have been

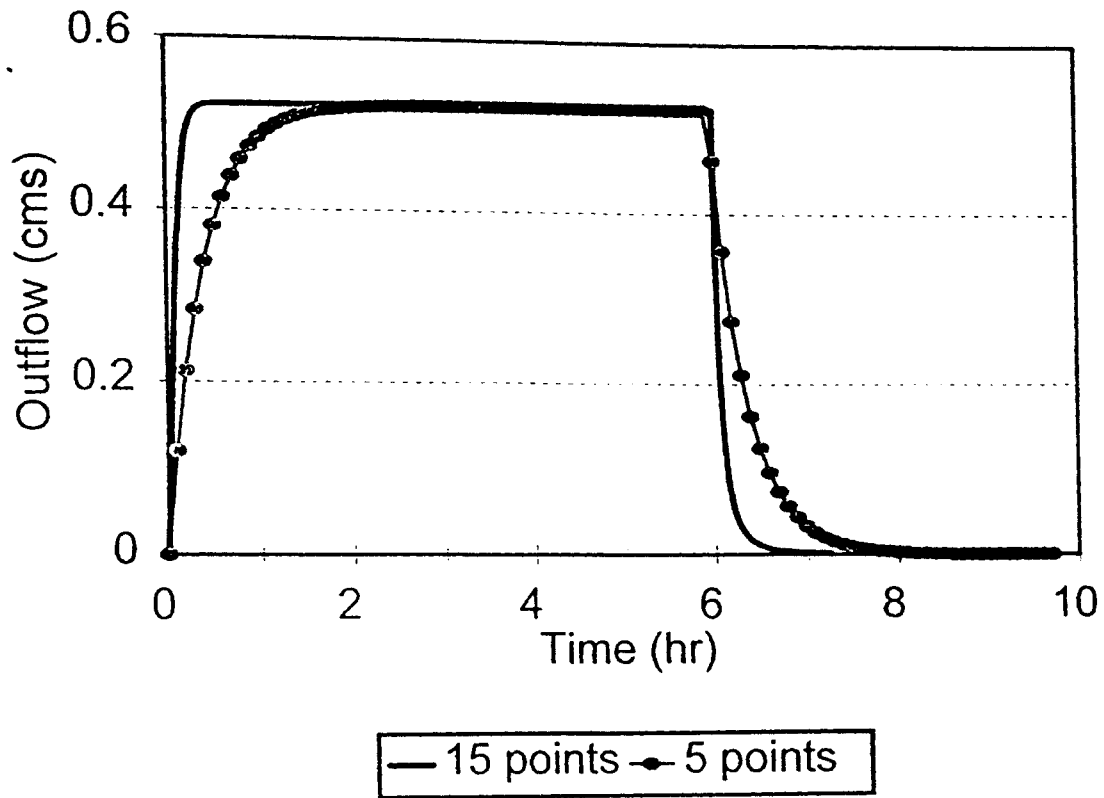


Figure 5.4: Outflow hydrograph comparison using five and fifteen stage-discharge points in the CSTRS model for the 7770 m<sup>3</sup> pond.

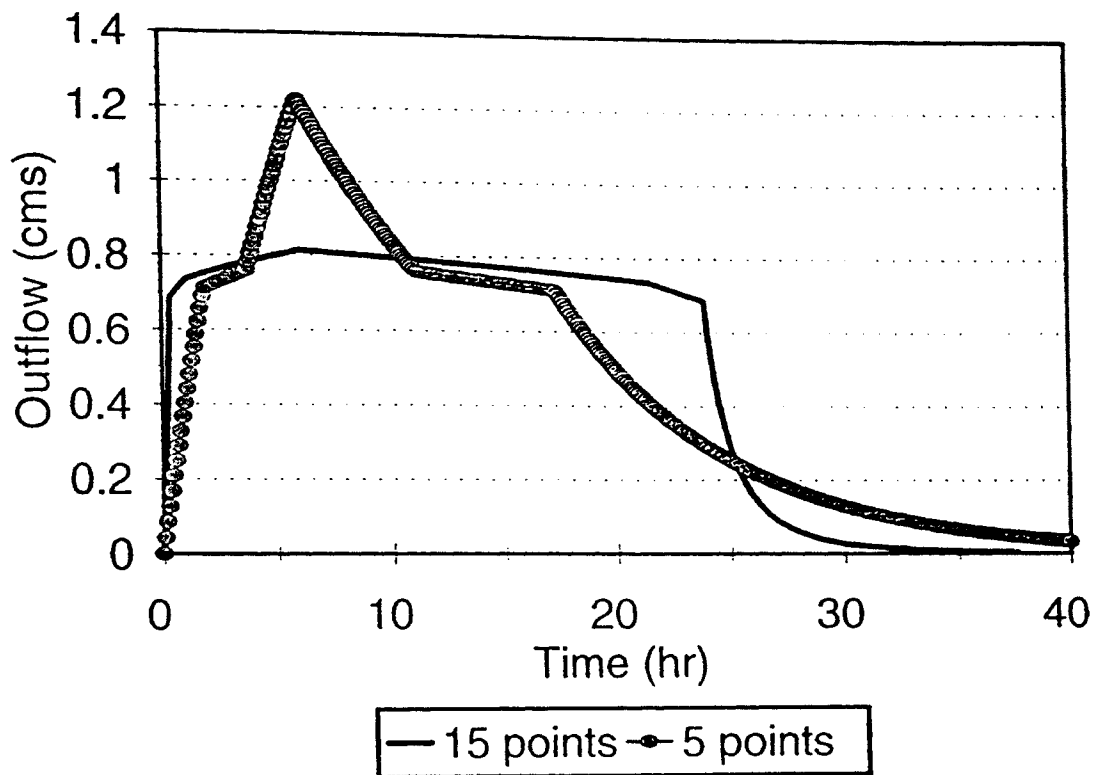


Figure 5.5: Outflow hydrograph comparison using five and fifteen stage-discharge points in the CSTRS model for a 15,663 m<sup>3</sup> pond.

validated previously in the literature (see Chapter 2). The stage-discharge relationships for perforated risers, open channels, and rock fill check dams have been modified for inclusion in the impoundment element. The modified methods of obtaining discharge will be validated. Specifically, the power function regression relationship utilized for perforated risers, the fourth-order polynomial regression relationship utilized for open channel outlets, and the numerical simplification of the Herrera (1989) method for determining flow through rock fill check dams will be validated.

### **Perforated Risers**

To accurately determine the discharge for a perforated riser with a given driving head, McEnroe et al. (1988) presented an experimentally validated procedure that requires an iterative, simultaneous solution of two of six possible equations. For a daily simulation lasting twenty years, this procedure would be far too computationally expensive. To determine the discharge directly from a given stage, a regression equation was developed using stage-discharge relationships for ten perforated risers computed according to the McEnroe et al., (1988) procedure described in the Model Development section (Chapter 3). Two stage-discharge relationships computed with the regression equation are compared to stage-discharge relationships computed according to the McEnroe et al. (1988) procedure to show that the regression equation provides a reasonable representation of the McEnroe et al. (1988) procedure.

The regression equation utilized to determine the discharge for a given



stage is presented as Equation 3.11 in the Model Development section. The regression equation is compared in Figures 5.6 and 5.7 against two stage-discharge relationships computed by the McEnroe et al. (1988) procedure. The two perforated risers had a 102 mm riser diameter, 1.1 m riser height, 12.7 mm diameter slots covering the upper 0.9 m of riser height ( $h_s = 0.9$  m) and bottom orifice plate diameter of 50.8 mm. One of the risers had a bottom orifice plate located at the base of the slots ( $h_b = 0$  m) and the other had a bottom orifice plate located 0.9 m below the bottom of the slots ( $h_b = 0.9$  m). Figure 2.12 illustrates a schematic of the perforated riser and should be consulted for a definition of terms. The excellent agreement seen in Figures 5.6 and 5.7 indicates that the regression relationship presented in Equation 3.11 does a reasonable job of predicting the discharge for a given stage as compared to the validated McEnroe et al. (1988) procedure.

### **Emergency Spillways and Open Channels**

To accurately determine the discharge through an open channel or emergency spillway outlet, a water surface profile must be employed. The steady-state standard step method (Chow, 1959) has seen wide spread use. For a twenty-year simulation performed on a daily basis, utilizing the iterative standard step method would be far too computationally expensive. To expedite the determination of discharge for a given stage, a fourth-order polynomial is utilized with the coefficients of the polynomial computed from a series of stage-discharge points calculated with the steady state standard step method.

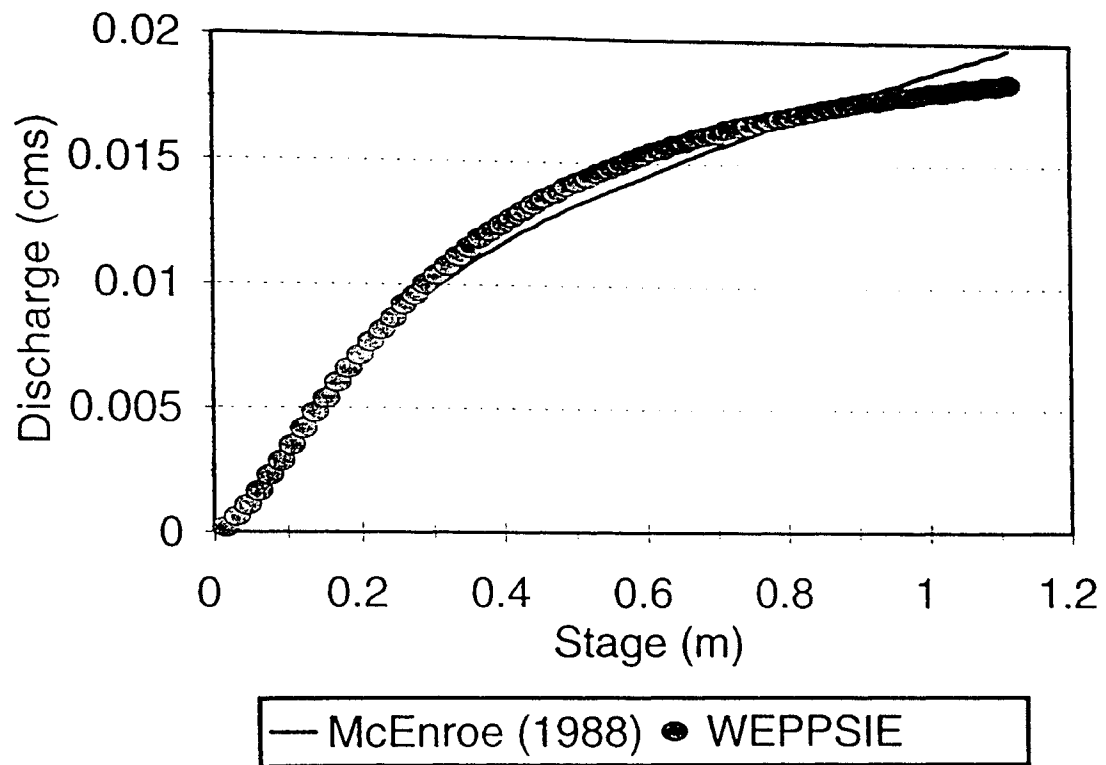


Figure 5.6: Comparison between the stage-discharge relationship computed according to the McEnroe et al. (1988) procedure and the regression relationship in WEPPSIE ( $h_b = 0.0$  m).

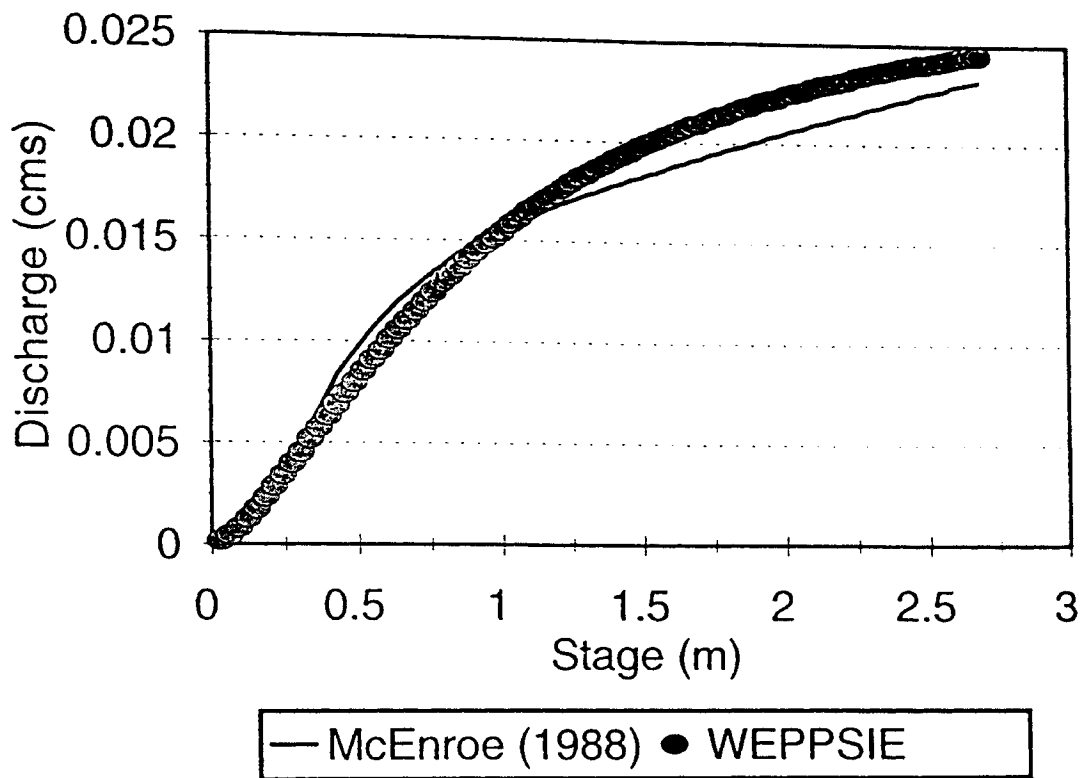


Figure 5.7: Comparison between the stage-discharge relationship computed according to the McEnroe et al. (1988) procedure and the regression relationship in WEPPSIE ( $h_b = 0.9$  m).

The fourth-order polynomial was chosen because it provided a reasonable compromise between accuracy, stability, and complexity. The stage-discharge relationship is computed with a steady-state standard step method routine written and validated by Fogle and Barfield (1992). To show that the polynomial regression adequately represents discharge as predicted by the steady-state standard step method, the stage-discharge relationship computed with the Fogle and Barfield (1992) routine is compared to the stage-discharge relationship computed with the polynomial regression equation presented as Equation 3.14.

Comparisons have been made for two different open channel outlets. One was a trapezoidal open channel 6 m wide with 3:1 side slopes without a control section. It had 12.2 m approach on a -4 % slope, a 3 m flat crest, and an exit slope of 0.015 %. Figure 5.8 presents a comparison of the stage-discharge relationship computed with the Fogle and Barfield (1992) routine and the stage-discharge relationship computed with the polynomial regression equation, Equation 3.14. The other channel was a trapezoidal emergency spillway 10 m wide with 4:1 side slopes and a control section. It had a 40.2 m approach on a -10 % slope, a 10 m flat crest, and an exit slope of 0.15 %. Figure 5.9 presents a comparison of the stage-discharge relationship computed with the Fogle and Barfield (1992) routine and the stage-discharge relationship computed with the polynomial regression equation, Equation 3.14. The agreement seen in Figures 5.8 and 5.9 lends credibility to the use of a

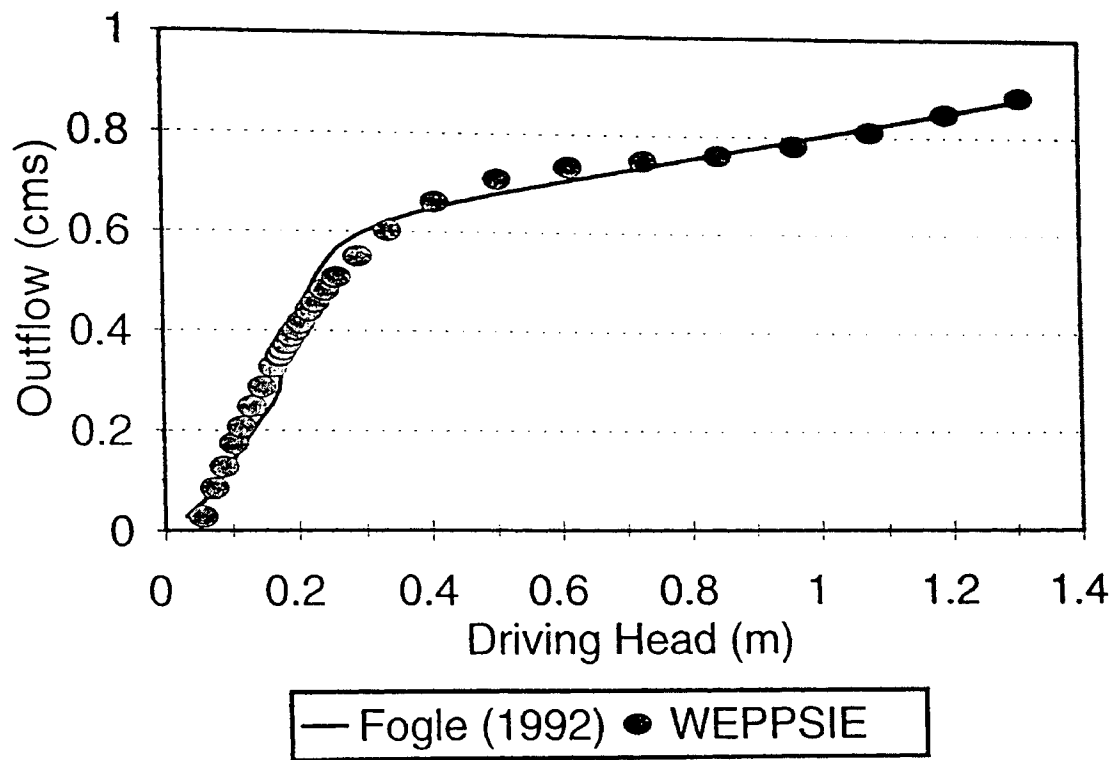


Figure 5.8: Comparison of the stage-discharge relationship for an open channel outlet without control produced by the steady-state standard step method and the polynomial regression equation included in WEPPSIE.

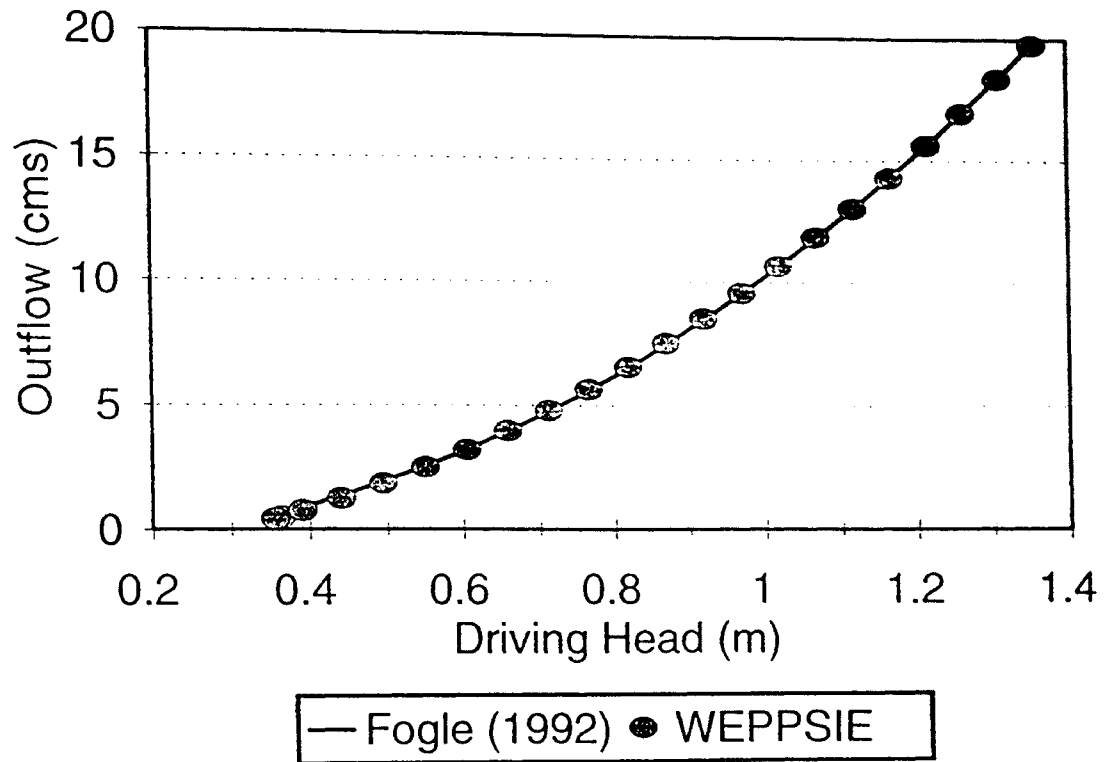


Figure 5.9: Comparison of the stage-discharge relationship for an emergency spillway with control outlet produced by the steady-state standard step method and the polynomial regression equation included in WEPPSIE.

polynomial to provide a stage-discharge relationship through an open channel.

### **Rock Fill Check Dams**

The Herrera (1989) procedure is the best procedure available to compute the discharge for a given stage through a rock fill check dam. However, the Herrera (1989) procedure requires a time consuming iterative process. Haan et al. (1994) published a graphical adaptation of the Herrera (1989) procedure limited to two reasonable assumptions; (1) a rock fill porosity of 0.46; and (2) a standard deviation of the rock fill diameter equal to half the mean rock fill diameter. In order to quickly determine the discharge for a given stage through a rock fill check dam, WEPPSIE employs a numerical adaptation of the Haan et al. (1994) graphical procedure. The procedure is described in the Model Development section (Chapter 3), and is subject to the same limiting assumptions for porosity and rock fill standard deviation. In order to validate that the numerical adaptation of the Haan et al. (1994) procedure is correctly utilized in WEPPSIE, the results using the Herrera (1989) procedure are compared to the results using the procedure included in WEPPSIE.

The WEPPSIE procedure has been validated for four flow rates on four different rock fill structures. The four rock fill check dams utilized rock fill with mean diameters of 0.025 m and 0.25 m. Each rock fill diameter was used for two check dams; 1.6 m and 2.3 m long. The results are shown in Figure 5.10 comparing the Haan et al. (1994) procedure included in WEPPSIE with flow rates computed according to the Herrera (1989) procedure for identical rock fill

check dams. The points plotted in Figure 5.10 illustrate that the WEPPSIE procedure performs well when the limiting assumptions are met.

## **Sedimentation Algorithms**

The sedimentation algorithms were validated against a database created with the CSTRS model and experimental data gathered by Tapp et al. (1981) and Wilson et al. (1984). Validation against the CSTRS model is particularly valuable since an extensive data set can be created for impoundments with a wide range of shapes, sizes, and outflow structures. The CSTRS model has been previously shown to have acceptable accuracy (Wilson and Barfield, 1984). Validation against real data is also valuable, showing that WEPPSIE adequately represents experimental data. Unfortunately there are few data sets that include all the information necessary to make a good validation run. WEPPSIE was validated against experimental data collected by Tapp et al. (1981) and Wilson et al. (1984) for eleven events on two small experimental sediment ponds.

A detailed description of the validation runs against the CSTRS database was presented in Chapter 4 to prove that the regression models used to predict the calibration coefficients,  $c_t$  and  $c_d$ , in WEPPSIE worked well. The results, based on the difference in predicted trapping efficiency, were very favorable. For small impoundments, the average difference in predicted trapping efficiency ranged from 0.1 % for sand particles to 5.8 % for small aggregates, and for large impoundments, the average difference in predicted trapping efficiency



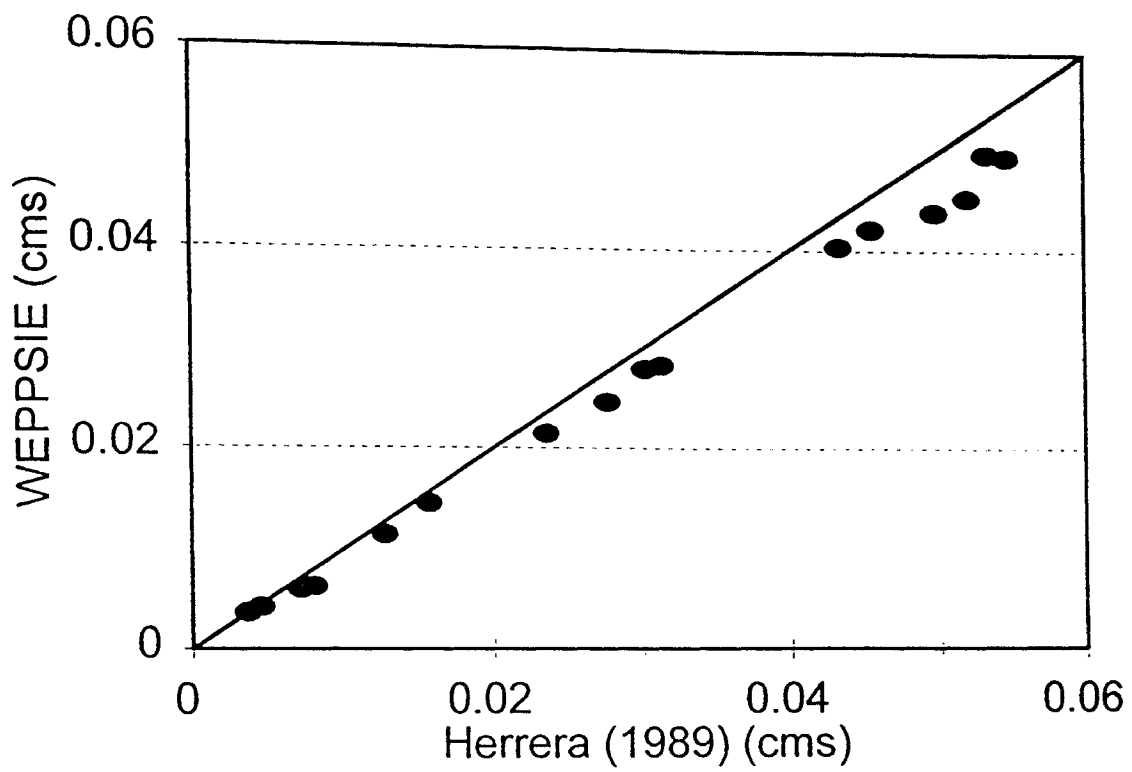


Figure 5.10: Comparison of the stage-discharge relationship for a rock fill check dam produced by the Herrera (1989) procedure and the procedure included in WEPPSIE.

ranged from 0.6% for large aggregates to 4.0 % for clay particles. However, the predicted trapping efficiency for clay particles was consistently higher than the trapping efficiency predicted by the CSTRS model.

Finding empirical data sets suitable for the validation of the sedimentation algorithms utilized in WEPPSIE proved very difficult. Suitable data sets for validation of WEPPSIE, had to include the following data:

1. Inflow hydrograph and influent sediment graph.
2. Outflow hydrograph and effluent sediment graph.
3. Influent sediment size distribution.
4. Stage-area and stage-length relationships.

Most of the data sets presented in the literature are missing one or more of the necessary pieces of information. Both Tapp et al. (1981) and Wilson et al. (1984) reported data on experimental scale impoundments with variable inflow rates and influent concentrations that included all the necessary information.

The Tapp et al. (1981) data set utilized a pilot scale pond 1.24 m wide and 6.1 m long. The Tapp et al. (1981) data set was collected to analyze the effects of chemical flocculation. Since flocculation processes are neglected in WEPPSIE, five of the Tapp et al. (1981) runs that did not include chemical flocculation were utilized to validate WEPPSIE. Peak inflow rates and peak influent concentrations for the five Tapp et al. (1981) runs utilized are summarized in Table 5.2. Tapp et al. (1981) encountered problems obtaining their data set. The inflow sediment size distribution was highly variable during

a run due to sediment deposition behind valves and in pipes. The sediment size distribution utilized in the validation of WEPPSIE was the average distribution computed near the peak inflow rate, as recommended by Tapp et al. (1981). Tapp et al. (1981) did not treat their system to prevent natural flocculation, which can have a significant effect on sediment size distribution and settling characteristics. Despite the shortcomings of the Tapp et al. (1981) data set, it was one of the only studies available that included the information necessary for the validation of the WEPPSIE sedimentation algorithms.

The Wilson et al. (1984) data set utilized a triangular shaped, pilot scale impoundment with a 3 m base width and a 3.4 m length. Six runs made by Wilson et al. (1984) were utilized to validate WEPPSIE. Peak inflow rates and peak influent concentrations for the Wilson et al. (1984) runs are summarized in Table 5.2. Wilson et al. (1984) improved upon the experimental apparatus used by Tapp et al. (1981) by redesigning the sediment delivery system to minimize deposition in pipes and behind valves. The influent particle size distributions were relatively constant with time. Wilson et al. (1984) also chemically treated the inflow to prevent natural flocculation.

Both the Tapp et al. (1981) and Wilson et al. (1984) data sets utilized variable inflow rates and influent concentrations. The WEPPSIE sedimentation algorithms were developed based upon the WEPP convention which specifies rectangular inflow hydrographs and sediment graphs. In order to validate the WEPPSIE sedimentation algorithms with variable inflow rates and influent

Table 5.2: Summary of inflow rates and influent sediment concentrations for empirical validation runs.

Data Set	Run Number	Peak Inflow Rate (l/min)	Peak Influent Concentration (mg/l)
Tapp et al. (1981)	18	53	1330
	19	59	19,500
	22	24	17,800
	24	102	17,800
	28	102	76,000
Wilson et al. (1984)	1	78	86,000
	2	38	104,000
	3	68	91,000
	4	31	25,000
	5	62	19,000
	6	36	15,000

sediment concentrations, break point inflow rate and influent sediment concentration were utilized for each time step. The depositional routines utilized in WEPPSIE include two statements for deposition, one to be utilized before the time of inflow and one to be used after. The inflow time is defined utilizing an equivalent rectangular inflow hydrograph as:

$$T_i = \frac{Vol_{in}}{Q_{in\ max}} \quad (5.1)$$

where the  $Vol_{in}$  is the inflow volume and  $Q_{in\ max}$  is the peak inflow rate. When  $t < T_i$ , Equation 3.35 is utilized to compute deposition. In a run following the WEPP convention, during this time there would be inflow at the constant peak inflow rate and deposition would be determined using the peak inflow rate and influent concentration. When  $t > T_i$ , Equation 3.36 is utilized in the computation of deposition. Following the WEPP convention, during this time there would be no inflow and Equation 3.36 computes deposition based upon the sediment concentration in the impoundment and settling velocity. To utilize the WEPPSIE code with a variable rate inflow hydrograph, the inflow time is determined according to Equation 5.1 and Equations 3.35 and 3.36 are utilized when  $t < T_i$  and  $t > T_i$ , respectively. Although not completely accurate, these adjustments make a rough comparison between the effluent concentrations predicted by the WEPPSIE sedimentation algorithms and the observed effluent concentrations possible. However, the assumption of a rectangular inflow

hydrograph and sediment graph upon which the WEPPSIE sedimentation algorithms are based have not been met. Therefore, computing deposition according to Equations 3.35 and 3.36 is not expected to agree perfectly. Since the depositional statement (Equation 3.36) used after the time of inflow does not include any settling of incoming sediment, the effluent sediment concentrations predicted by WEPPSIE are expected to be somewhat higher than the observed sediment concentrations.

The trapping efficiency predicted by WEPPSIE and the CSTRS model are compared to the observed trapping efficiency in Table 5.3. The trapping efficiency predicted with the CSTRS model is included as a comparison of the prediction accuracy of the WEPPSIE algorithms. Trapping efficiency is not predicted as well by WEPPSIE as CSTRS, and tends to be slightly lower than the observed trapping efficiency. The difference in the WEPPSIE predicted trapping efficiency and the observed trapping efficiency averaged 5.5 % with a maximum difference of 13 %; by comparison the difference between the observed trapping efficiency and the trapping efficiency predicted by the CSTRS model averaged 2.5 % with a maximum difference of 5 %.

Comparisons of the observed effluent sediment graph and the effluent sediment graph predicted by WEPPSIE are presented in Figures 5.11 through 5.15 for the Tapp et al. (1981) runs and in Figures 5.16 through 5.21 for the Wilson et al. (1984) runs. Effluent concentration is predicted well on the rising limb of effluent sediment graph for all the runs. After the time increases

beyond the time of inflow,  $t > T_i$ , the WEPPSIE prediction tends to drift above the observed effluent sediment graph for several of the runs. This is possibly due to the expressions used to determine deposition, and the assumption of an equivalent rectangular hydrograph.

During the time of inflow,  $t < T_i$ , deposition is determined with Equation 3.35, which is based upon the inflow rate, influent sediment concentration, and the detention time including the calibration coefficient  $c_t$  (see Equations 3.32 to 3.35). Equation 3.35 was formulated to predict deposition during the rising limb of an effluent sediment graph through the use of regression models to predict the calibration coefficient  $c_t$ . The agreement between the rising limbs of the effluent sediment graphs demonstrates that Equation 3.35 predicts deposition well. After the time of inflow,  $t > T_i$ , Equation 3.36 is utilized to compute deposition. Equation 3.36 is based upon the sediment concentration in the impoundment, the area of the impoundment, and the detention time including both of the calibration coefficients,  $c_t$  and  $c_d$  (see Equations 3.32 to 3.36). Equation 3.36 does not include any deposition of incoming sediment because the WEPP convention specifies rectangular inflow hydrographs and influent sediment graphs, eliminating any incoming sediment after the time of inflow. When attempting to utilize Equation 3.36 to predict deposition with a variable inflow rate, deposition of the sediment entering the impoundment after the time of inflow,  $t > T_i$ , is delayed until the incoming sediment is added to the overall impoundment sediment concentration. This causes the predicted

Table 5.3: Predicted and observed trapping efficiencies for the Tapp et al. (1981) and Wilson et al. (1984) data sets.

Data Set	Run Number	Trap Efficiency, percent		
		Observed	WEPPSIE	CSTRS
Tapp et al. (1981)	18	74	78	78
	19	85	72	84
	22	88	82	88
	24	85	78	89
	28	84	74	79
Wilson et al. (1984)	1	70	65	67
	2	84	82	81
	3	84	75	81
	4	88	85	88
	5	75	75	75
	6	78	79	83



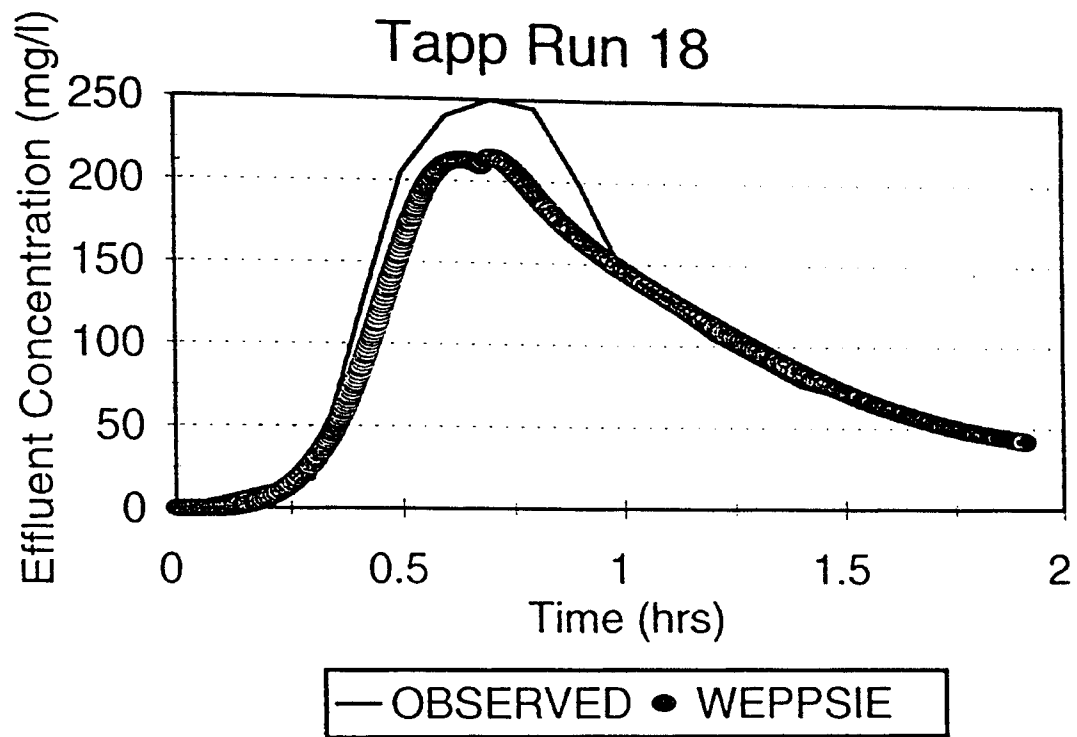


Figure 5.11: Predicted and observed effluent sediment concentrations for Tapp et al. (1981) Run 18.

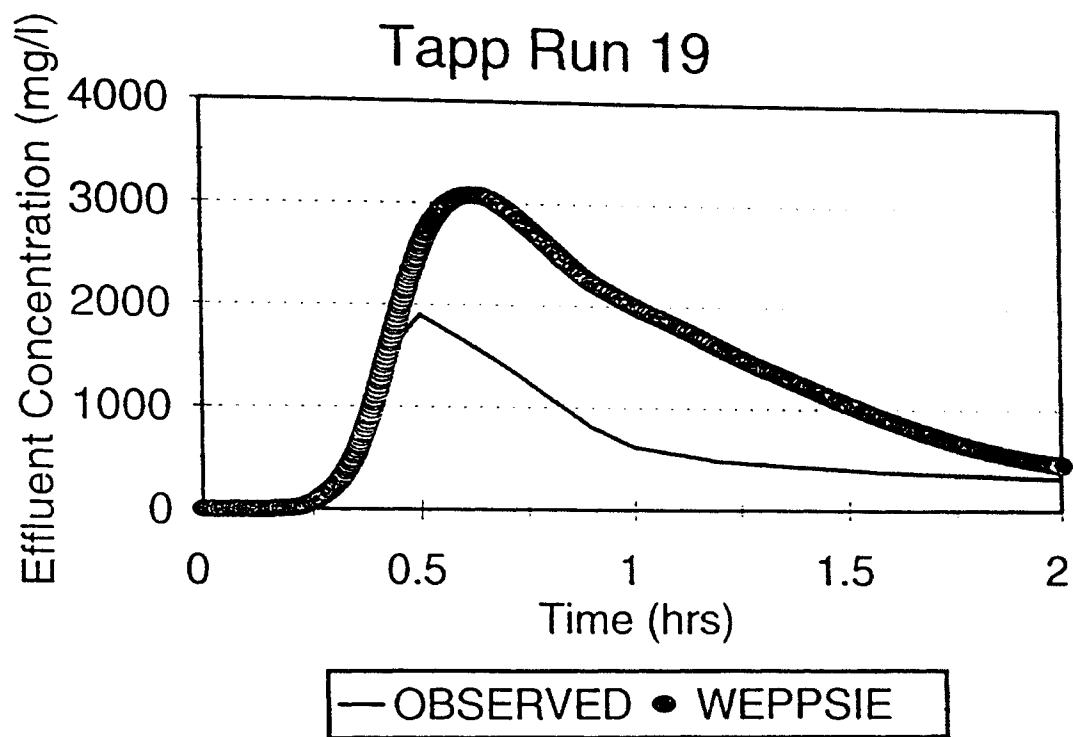


Figure 5.12: Predicted and observed effluent sediment concentrations for Tapp et al. (1981) Run 19.

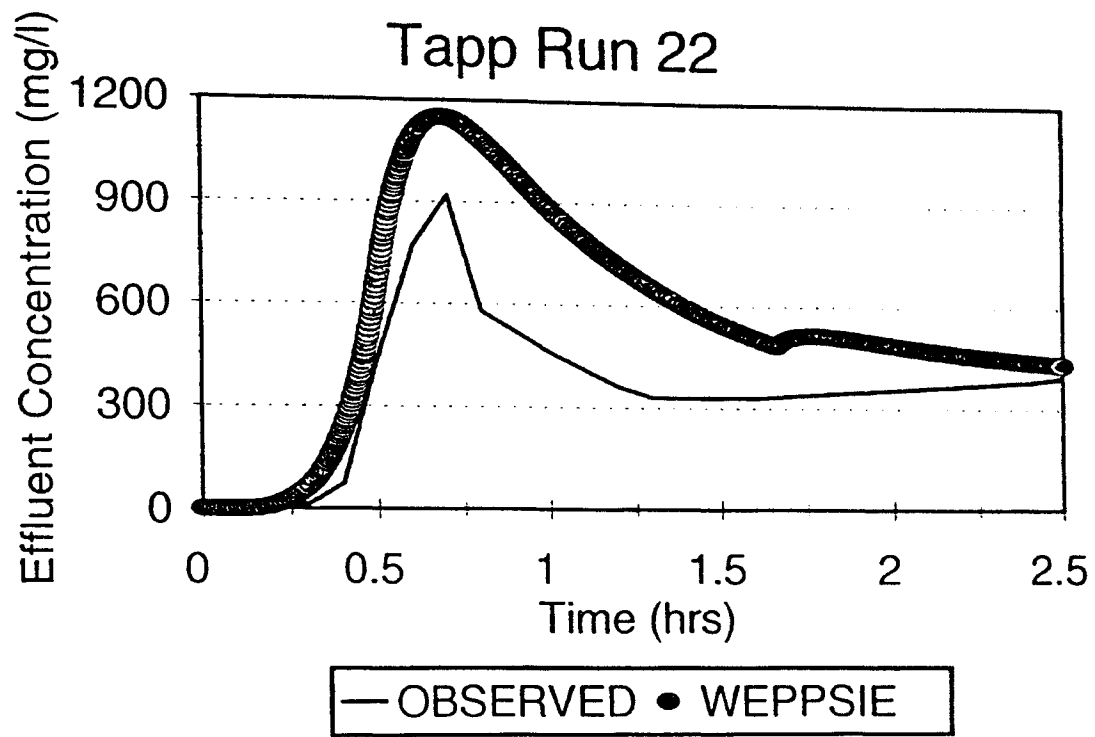


Figure 5.13: Predicted and observed effluent sediment concentrations for Tapp et al. (1981) Run 22.

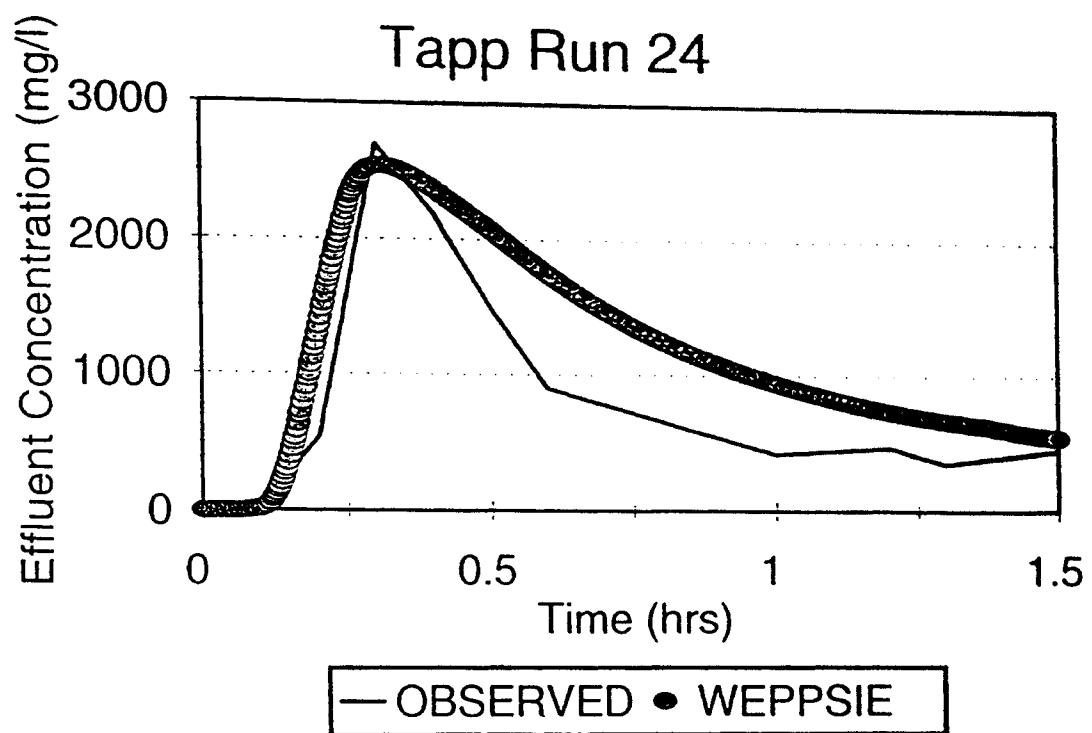


Figure 5.14: Predicted and observed effluent sediment concentrations for Tapp et al. (1981) Run 24.

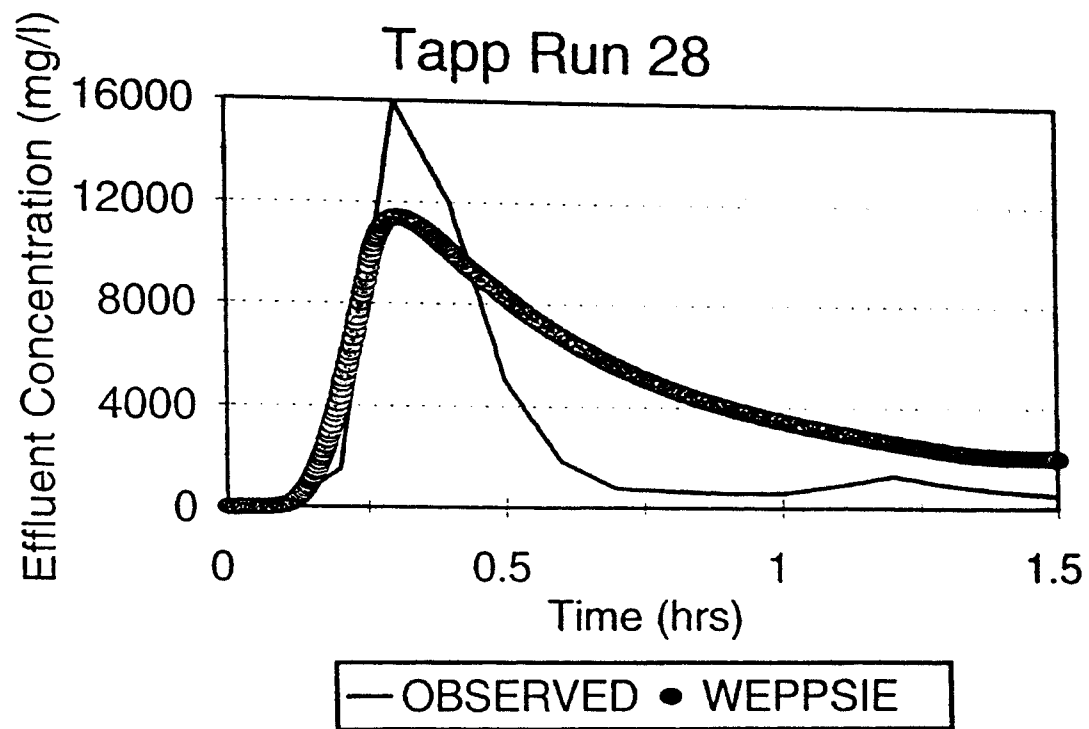


Figure 5.15: Predicted and observed effluent sediment concentrations for Tapp et al. (1981) Run 28.

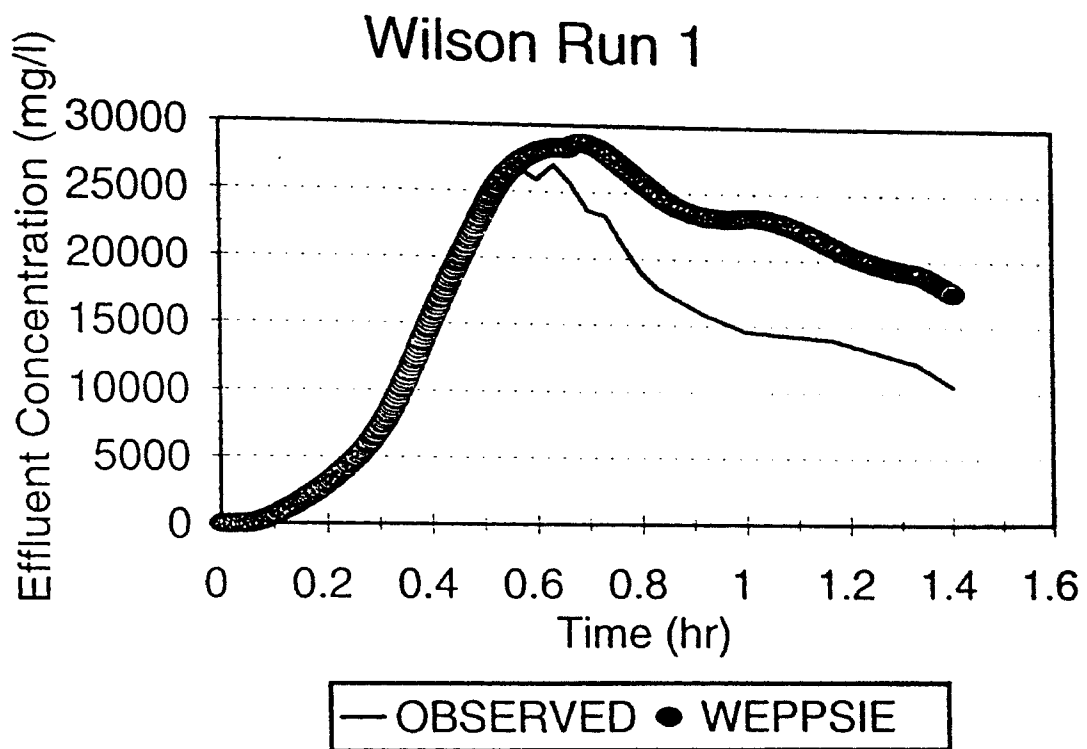


Figure 5.16: Predicted and observed effluent sediment concentrations for Wilson et al. (1984) Run 1.

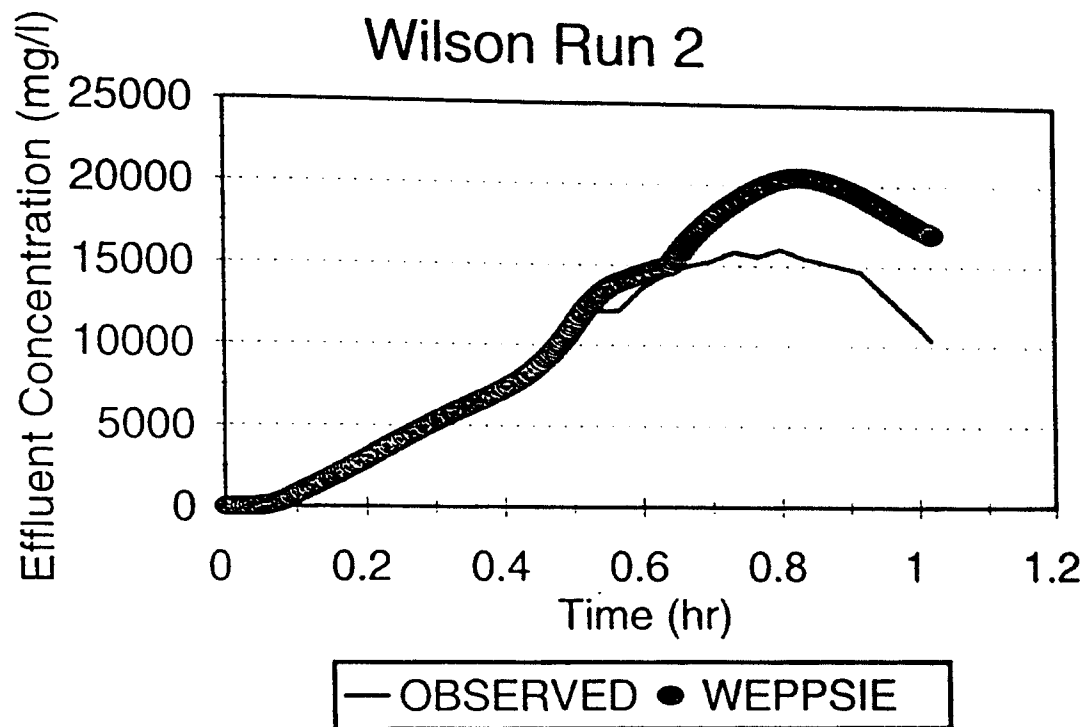


Figure 5.17: Predicted and observed effluent sediment concentrations for Wilson et al. (1984) Run 2.

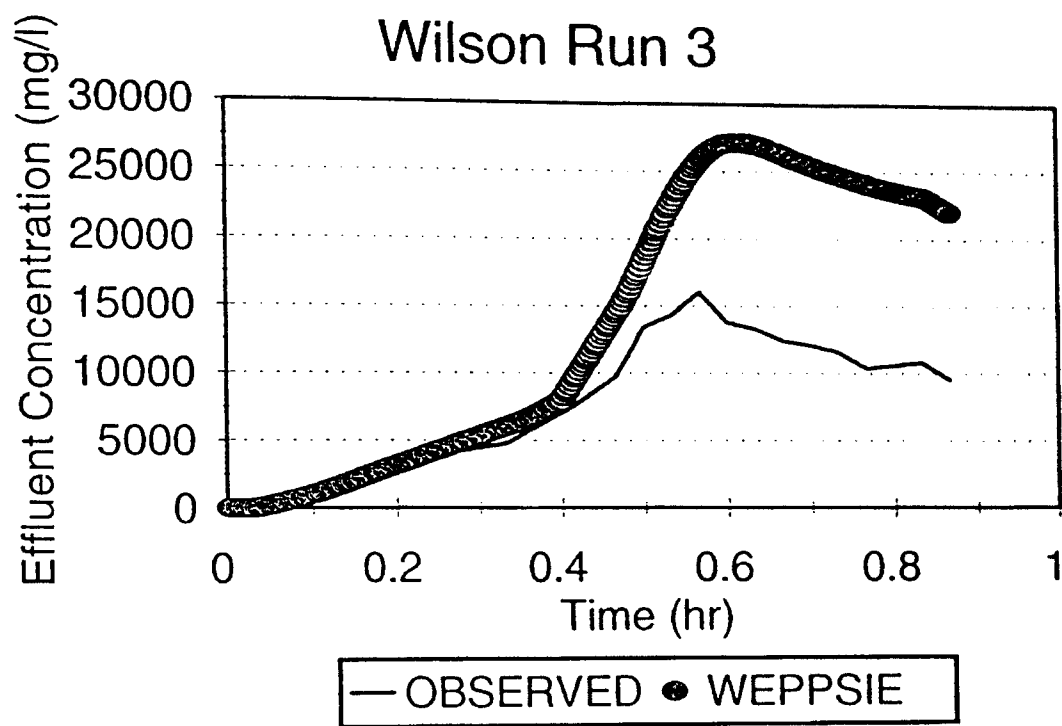


Figure 5.18: Predicted and observed effluent sediment concentrations for Wilson et al. (1984) Run 3.



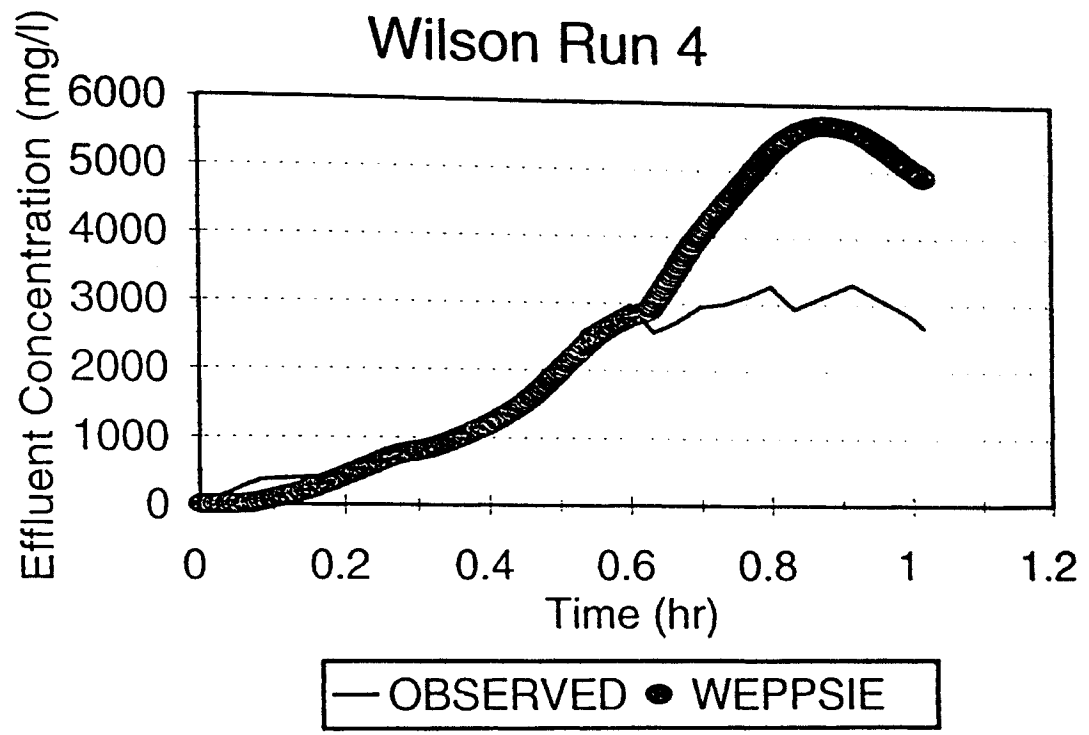


Figure 5.19: Predicted and observed effluent sediment concentrations for Wilson et al. (1984) Run 4.

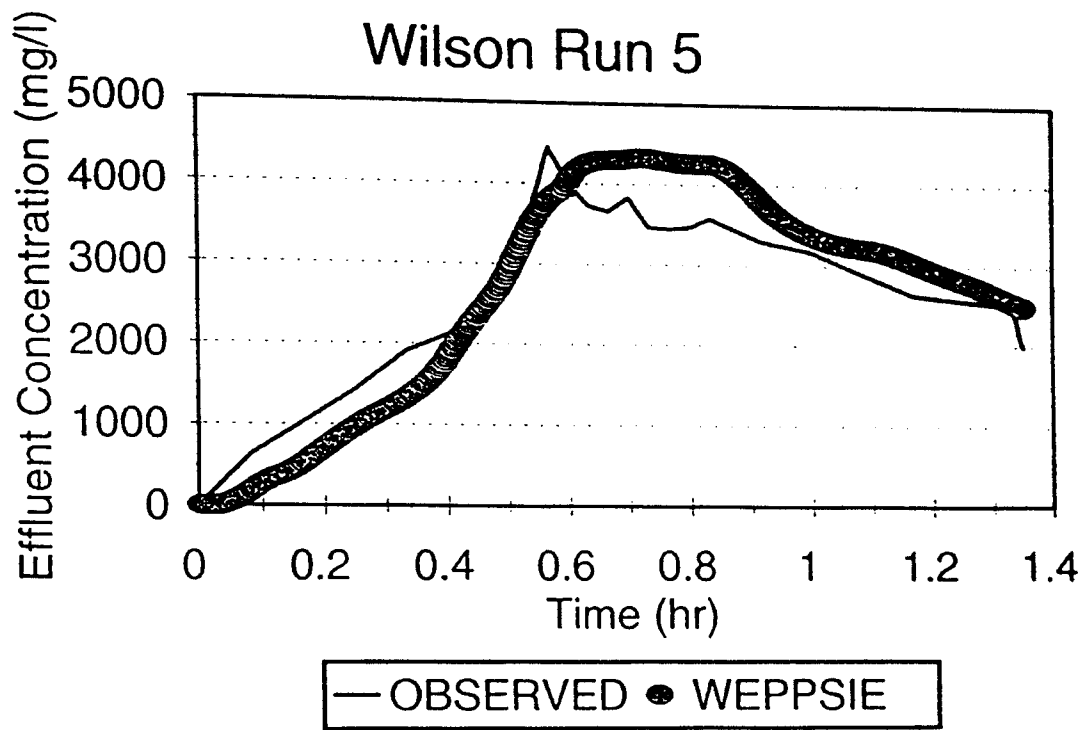


Figure 5.20: Predicted and observed effluent sediment concentrations for Wilson et al. (1984) Run 5.

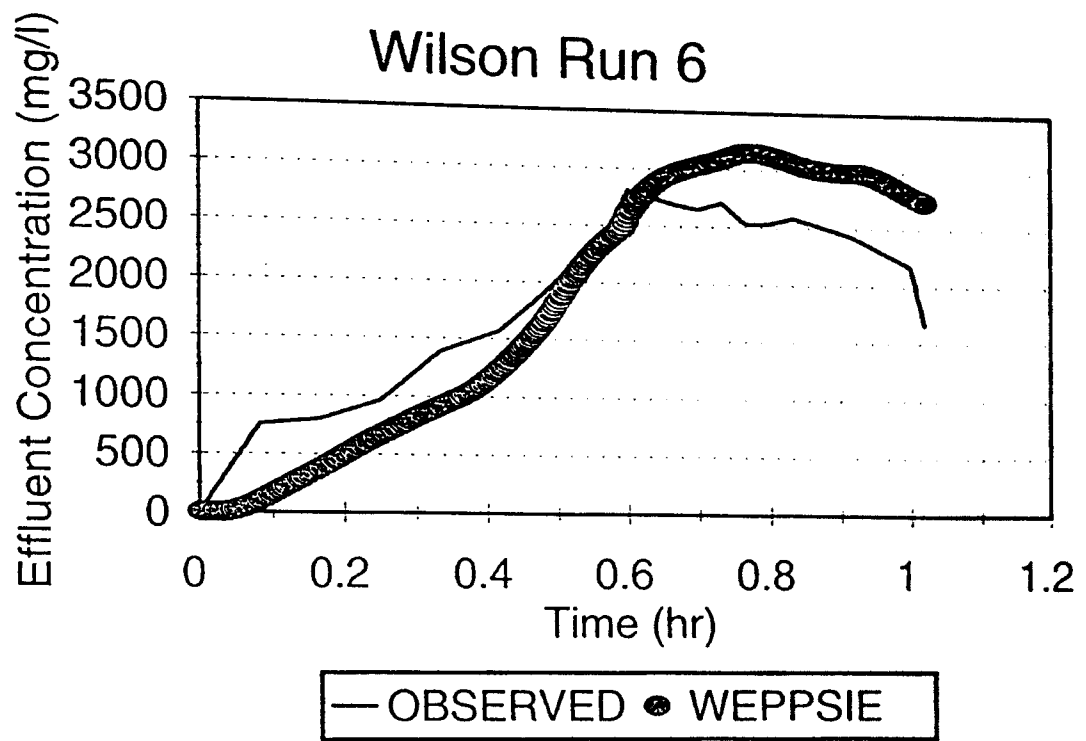


Figure 5.21: Predicted and observed effluent sediment concentrations for Wilson et al. (1984) Run 6.

effluent sediment concentration to be higher than the observed value. This phenomena has a greater effect on runs where there is a considerable amount of sediment entering the impoundment after  $T_i$ .

Differences in the effluent sediment concentration predicted by WEPPSIE and the observed effluent sediment concentration may also be due to inaccurate influent sediment size distributions. This is particularly true of the Tapp et al. (1981) runs. The measured influent sediment concentrations for the Tapp et al. (1981) runs were highly variable, making a prediction of the true influent sediment size distribution a rough estimate at best. The Tapp et al. (1981) runs also did not include chemical treatment to prevent natural flocculation. If natural flocculation did occur, the measured influent sediment size distributions would be skewed to include more larger particles causing predicted trapping efficiencies to be low. The trapping efficiencies predicted by WEPPSIE are lower than the observed trapping efficiencies for four of the five Tapp et al. (1981) runs.

Although there are differences between the trapping efficiencies and effluent sediment concentrations predicted by WEPPSIE and observed by Tapp et al. (1984) and Wilson et al. (1984), they are small and explainable. The average difference in the observed trapping efficiency and the trapping efficiency predicted by WEPPSIE of 5.5 % is satisfactory considering the many simplifying assumptions going into the WEPP convention and that the observed data sets do not follow this convention. Further, the validation runs against the

CSTRS database in which the simplifying assumptions made by the WEPP convention are met indicate that the WEPPSIE sedimentation algorithms perform well. The effluent trapping efficiencies predicted by WEPPSIE are generally more conservative than the measured trapping efficiencies.

## **Chapter 6: Summary and Conclusions**

### **Summary**

Algorithms and computer code for the WEPP Surface Impoundment Element were developed and validated for a variety of possible impoundment geometries and outflow structures. The WEPP Surface Impoundment Element performs hydraulic and sedimentologic routing for impoundments with any combination of the following outflow structures:

1. Drop spillway.
2. Perforated riser.
3. Culvert or trickle tube spillway.
4. Open channel or emergency spillway outlets.
5. Rock fill check dams.
6. Filter fence or straw bale check dams.

Hydraulic routing is performed by a direct numerical integration of an expression of continuity. Continuous functions are utilized to determine the discharge and area as functions of stage in the hydraulic routing. To speed up the routing process, an adaptive time step procedure that increases the time step when the inflow and outflow rates are relatively constant is utilized. The hydraulic routing procedure was validated against the PULS routing method included in the impoundment components of the SEDIMOT (Wilson et al., 1982) and SEDCAD (Warner and Schwab, 1992) models. The continuous

functions utilized to compute the discharge for a given stage have been validated for perforated risers, open channels, and rock fill check dams. The continuous outflow functions used for drop spillways, culverts, filter fence check dams, and straw bale check dams are taken directly from the literature and have been previously validated.

The sedimentation algorithms presented here are based upon an analogy to the overflow rate and conservation of mass. To adjust the simplified modeling approach used in WEPPSIE, two parameters have been included in the determination of deposition,  $c_t$  and  $c_d$ . These parameters are empirical factors used to account for the effects of impoundment geometry, hydraulic response, and stratification of the suspended sediment. An optimization procedure was utilized to determine optimal values of  $c_t$  and  $c_d$  for a variety of farm ponds, terraces, and check dams. Regression models have been developed to determine  $c_t$  and  $c_d$  for either small impoundments with little to no permanent pool, or large impoundments with a permanent pool. The results of WEPPSIE have been validated against results obtained with the CSTRS model for a large database including a range of impoundment geometries and outflow structures. For small impoundments without permanent pool, the average difference in predicted trapping efficiency ranged from 0.1 % for sand particles to 5.8 % for clay particles, and for large impoundments with permanent pool, the average difference in predicted trapping efficiency ranged from 0.6% for large aggregates to 4.0 % for clay particles. Further, the WEPPSIE sedimentation

algorithms were validated against data collected on two experimental impoundments. The difference in the WEPPSIE predicted trapping efficiency and the observed trapping efficiency averaged 5.5 % with a maximum difference of 13 %.

### **Conclusions**

The following conclusions can be drawn from observations made during this study:

1. The hydraulic routing procedure performs well and is an improvement over the PULS routing procedure used in SEDIMOT (Wilson et al., 1982) and SEDCAD (Warner and Schwab, 1992).
2. The continuous function utilized to predict discharge through a rock fill check dam is based on a simple graphical procedure by Haan et al. (1994). It is subject to the same limiting assumptions as the Haan et al. (1994) graphical procedure: a porosity of 0.46, a standard deviation of the rock fill diameter equal to half the average diameter, and a down stream depth of zero. If the conditions in the field are very different from these assumptions, the discharge predicted may not be accurate.
3. The sedimentation algorithms perform well as compared to the CSTRS model (Wilson and Barfield, 1984) when the conventional WEPP rectangular inflow hydrograph and influent sediment graph is used. The overall average difference in the trapping efficiency



predicted by CSTRS and WEPPSIE was 2.6 %. Note that trapping efficiencies predicted for clay particles with WEPPSIE were consistently high than trapping efficiencies predicted by CSTRS.

4. When compared to empirical data collected on pilot scale impoundments with variable flow rates, the sedimentation algorithms predict the rising limb of effluent sediment graphs well, but for the falling limb generally predict effluent sediment concentrations that are some what higher than the observed concentrations. However, the average difference in the observed trapping efficiency and the predicted trapping efficiency is 5.5 % which is acceptable considering the simplifying assumptions included in the WEPP convention.
5. Taken as a whole the WEPP Surface Impoundment Element satisfies the objectives of this project by producing reasonable predictions of the hydraulic routing of flow and effluent sedimentation concentration for impoundments covering a wide range of geometries and outflow structures.
6. The use of a slurry flow rate to compute the discharge through a filter fence or straw bale check dam provides only a rough estimate of discharge because there is little knowledge of the what is the correct slurry flow rate for a given material filtering flows of sediment laden water with a given sediment

concentration and size distribution. Further, the slurry flow rate changes as pores become blocked by sediment. The discharge predicted through filter fence and straw bale check dams is only as accurate as the estimation of the slurry flow rate.

#### **Recommendations for Further Study**

1. Work is needed to improve the range of applicability of the stage-discharge relationship used for rock fill check dams.
2. Work is needed to improve upon the slurry flow rate concept employed to determine the discharge for filter fence and straw bale check dams.
3. Work is needed to quantify the effects of deposited organic matter and sediment on structure inlet hydraulics, particularly for culvert inlets which often become partially blocked by sediment, trash, and organic matter.
5. The effects of natural flocculation, scour, and thermal stratification are neglected by WEPPSIE. These phenomena can be important in predicting effluent sediment concentration, and perhaps correction factors could be added to account for these phenomena.
6. The conditions under which rock fill, filter fence, and straw bale check dams wash out need to be studied and included in WEPPSIE.

## References

- Barfield, B.J., R.C. Warner, and C.T. Haan. 1981. Applied Hydrology and Sedimentology for Disturbed areas. Oklahoma Technical Press, Stillwater, OK.
- Camp, T.R. 1946. Sedimentation and the Design of Settling Tanks. Transactions of the ASCE. 111: 895-958.
- Carter, R.W. 1957. Computation of Peak Discharge at Culverts. U.S. Geological Survey, Circular 376, U.S. Government Printing Office, Washington, D.C.
- Chen, C. 1975. Design of Sediment Retention Basins. Proceedings National Symposium on Urban Hydrology and Sediment Control. UK BU 109, College of Engineering, University of Kentucky, Lexington, KY, pp 169-178.
- Chow, V.T. 1959. Open Channel Hydraulics. McGraw-Hill, New York, NY.
- Dobbins, W.E. 1944. Effect of Turbulence on Sedimentation. Transactions of the ASCE. 109: 629-678.
- Driscoll, E.D., D. DiToro, D. Gaboury, and P. Shelly. 1986. Methodology for Analysis of Detention Basins for Control of Urban Runoff Quality. Report No. EPA 440/5-87-01. (NTIS No. PB87-116562) U.S. EPA, Washington D.C.
- Einstein, H.A. 1950. The Bed-Load Function for Sediment Transportation in Open Channel Flows. USDA, Technical Bulletin No. 1026. Washington, D.C.
- Federal Highway Administration. 1985. Hydraulic Design of Highway Culverts. Hydraulic Design Series No 5. Report No. FHA-IP-85-15, FHA, Washington, D.C.
- Fisher, L.S. and A.R. Jarrett. 1984. Sediment Retention Efficiency of Synthetic Filter Fabric. Transactions of the ASAE. 27(2): 429-436.
- Fogle, A.W. and B.J. Barfield. 1992. Channel-A Model of Channel Erosion by Shear, Scour, and Channel Headwall Propagation: Part 1 Model Development. Research Report No. 186, University of Kentucky, Water Resources Research Institute, Lexington, KY.

- Foster, G.R. and L.J. Lane. 1987. User Requirements: USDA - Water Erosion Prediction Project (WEPP). National Soil Erosion Research Laboratory, West Lafayette, IN.
- Foster, G.R., R.A. Young, and W.H. Neibling. 1985. Sediment Composition for Nonpoint Source Pollution Analyses. Transactions of the ASAE. 28(1):133-139,146.
- Graf, W.H. 1971. Hydraulics of Sediment Transport. McGraw-Hill, New York, NY.
- Grant, D.A. 1978. Open Channel Flow Measurement Handbook. First Edition. Instrument Specialties Co., Lincoln, NE.
- Griffin, M.L., B.J. Barfield, and R.C. Warner. 1985. Laboratory Studies of Dead Storage in Sediment Ponds. Transactions of the ASAE. 28(3):799-804.
- Griffin, M.L. 1983. Characterizing the Hydraulic Efficiency of Sediment Ponds. M.S. Thesis. University of Kentucky, Lexington, KY.
- Gupta, R.S. 1989. Hydrology and Hydraulic Systems. Prentice Hall, Englewood Cliffs, NJ.
- Haan, C.T., B.J. Barfield, and J.C. Hayes. 1994. Design Hydrology and Sedimentology for Small Catchments. Academic Press, New York (In Press).
- Haan, C.T. 1977. Statistical Methods in Hydrology. Iowa State University Press, Ames, IA.
- Haan, C.T. and H.P. Johnson. 1967. Geometrical Properties of Depressions in North-Central Iowa. Iowa State Journal of Science. 42(2): 149-160.
- Hill, R.D. 1976. Sedimentation Ponds - A Critical Review. Proceedings Sixth Symposium on Coal Mine Drainage Research, Louisville, KY.
- Herrera, N.M. 1989. Defining the Hydraulics of Flow through a Rockfill of Varying Gradation Using Sediment-Free Water. Ph.D. Dissertation. University of Kentucky, Lexington, KY.
- Herrera, N.M. and G.K. Felton. 1991. Hydraulics of Flow Through a Rockfill Dam Using Sediment-Free Water. Transactions of the ASAE. 34(3):871-875.

- Kao, T.Y. 1975. Hydraulic Design of Storm Water Detention Structures. Proceedings of the National Symposium on Urban Hydrology and Sediment Control, UKY BU 111, College of Engineering, University of Kentucky, Lexington, KY.
- Kohler, M.A., T.J. Nordenson, and W.E. Fox. 1955. Evaporation from Pans and Lakes. U.S. Weather Bureau Research Paper No. 38.
- Lafren, J.M. 1972. Simulation of Sedimentation in Tile-Outlet Terraces. Ph.D Dissertation. Iowa State University, Ames, IA.
- Lake, E.B. and A.M. Shady. 1993. Erosion Reaches Crisis Proportions. Agricultural Engineering. 74(6):8-13.
- Lindley, M.R., B.J. Barfield, B.N. Wilson, and J.M. Lafren. 1993. WEPP Surface Impoundment Element: Farm Pond Sedimentation. Paper No. 932108. Presented at ASAE Meeting, Spokane, WA.
- Lindley, M.R., B.J. Barfield, B.N. Wilson, and J.M. Lafren. 1992. Surface Impoundment Element For WEPP: Farm Pond Hydraulics. Paper No. 922643. Presented at ASAE Meeting, Nashville, TN.
- Mavis, F.T. 1942. The Hydraulics of Culverts. The Pennsylvania State College, Engineering Experiment Station, Bulletin 56, State College, Pennsylvania.
- Maryland Water Resources Administration. 1983. Maryland Standards and Specifications for Soil Erosion and Sediment Control. Maryland Water Resources Administration, Annapolis, MD.
- McEnroe, B.M., J.M. Steichen, and R.M. Schweiger. 1988. Hydraulics of Perforated Riser Inlets for Underground-Outlet Terraces. Transactions of the ASAE, 31(4):1082-1085.
- Peavy, H.S., D.R. Rowe, and G. Tchobanoglous. 1985. Environmental Engineering. McGraw-Hill, New York, NY.
- Press, W.H., S.A. Teukolsky, W.T. Vetterling, and B.P. Flannery. 1986. Numerical Recipes in FORTRAN: The Art of Scientific Computing. Cambridge University Press, Cambridge, New York.
- Rochester, E.W. and C.D. Busch. 1974. Hydraulic Design for Impoundment Terraces. Transactions of the ASAE. 17(4): 694-696.

- SAS Institute, Inc. 1984. SAS/ETS Users Guide Version 5 Edition. SAS Institute, Inc, Cary, NC.
- Schwab, G.O., R.K. Frevent, T.W. Edminster, and K.K. Barnes. 1981. Soil and Water Conservation Engineering. 3<sup>rd</sup> Edition. John Wiley and Sons, New York, NY.
- Simons, D.B. and F. Senturk. 1977. Sediment Transport Technology. Water Resources Publications. Fort Collins, CO.
- Soil Conservation Service. 1984. Engineering Field Manual. USDA, Washington, D.C.
- Soil Conservation Service. 1951. Engineering Handbook, Hydraulics Section 5. USDA, Washington, D.C.
- Stephenson, D. 1979. Rockfill in Hydraulic Engineering. Elsevier Scientific Publishing, New York, NY.
- Streeter, V.L. 1971. Fluid Mechanics. 5<sup>th</sup> Edition. McGraw-Hill, New York, NY.
- Tapp, J.S., B.J. Barfield, and M.L. Griffin. 1981. Predicting Suspended Solids Removal in Pilot Size Sediment Ponds Using Chemical Flocculation. Institute for Mining and Minerals Research Report IMMR 81/063, University of Kentucky, Lexington, KY.
- United States Department of Agriculture. 1980. CREAMS - A Field Scale Model for Chemicals, Runoff, and Erosion from Agricultural Management Systems. USDA Conservation Research Report No. 26, Washington D.C.
- Vetter, C.P. 1940 Technical Aspects of the Silt Problem on the Colorado River. Civil Engineering. 10:698-701.
- Virginia Soil and Water Conservation Commission. 1980. Virginia Erosion and Sediment Control Handbook. Richmond, VA.
- Ward, A.D., C.T. Haan, and B.J. Barfield. 1979. Prediction of Sediment Basin Performance. Transactions of the ASAE. 22(1):126-136.
- Ward, A.D., C.T. Haan, and B.J. Barfield. 1977. Simulation of the Sedimentology of Sediment Detention Basins. Research Report No. 103, Water Resources Research Institute, University of Kentucky, Lexington, KY.

- Wilson, B.N. and B.J. Barfield. 1985. Modeling Sediment Detention Ponds Using Reactor Theory and Advection-Diffusion Concepts. Water Resources Research. 21(4):423-432.
- Wilson, B.N. and B.J. Barfield. 1984. A Sediment Detention Pond Model Using CSTRS Mixing Theory. Transactions of the ASAE. 27(5):1339-1344.
- Wilson, B.N., B.J. Barfield, and I.D. Moore. 1982. SEDIMOT II: A Simulation Model of the Hydrology and Sedimentology of Surface Mined Lands. Part I: Modeling Techniques. University of Kentucky Agricultural Engineering Department, Final Report of EPA Project KY01212.

# VITA

**Mark Lindley**

Candidate for the Degree of

Master of Science

**Thesis: THE SURFACE IMPOUNDMENT ELEMENT FOR THE WATER  
EROSION PREDICTION PROJECT**

**Major Field: Biosystems Engineering**

**Biographical:**

**Personal Data: Born in Evanston, Illinois, on November 4, 1966, the son  
of Carl and Christine Lindley.**

**Education: Graduated from Buffalo Grove High School, Buffalo Grove,  
Illinois in May 1984. Received a Bachelor of Science degree in  
Mechanical Engineering from the University of Kentucky,  
Lexington, Kentucky in May, 1989. Completed the requirements  
for the Master of Science degree in Biosystems Engineering in  
July, 1994.**

**Experience: Raised in Arlington Heights, Illinois; employed as a  
warehouse worker during high school and during the summers.  
Employed as a Research Engineer by the Biological and  
Agricultural Engineering Department of the University of Kentucky,  
Lexington, Kentucky from May, 1988 to January, 1992.  
Employed as a Research Assistant by the Biosystems and  
Agricultural Engineering Department at the Oklahoma State  
University, Stillwater, Oklahoma from January, 1992 to May  
1994.**

**Professional Memberships: American Society of Agricultural Engineers  
and the American Society of Mechanical Engineers.**